1-1-2011

Effect of high intensity focused ultrasound on neural compound action potential : an in vitro study

Shahrad Jabbary.
Ryerson University

EFFECT OF HIGH INTENSITY FOCUSED ULTRASOUND ON NEURAL COMPOUND ACTION POTENTIAL: AN *IN VITRO* STUDY

By: Shahrad Jabbary

B.Eng. Bradford University, 2006, Bradford, England

A thesis

presented to Ryerson University

in partial fulfillment of the

requirements for the degree of

Master of Science

in the program of

Biomedical Physics

Toronto, Ontario, Canada, 2011

Author’s Declaration

I hereby declare that I am the sole author of this thesis.

I authorize Ryerson University to lend this thesis or dissertation to other institutions or individuals for the purpose of scholarly research.

_____

Shahrad Jabbary

I further authorize Ryerson University to reproduce this thesis or dissertation by photocopying or by other means, in total or in part, at the request of other institutions or individuals for the purpose of scholarly research.

_____

Shahrad Jabbary

Abstract

‘’Effect of High Intensity Focused Ultrasound on Neural Compound Action Potential: An *In Vitro* Study’’, Shahrad Jabbary, M.Sc., Biomedical Physics, Ryerson University, 2011

Therapeutic ultrasound is a promising field with many novel applications in medicine and biology. High intensity focused ultrasound (HIFU) provides the ability to localize the deposition of acoustic energy within the body by thermal effect. In this work a brief description of how the HIFU system works and how it can be used to produce localized thermal lesions on the pathogenic tissues in the human body will be presented. Results of acoustic characterization of a hand-held HIFU system developed in our lab will also be presented. The capabilities of creating controlled reversible and irreversible changes in the compound action potential (CAP) values of a specific neural tissue, i.e. lobster abdominal nerves by adjusting different ultrasound parameters (intensity, exposure duration, etc.) in the HIFU system will be also described. Lobster abdominal nerves were exposed to a 10s HIFU exposure. The focal intensity values for this study were chosen as 100, 175, 275, 400, 525 and 700 $W.cm^{-2}$. It was shown that a trend of small changes in the measured CAP values (increase in the CAP amplitude) could be achieved in the five intermediate intensities, while a drastic decrease in the measured CAP values and total degeneration of the nerve could be observed with the highest focal intensity of 700 $W.cm^{-2}$.

Acknowledgements

I would like to give my sincere thanks to my supervisor, Dr. Jahan Tavakkoli, for his excellent and continuous support during the tenure of this thesis. His thoughtful insights, comments and intelligence have always been most helpful in solving the problems and finding novel ways to approach the goal. It has been a privilege to have worked with such professional scientist.

I would also like to thank all the faculty and staff of the department of physics at Ryerson University for their help and support. Special thanks go to Mr. Arthur Worthington for his continues technical support that was vital to this project.

I would also like to show my appreciation to my supervisory committee, Dr. Michael Kolios and Dr. Carl Kumaradas for their valuable guidance and support throughout this project.

Moreover, I would like to thank my colleagues in the physics department who have helped and supported me in this thesis. I am also thankful to my dear parents for their continuous support in this stage of my professional life.

Research support from the Toronto Polyclinic Inc., Toronto, Ontario, was vital to the success of this project. This work was also supported by the Ontario Research Fund- Research Excellence (ORF-RE) grant and the Ryerson University Dean's Start-up Fund that were awarded to Dr. Tavakkoli.

Winter of 2011

Table of Contents

List of Figures

List of Tables

Chapter 1 Introduction and Background

In this chapter we will provide some basic knowledge and background studies about the topics that were directly dealt with in this research work. These include: anatomy of nerve and its properties, neural compound action potential (CAP) and its measurement, basics of physics of ultrasound, high intensity focused ultrasound (HIFU) and its applications in neurology and neurosurgery. At the end of the chapter, the hypothesis of the research work and the specific aims that were set to test it are postulated.

1.1 Nerve

1.1.1 Anatomy of Mammalian Nerves

A nerve is an enclosed, cable-like bundle of axons (Hang et al. 2004). Neurons are sometimes called nerve cells, however, this term is technically inaccurate since many neurons do not form nerves, and nerves also include the non-axon glial cells that ensheath the axons in myelin. Schwann cells function to support neurons and wrap around axons of motor and sensory neurons to form the myelin sheath. These cells are also involved in many important aspects of nerve biology, tasks such as the conduction of nervous impulses along axons, nerve development and regeneration are the two most important functions that Schwann cells are involved in (Bhatheja et al. 2006).

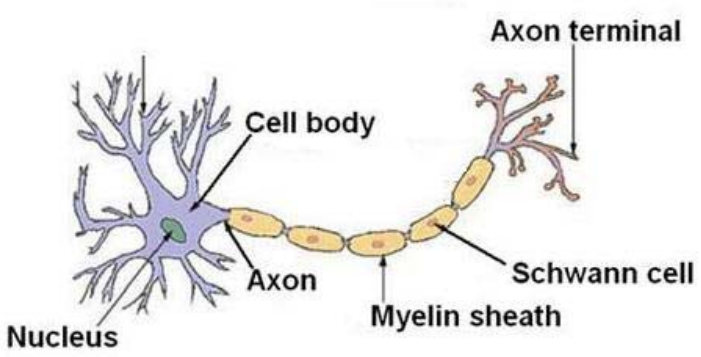

Figure 1.1 – Nerve's anatomy – Nerves are made up of bundle of axons, also protected by a Myelin sheath – courtesy of Hang et al. 2004

Nerves are part of the peripheral nervous system. Afferent nerves convey sensory signals to the central nervous system, for instance, from skin or organs, while efferent nerves conduct stimulatory signals from the central nervous system to the muscles and glands (Kalat et al. 2007). Afferent and efferent axons are often arranged together, forming mixed nerves. For example, the median nerve controls motor and sensory function in the hand. Neurons (long nerve cells) receive and transmit chemical-electrical messages to and from the brain. Each neuron is long and thin. One end receives messages and the other end transmits the message to the next neuron. These messages jump across a gap (synapse), from one neuron to another.

Damage to nerves can be caused by physical injury, swelling, autoimmune diseases, infection or failure of the blood vessels surrounding the nerve (Purves et al. 2008). A pinched nerve occurs when pressure is placed on a nerve, usually from swelling due to an injury or pregnancy in women. Nerve damage or pinched nerves are usually accompanied by pain, numbness, weakness or even paralysis. This is the reason why it is important to investigate and develop new and novel techniques and modalities to fight any discomfort/pain that can arise from any failure in the nervous system.

In mammals, the spinal cord contains a series of segmental ganglia, each giving rise to motor and sensory nerves that innervate a portion of the body surface and underlying musculature. On the limbs, the layout of the nerve supply is complex, but on the trunk it gives rise to a series of narrow bands (Marieb et al. 2007).

Myelin is an electrically insulating material that forms a layer, the myelin sheath, usually around only the axon of a neuron. This sheath is essential for the proper functioning of the nervous system (Trail et al. 1988). As mentioned earlier, this sheath is an outgrowth of the Schwann cells. The main purpose of a myelin sheath is to increase the speed at which impulses propagate along the myelinated fiber. It also increases electrical resistance across the cell membrane by a factor of 5000 and decreases capacitance by a factor of 50 (Duncan et al. 1934). In general, myelination helps prevent the electrical current from leaving the axon.

1.1.2 Frog Sciatic Nerve

The sciatic nerve is the main nerve trunk from the spinal cord to the leg. It consists of a bundle of nerve fibers, each of which is the axon of a neuron, whose cell body is in (or near) the spinal cord. Some axons conduct action potentials toward the brain (afferent fibers). Other axons (efferent fibers), conduct action potentials away from the brain. The frog sciatic nerve contains both efferent and afferent fibers (Figure 1.2).

The fibers may be large (15-25 μm) and myelinated, or small (around 0.2 μm) and un-myelinated. Regardless of the type or size of the fibers, they all have certain properties in common; e.g., they all conduct action potentials. However, there are also certain differences, for

example the conduction velocity of the fibers depends on their size (diameter) and whether they are myelinated or non-myelinated.

In general, small (lengths less than 25mm), myelinated and un-myelinated fibers are a feature of vertebrates, while large (lengths up to 500 mm or larger), un-myelinated fibers are a feature of invertebrates in vertebrates (including human). The whole nerve is encased in a connective tissue sheath called the Epineurium.

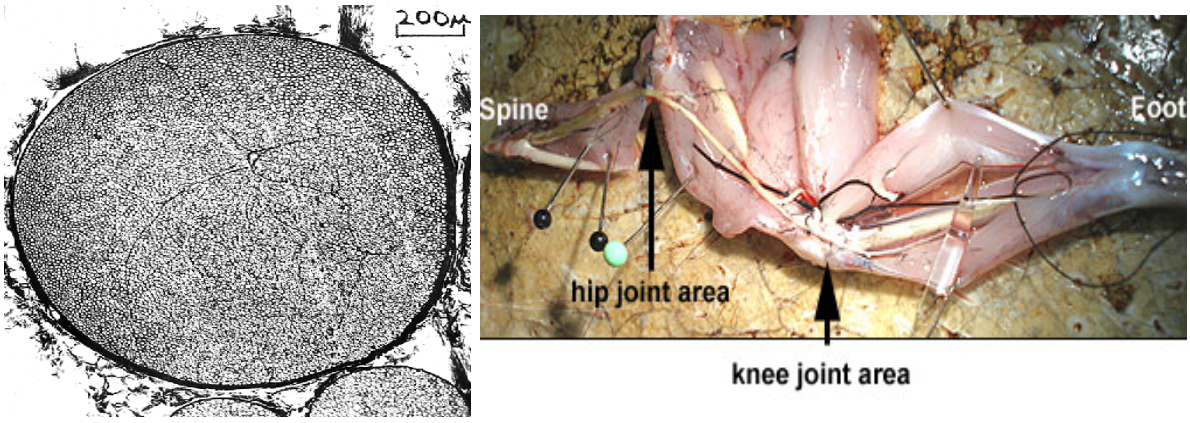

Figure 1.2 – Left: Frog's sciatic nerve consists of only a single bundle of fibers, surrounded by the perineum and loose epineurium – Right: Dissection of a frog's sciatic nerve

1.1.3 Lobster Nerve

The lobster abdominal nerve cord has been widely investigated because of its relative simplicity. The cord consists of six ganglia joined by connectives. From each ganglion, three bilateral (left and right) pairs of nerves innervate the muscles and sensory receptors in that abdominal segment (Shona et al. 2004). Each of the roots has a different destination in its segment of the abdomen. As it is shown in the figure 1.3 below, the nerve of lobster is starting from its brain running along into the middle of the tail of the animal.

Unlike mammalians, the myelin sheath does not exist in lobsters. In lobster with fibers of medium size (10-20 μm), the Schwann cells are usually very thin (0.1 μm). Therefore, this leaves the lobster nerve with no myelin sheath, which is responsible for protecting the neurons. Having no myelin sheath also causes the electrical-chemical signals to travel with a slower rate compared to the nervous system of mammalians (Schmitt et al. 1956).

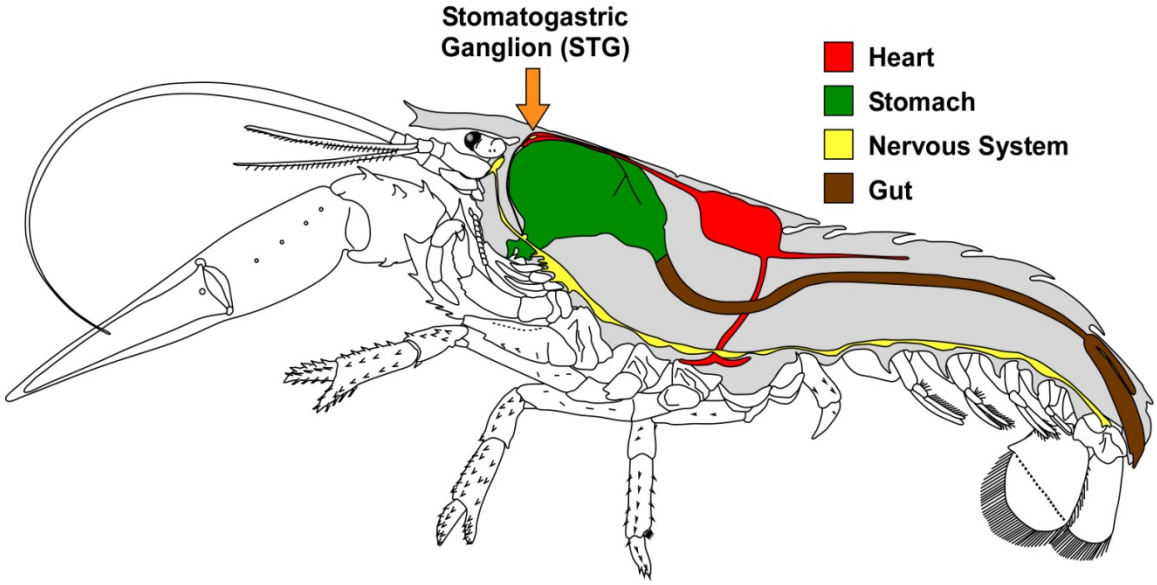

Figure1. 3 – Lobster's anatomy – Lobster's nervous system is starting from the brain running along into the middle of the tail – courtesy of Colin et al. 2004

1.2 Nerve Electro-physiology

The signals that nerves carry, sometimes called nerve impulses, are known as Action Potentials. Action potentials are electrochemical impulses that are produced by only nerve and muscle fibers which are excitable and capable of self-generation of these impulses (Barnett et al. 2007). The electrical potential that is generated following the propagation of an action potential along an axon can be recorded from the surface of the nerve (Figure 1.4). When a nerve bundle is

stimulated, many axons produce action potentials synchronously. The resulting electrical responses recorded from the surface of the nerve are called Compound Action Potentials (CAP), which represent the sum of many individual action potentials that distinguish them from the action potential generated by a single axon. The CAP is produced clinically or experimentally by placing extra-cellular stimulating electrodes on one end of the nerve and extra-cellular recording electrodes along the nerve. The stimulus for excitation of the nerve is provided by a stimulator which produces a stimulating pulse of variable intensity (voltage), duration and frequency.

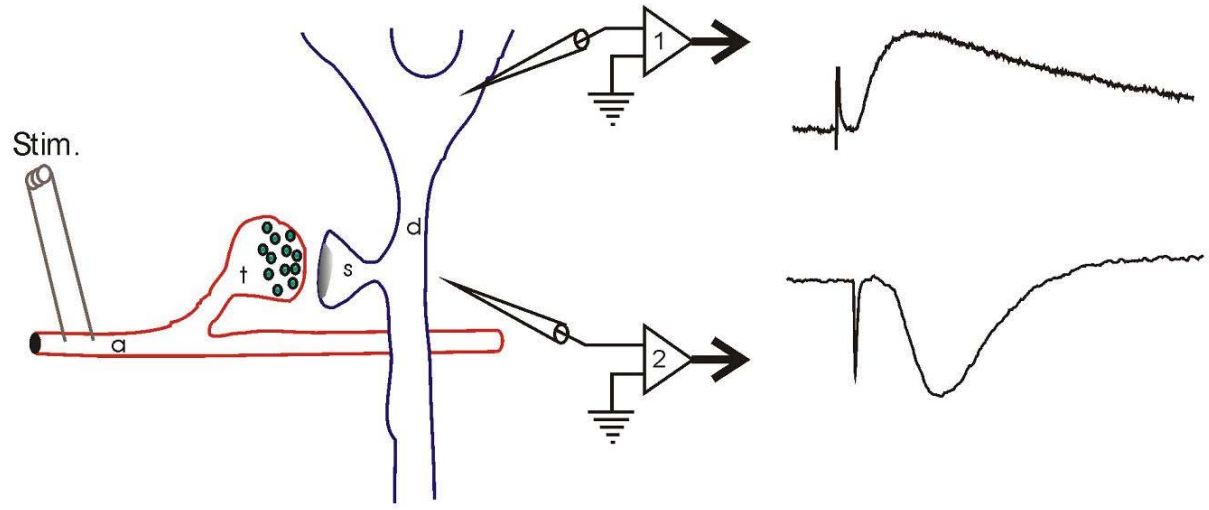

Figure 1.4 – A generic Electrophysiology – A schematic diagram showing action potential recording from rat neurons – (1) records the change in membrane potential that the incoming current causes – (2) detects the negativity deflection – courtesy of Gibson et al. 2008

1.3 Compound Action Potential (CAP)

As action potentials propagate along an axon, they produce electric potentials that can be recorded from the surface of the nerve. A single compound action potential is shown in figure 1.5.

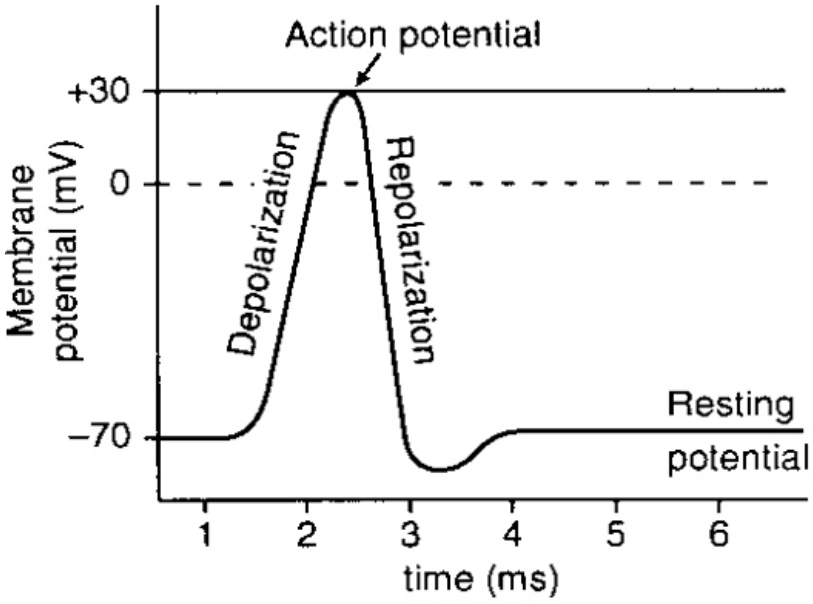

Figure 1.5 – Compound action potential – Showing different phases that a signal goes through in order to produce a CAP – courtesy of Barnett et al. 2007

As mentioned before, nerve signals are transmitted by action potentials, which are rapid changes in cell membrane from the 'resting' state. In the depolarization stage, voltage-dependant Na^+ channels are activated, leading to a rapid flux of Na^+ ions into the nerve cell and action potential reaches its peak. A very short time after peak action potential, voltage-dependant K^+ channels open and K^+ ions rapidly exit to the extra-cellular space. As K^+ flows outward, the Na^+ channels gradually become deactivated, Na^+ flux drops off and membrane repolarization has occurred (Doyle et al. 1998). Measurements of action potential amplitude, area, latency and conduction velocity may provide information about membrane Na^+ and K^+ transport (Figure 1.6). CAP amplitude and conduction velocity are positively correlated with sodium transport. In addition, the action potential amplitude and area recorded from a nerve can be used to estimate the number of activated nerve fibrils (Jiang et al. 2003).

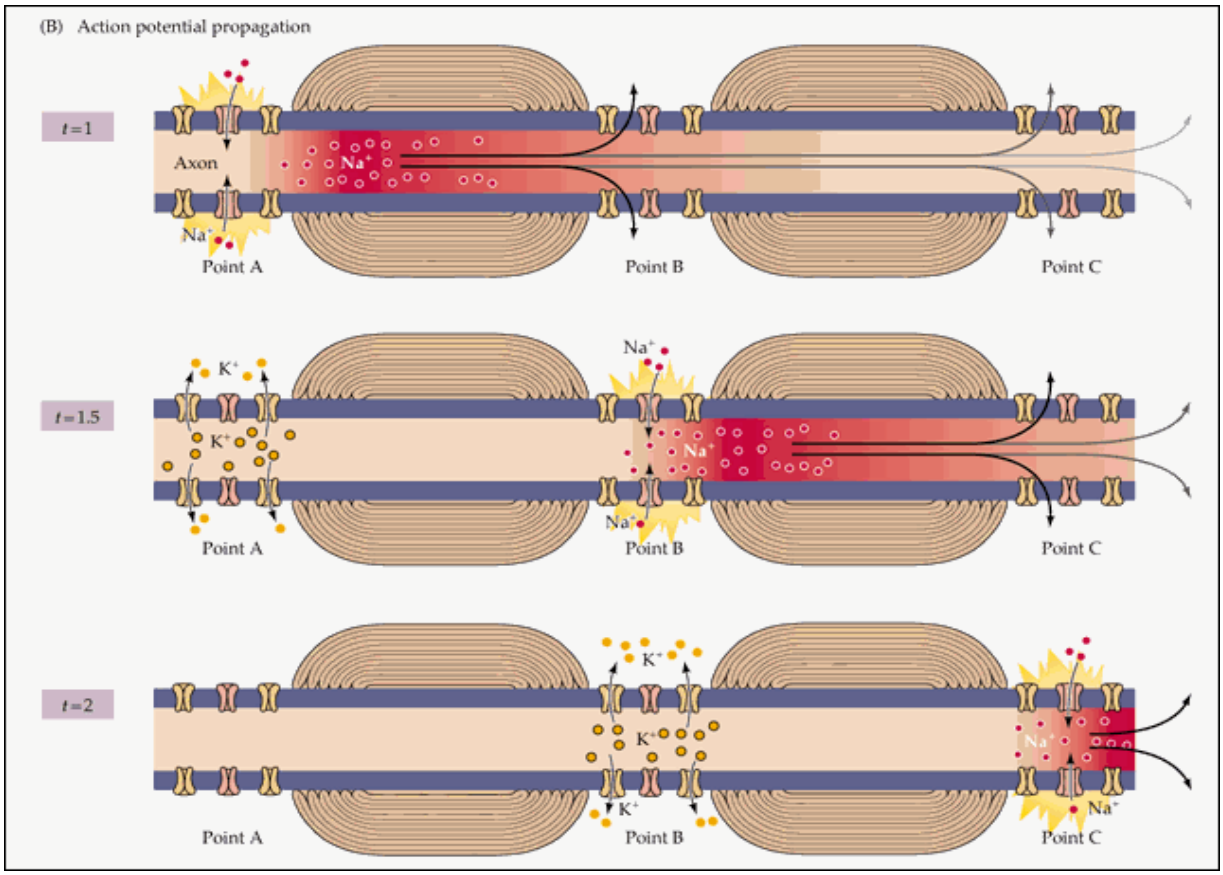

Figure 1.6 – Action potential propagation – Showing the flow of Na^+ and K^+ in and out of a nerve cell – courtesy of Jiang et al. 2003

1.4 CAP Measurement

Stimulus electrodes are applied to one end of the nerve; recording electrodes are located along the nerve. If the nerve is stimulated with a current pulse of sufficient amplitude, the action potentials produced in the fibers propagate toward the reading electrodes. The aggregate effect of the many action potentials is an extra-cellular wave of negative potential, moving along the surface of the nerve (figure 1.8). If the recording electrodes are widely spaced, the wave of negative potential produces a negative pulse in recorded voltage as it passes the positive recording electrode. At a later time, the negative wave of extra-cellular potential passes the

negative recording electrode, where it contributes a positive pulse to the recorded voltage. This concept is further illustrated in the upcoming pages of this chapter. Once the electrodes are spaced, the negative and positive parts of the recorded voltage merge, and the resulting waveform is called a biphasic compound action potential (Figure 1.7). The propagation can be blocked by a number of methods including mechanical, electrical and chemical methods. If the compound action potential is blocked between the two recording electrodes so that it does not reach the recording end, a monophasic compound action potential is recorded.

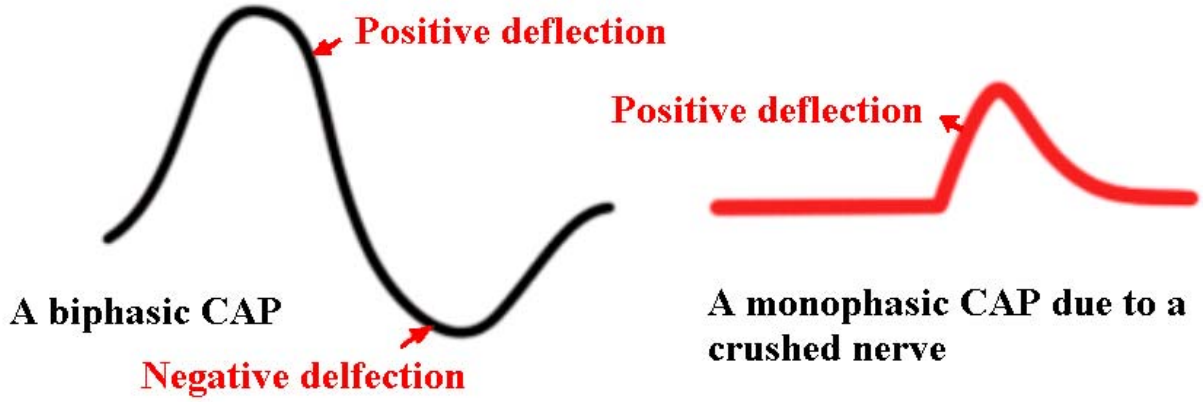

Figure 1.7 – Biphasic and Monophasic CAP

The maximum amplitude of CAP varies with the recording conditions though rarely exceeds a few milli-volts. Multiple peaks might represent repeated action potentials produced by the same fibers or alternatively, sub-populations of fibers that differ in their propagation velocities and therefore produce components with different delays.

The shape of the compound action potential depends on the population of excited fibers within the nerve. If all of the fibers in the nerve have similar diameters, then the propagation

velocities for action potentials will be similar. The resulting monophasic compound action potential will be brief. If the nerve contains a heterogeneous mix of fibers with different diameters, then the monophasic compound action potential will become broader as it propagates. If the distance between the stimulating and recording electrodes is sufficiently large, the monophasic compound action potential may consist of several peaks – each corresponding to a different sub-population of fibers that conducts action potentials at a different velocity.

The series of diagrams in figure 1.8 explain the CAP recording in further details. In these diagrams, single nerve fibers are shown in yellow (Biopac nerve conduction manual, Biopac Systems Inc., 2003). At rest, they have a positive external polarity with respect to a negative internal polarity. If an adequate stimulus is applied to the nerve fiber, an action potential will be generated at the site of the stimulus. As mentioned earlier, this action potential creates a nerve impulse, which consists of a traveling wave of depolarization followed immediately by a wave of repolarization. Once generated, this impulse will propagate along the fiber away from the stimulus site without change in amplitude or velocity. Viewed from the outside of the nerve fiber, the impulse begins by creating a negative polarity shift at the region of stimulation, shown in blue. The impulse proceeds as a wave of negative polarity along the outside of the fiber.

The diagrams in figure 1.8 show a voltmeter connected externally to the nerve fiber to record the voltage difference across two points. A graph will be plotted of voltage vs. time measured by the voltmeter beginning when the stimulus first generates an action potential. It is important to note that the voltmeter reads the potential difference between its positive and negative terminals. If the nerve fiber is at rest, the voltmeter will read 0 because both of its terminals are at the same voltage potential. If the voltmeter's negative terminal is more negative than its positive terminal, the voltmeter will indicate a positive voltage and vice versa.

Figure 1.8 shows five ‘’snap-shots’’ in time of events occurring on a single nerve fiber beginning with A and ending with E (Biopac nerve conduction manual). The recording is considered biphasic because the voltmeter can record both a positive and negative deflection:

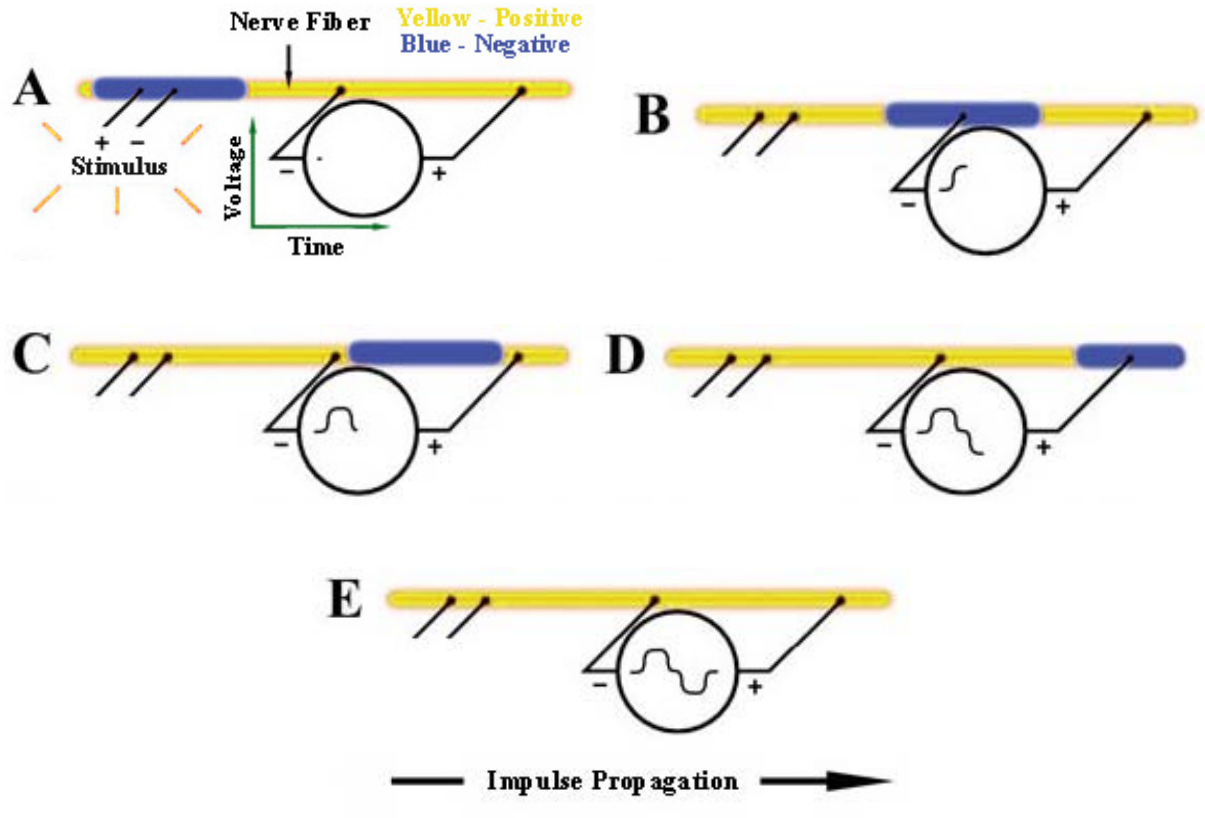

Figure 1.8 – (A) When an external stimulus that exceeds a certain threshold level is applied, an action potential will occur, creating the nerve impulse shown in blue. Since the voltmeter's negative and positive terminals at this instant are at the same voltage potential, it records 0 Volts. (B) The nerve impulse will propagate along the nerve with constant amplitude and velocity until it eventually passes through the voltmeter's negative terminal, causing it to record a positive voltage reading. (C) Propagation will continue and a point may be reached where the nerve impulse is between the voltmeter's negative and positive terminals, causing it to record 0 Volts. (D) Propagation will continue and eventually pass the voltmeter's positive terminal, causing it to record a negative (downward) voltage reading. (E) At some point, the impulse propagation will be complete, with the entire nerve fiber returned to its resting state and the voltmeter recording 0 Volts. The Voltage vs. Time recording will then be complete.

It only matters that the stimulus level exceeds the nerve fibers threshold, because a nerve impulse is generated in an *''all or none''* fashion. This means that regardless of the stimulus strength above threshold strength, the corresponding nerve impulse amplitude, duration and propagating velocity will be the same (Hartline et al. 2007). And since the voltmeter measures the differential voltage between its terminals, if the terminals come too close together, the voltage recording will be reduced in amplitude and a complete loss of recording ability may result.

1.5 Elements of Ultrasound Physics

Sound is mechanical energy that is transmitted by pressure waves through a medium, illustrated in figure1.9. Periodic changes in the pressure of the medium are created by forces acting on the molecules, causing them to oscillate about their normal positions. And since the motion of the molecules is repetitive, the term cycle is used to describe any sequence of changes in molecular motion that recurs at regular intervals (Hedrick et al. 2005).

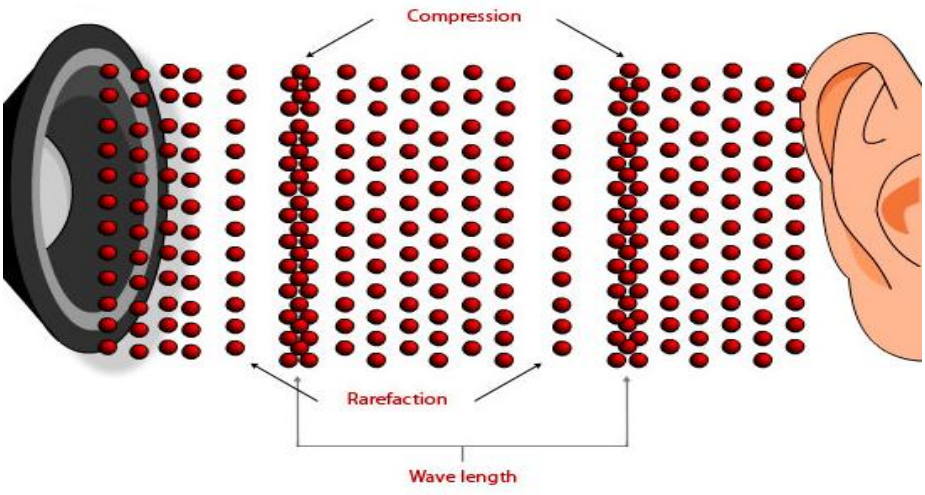

Figure 1.9 – Concept of molecular motion – Oscillation of air molecules produced by a speaker

Sound waves are mechanical in nature; however, they are not restricted to transmission through air. These mechanical pressure waves require an elastic deformable medium for propagation, which can be gas, liquid or solid. Something to note is that sound transmission cannot occur in a vacuum, since no molecules are available to transfer the mechanical vibrations that are caused by the sound waves.

Ultrasound is defined as mechanical waves with higher frequencies than those human can detect, i.e.; waves with frequencies of greater than 20,000 Hz. Any sound waves with frequencies less than 20 Hz are known as Infrasound (Hedrick et al. 2005). Ultrasound and infrasound waves however have similar properties which will be discussed in upcoming pages.

1.6 Types of Ultrasound Waves

Ultrasound waves are divided into two different types; longitudinal and transverse (Cobbold et al. 2007). In longitudinal waves particles are moving along the direction of the wave energy propagation, (Figure 1.10) meaning that the molecules are vibrating back and forth in the same direction as the wave is travelling. Ultrasound waves in liquids and tissues are known as longitudinal waves.

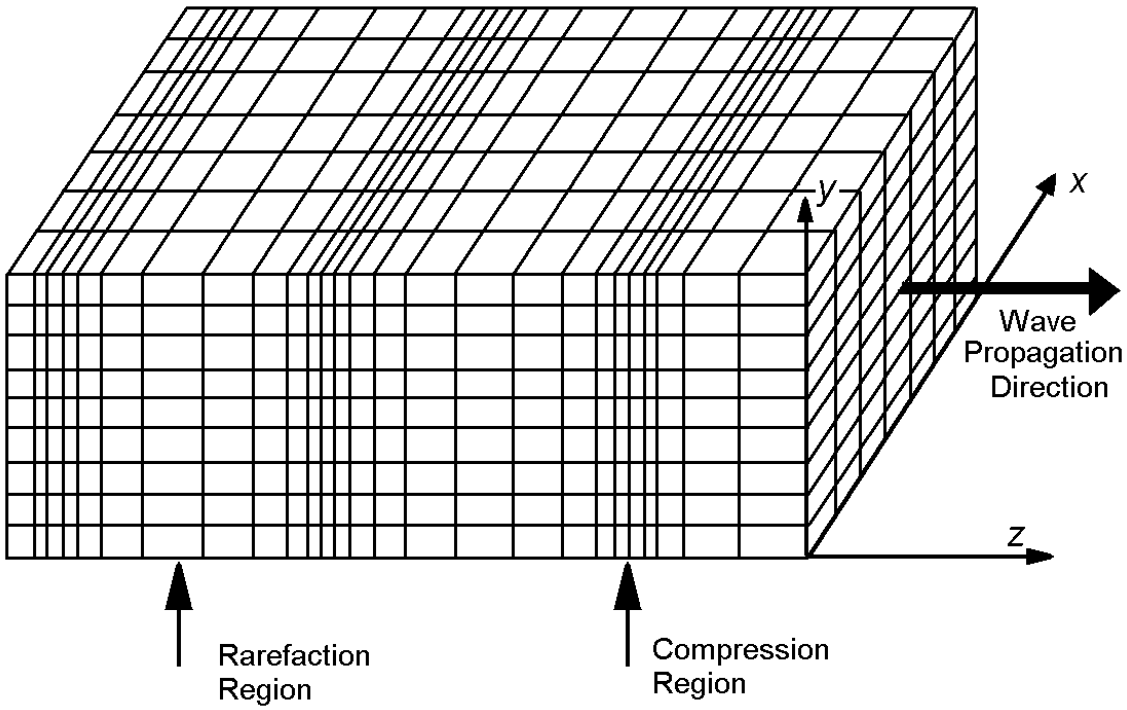

Figure 1.10 – Longitudinal wave – Molecular motion is along the direction of propagation – courtesy of Cobbold et al. 2007

Transverse ultrasound waves are those in which the motion of the particles is perpendicular to the direction of propagation of the wave energy (Figure 1.11). Observing the wave motion resulting from throwing a stone into a pool of water is a good example of illustrating this type of waves. The water molecules vibrate up and down, similar to a crack floating on the water, as the wave moves away from the point of origin across the surface of the water. These ultrasound transverse waves are also known as shear waves or stress waves, which can be observed in bone which is counted as the only biologic tissue that can cause the production of these waves when exposed to ultrasound (Hedrick et al. 2005).

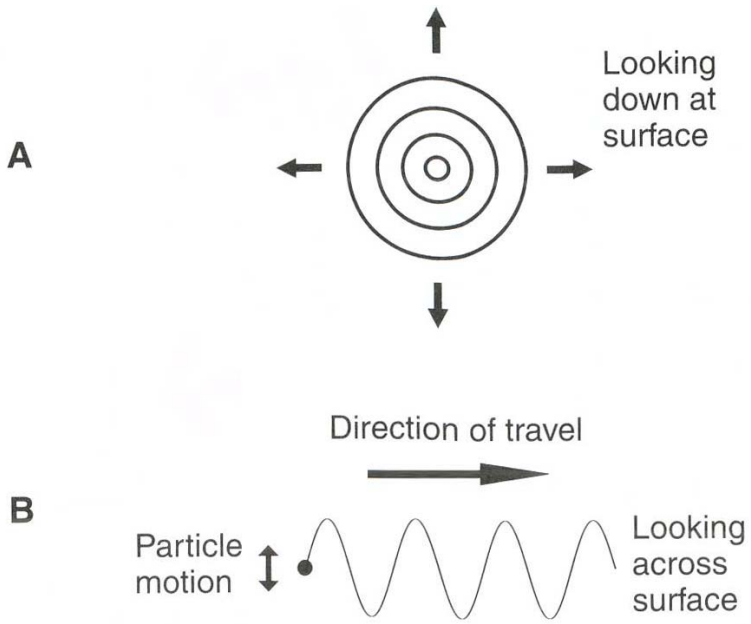

Figure 1.11 – Transverse ultrasound wave – A: direction of wave travelling is outward from sound source, B: producing particular motion perpendicular to the direction of travel – Hedrick et al. 2005

1.7 Properties of Ultrasound Waves

Ultrasound waves have certain physical characteristics that are used to describe them. Some of these characteristics are discussed in this chapter.

1.7.1 Wavelength

The spatial extent of one complete cycle is called wavelength (Figure 1.12). When particle density (mass per unit volume) is plotted against distance, amplitude describes the variation in density. Wavelength is the distance between two successive equivalent density zones (Carson et al. 1995).

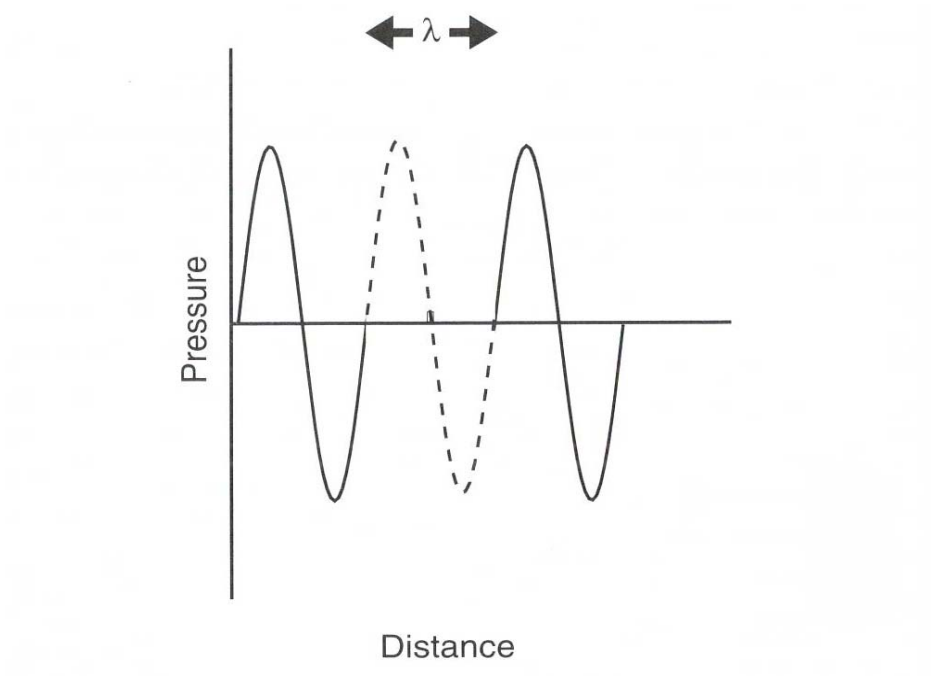

Figure 1.12 – Amplitude of particle density as a function of the distance in which wave travels

1.7.2 Frequency

The number of cycles (pressure oscillations) occurring at a given point in one unit of time is known as frequency. The unit of frequency is the hertz, which is equal to 1 cycle per second. Inverse of the frequency is termed as period with the units of second. The following equations define the relationship between period and frequency:

$$\tau = \frac{1}{f} \tag{1.1}$$

where τ represents the period in seconds and f is frequency in Hz.

1.7.3 Ultrasound Speed

The speed at which an ultrasound wave propagates through the medium is called the ultrasound speed (*c*). Velocity (m/s) is usually considered as a vector quantity which magnitude and direction are both assigned. However, the ultrasound speed refers to magnitude only (a scalar quantity). The velocity of sound is determined by the rate at which the wave energy is transmitted through the medium, in which the density and compressibility of the medium becomes important (Hedrick et al. 2005).

1.7.4 Medium Density and Compressibility

Density is the mass of a medium per unit volume (ρ). An increase in density of the medium will impede the rate of sound propagation through that particular medium (Kremkau et al. 2002). Thus on the basis of density alone, ultrasound is expected to have a greater velocity in air (low density) than in bone which is much denser and therefore has a much higher density than air. However, this is not the case, and other factors must influence ultrasound speed.

Compressibility indicates the fractional decrease in volume when pressure is applied to the material. The easier a medium is to reduce in volume, the higher is its compressibility (*K*) (N/m^2). The ultrasound speed in a medium is also inversely proportional to the square root of the compressibility of that medium (Hedrick et al. 2005).

Combining the compressibility and density into one equation, can determine the ultrasound speed for a particular medium as (Hedrick et al. 2005):

$$c = \frac{1}{\sqrt{K\rho}} \qquad (1.2)$$

where c represents ultrasound speed (m/s), K (N/m^2) is compressibility and ρ(kg/m^3) is the density.

In linear propagation regime, the speed of sound or ultrasound remains constant for a particular medium (Hedrick et al. 2005). The velocity (c) is equal to the frequency (f) times the wavelength (λ). Stated mathematically:

$$c = f\lambda \tag{1.3}$$

This is a very fundamental yet important equation used in biomedical ultrasound. Because the velocity is constant for a particular medium, increasing the frequency causes the wavelength to decrease.

1.7.5 Absorption

This is the only process whereby sound energy is dissipated in a medium. All other modes of interactions decrease the intensity by redirecting the energy of the beam. Absorption is the process that ultrasonic energy is transformed into other energy forms, primarily heat (Wells et al. 1977). Absorption is responsible for the medical applications of therapeutic ultrasound. Ultrasound propagation through homogeneous media is associated only with absorption and can be characterized with absorption coefficient only. Propagation through heterogeneous media requires taking into account scattering as well (Dukhin et al. 2002)

$$\mu = -\frac{1}{z} ln \frac{p(z)}{p0} \tag{1.4}$$

where μ represents absorption coefficient, z is the distance from the source, $p(z)$ is the pressure amplitude at point z and p_0 presents the pressure at the surface of the source.

1.7.6 Intensity

The intensity of an ultrasonic beam is the physical parameter that describes the amount of energy flowing through a cross-sectional area per second. Simply, it is the rate at which the energy is transmitted by the wave over a unit area (Zagzebski et al. 1996). The term intensity is used to describe the loudness of sound in the field of audible acoustics. For ultrasound, increasing intensity means that the distribution of particles within the compression regions becomes much denser, acoustic pressure is higher and maximum particle velocity is greater (Zagzebski et al. 1996). The intensity of ultrasound beam decreases as the beam propagates through tissue.

The intensity of an ultrasound beam is proportional to the square of the pressure amplitude and particle-velocity amplitude. The equation for instantaneous intensity is given by (Hedrick et al. 2005):

$$i(t) = \frac{p(t)^2}{\rho c} \tag{1.5}$$

where *p(t)* is the instantaneous acoustic pressure, *c* is the speed of sound, and ρ is the density. Often the time-averaged intensity is of interest. At any point through which an ultrasound beam passes, the pressure oscillates between high and low values. The greatest deviation from average pressure during a cycle is the maximum pressure or peak-pressure amplitude (P_0). By averaging the instantaneous intensity over one cycle it is possible to find the time-averaged intensity:

$$I = \frac{P0^2}{2\rho c} \tag{1.6}$$

1.7.7 Power

The power (W) of an ultrasound beam is a measure of the total energy transmitted per unit time summed over the entire cross-sectional area of the beam:

$$W = I \times A \tag{1.7}$$

where I represents the intensity and A represents cross-sectional area of the beam.

The emitted power from the transducer assembly is not constant but fluctuates over the wave cycle. Ultrasonic power, averaged over a time period, is referred to as the temporal average power. Unit of power is J/s or Watt.

1.8 History of Ultrasound in Medicine

The development of the mechanisms responsible for ultrasound-induced biological effects is closely linked to the unique history of the development of diagnostic applications in human medicine and the basis for the development of standards (O'Brien et al. 1998). A brief overview of the historical development of ultrasonic biophysics is therefore provided.

More than three decades after the 1880 discovery of the piezoelectric effect by the brothers Paul-Jacques and Pierre Curie (William et al. 2007), a discovery which revolutionized the production and reception of high-frequency sound (ultrasound), the French scientist Paul Langevin developed one of the first uses of ultrasound for underwater echo ranging of submerged objects with a quartz crystal at an approximate frequency of 150 kHz (Hunt et al. 1982). Langevin was, perhaps, the first to observe that ultrasonic energy could have a detrimental effect upon biological material wherein he reported ‘’fish placed in the beam in the

neighborhood of the source operation in a small tank were killed immediately, and certain observers experienced a painful sensation on plunging the hand in this region.'' Langevin also reported observing incipient cavitation in water when the source was active (William et al. 2007).

Another decade passed before a more detailed, experimental study was conducted (Wood et al. 1927) to investigate Langevin's observation. Although the ultrasonic levels were not specified, their experimental studies showed that ultrasonic energy had a range of effects from rupture of Spirogyra (a genus of filamentous, commonly found in freshwater areas (Whitton et al. 2002)) and Paramecium (a group of unicellular ciliate, which are also widespread in freshwater environments (Aury et al. 2006)) to death of small fishes and frogs by a 1-2 minute exposure, the latter also observed by Langevin with a Poulsen arc oscillator (a device that uses an electric arc to convert direct current electrically into radio frequency current (Pinto et al. 1921)).

Ultrasound-induced tissue heating was applied extensively as a therapeutic agent in the 1930s and 1940s. However, while it was clear that ultrasound could effectively heat tissue, and excess enthusiasm resulted in numerous clinical applications being proposed and tried, the inferior clinical experience caused this modality to fall into disfavor.

Also, during the 1930s and 1940s, with an understanding that ultrasound at sufficient levels could have a dramatic effect on tissues, and produce large temperature increases, the potential for ultrasonic surgery was proposed. This ability to non-invasively burn local tissue volumes deep in the body using ultrasound was first proposed in 1942 (Lynn et al. 1942) as a neurosurgery technique. Ultrasound surgery and its biophysical heating mechanism were further

developed in the late 1940s and early 1950s (Fry et al. 1955). Also proposed in 1948 and applied in 1952 was the application of ultrasound surgery to destroy the vestibular function to treat the symptoms of Meniere's disease is human ears (Sjoberg et al. 1963).

During the 1950s and 1960s, the ability to quantify ultrasonic fields improved but only to a limited extent; there were still no widely-accepted ultrasound measurement standards or procedures. All of the improvements dealt with absolute procedures to quantify second-order quantities, and consisted of ultrasonic intensity via thermocouple probe, electro-dynamic method, and ultrasonic power via radiation pressure, calorimetry (Wells et al. 1963) and radiation pressure balance (Hueter et al. 1956).

Until 1950s the scientific community saw only a few advances in the understanding of how ultrasound interacts with biological materials. Perhaps the first major symposium on ''Ultrasound in Biology and Medicine'' was held at the university of Illinois in 1952 to examine phenomena of how ultrasonic energy interacted with and acted upon biological materials. There were scattered reports about ultrasound having an effect on biological systems during this period, however, these reports in general did not deal with the types of exposure that would be expected from ultrasound equipment, nor did they provide any kind of a consistent message.

One interesting observation made in the late 1960s that would wait more than two decades before it would become an active area of basic and clinical research was the identification of the production of cavitation at the tip of catheters when various liquids were injected through the catheter. The cavitation was a primary source of echoes in an echocardiograph image, and the first application of an injected contrast agent was identified (Kremkau et al. 1970).

1.9 Therapeutic Ultrasound

It has been known for some time that ultrasound interacts with tissue to produce biological change. Although there has been natural concern about possible hazard associated with diagnostic ultrasonic imaging, most of the early effort was put into using ultrasonically induced changes in tissue for therapeutic benefit.

Therapeutic ultrasound can be divided into two different classes: at low intensities (time-averaged intensities of less than 3.0 $W.cm^{-2}$, at frequencies of a few megahertz) – the aim is to produce non-destructive heating or other, non-thermal effects and to stimulate or accelerate normal physiological response to injury; at higher intensities (time-averaged intensities of greater than 5 $W.cm^{-2}$) – the aim is rather to produce controlled selective destruction of tissues. The first category includes the majority of physiotherapeutic uses, whereas beam surgery and the use of thermal effects fall into the second class (Hedrick et al. 2005).

High intensity therapeutic ultrasound applications include high intensity focused ultrasound (HIFU), lithotripsy and histotripsy, and low intensity application, encompass sonophoresis, sonoporation, gene therapy and bone healing (Bailey et al. 2003).

For diagnostic applications of ultrasound, exposures are chosen primarily for their ability to give images with good spatial and temporal resolutions, using sufficient pressure amplitude to give an acceptable signal to noise ratio. The aim is to obtain the required diagnostic information without causing biologically significant cellular effects. In contrast, therapeutic applications require that the exposed target tissue undergoes reversible or irreversible change, depending on the goal of the treatment.

In common with diagnostic ultrasound, therapy ultrasound exposures can be described in terms of the acoustic pressure or of the intensity. The description of intensity for pulsed exposures presents some problems. The acoustic pressure in the acoustic field is spatially variant, and the pulsing introduces temporal variation in addition. It is possible to calculate the intensity based on the maximum pressure measured in the field or based on a pressure averaged over a specified area such as, for example, the -3 dB beam width of the pressure profile. When describing the energy delivery, it is also important to distinguish whether the intensity quoted is averaged solely while the pulse is on or has been averaged over a longer time, which includes pulse ‘’on’’ and ‘’off’’ times.

Most ultrasound transducers are made of high power piezo-ceramic such as lead zirconate titanate 4 (PZT4) (Whittingham et al. 1999). Whereas imaging transducers have such a backing which provides the damping required to produce short pulses, therapy transducers are usually air backed. Depending on the application, single element and phased array sources may be used. Frequencies range from 0.02 to 20 MHz, with the choice of frequency being a compromise between the depth of the tissue to be treated, and the requirement for ultrasound absorption within the target to provide heating.

For therapeutic applications, a number of methods are used to couple the ultrasound into the tissue. Where the acoustic window is relatively flat, and the transducer’s emitting surface is plane, aqueous gel may be used between the source’s front face and the skin. However, for awkward tissue geometries and when, for example concave spherical bowl transducers are used, water may provide a better coupling medium. For the high power applications, it is important that the water couplant is degassed to prevent the occurrence of cavitation bubbles.

The main aim of many therapeutic applications of ultrasound is tissue heating. Rising the temperature above normothermic levels by a few degrees may have a number of beneficial physiological effects, such as, for instance, increasing the blood supply to the affected area. The basis of HIFU is that tissues are raised very rapidly to temperatures in excess of 56 degrees Celsius. This leads to instantaneous cell death through cellular coagulation necrosis (ter Haar et al. 2007). Hyperthermia treatments rely on cells being held at temperatures of 43-50 degrees Celsius for times up to an hour. This leads to an inability for the cell to divide. For hyperthermic treatments, heating is usually accompanied by chemo or radiotherapy. The magnitude of the temperature rise depends on the ultrasound intensity, the acoustic absorption coefficient of the exposed tissue, tissue perfusion and the time for which the ultrasound is on.

The more recently emerging therapeutic applications of ultrasound often rely, at least in part, on acoustic cavitation or the action of ultrasonically driven micro-bubbles to deliver their effects (Holt et al. 2001). There is good evidence for example, that the effects of sonophoresis and gene transfection are enhanced in the pressure of bubbles (Hanajiri et al. 2006). Micro-streaming is set up in the fluids around acoustically driven bubbles. This leads to shear stresses on cell membranes in the vicinity, which may create transient pores through which ions and molecules may be transported. In addition, it is now recognized that acoustic cavitation enhances heating (Bailey et al. 2003). This may be used to advantage in HIFU applications.

1.9.1 Sonophoresis

Ultrasound may be used to increase the penetration of pharmacologically active drugs through the skin. This technique is known as sono or phonophoresis (Skauen et al. 1984). The

first indication that ultrasound might enhance transdermal transit of hydrocortisone came in 1954 (Fellinger and Schmidt). Small scale clinical trials have since been carried out on pain relief and inflammatory response (Davick et al. 1988). Attempts to enhance the effect of the topically applied anesthetics lignocaine, lidocaine and xylocaine have shown uncertain results (Becker et al. 2005). Mechanisms by which sonophoresis is achieved are unclear. It is thought that stratum corneum is rendered temporally permeable by acoustic cavitation or streaming, thus allowing the enhanced perfusion (Mitragotri et al. 1995). Low frequencies (less than 100 kHz) appear to be more effective than high, although frequencies up to 16 MHz have been investigated. In contrast to other findings, Bommannan et al. (1992) (William et al. 2007) showed that whereas a 20 min exposure of 0.2 $W.cm^{-2}$, 2 MHz ultrasound had no effect on the transport of salicyclic acid through the skin, 10 and 16 MHz increased it by 4 and 2.5-fold, respectively. Clearly, local heating may be a possibility at the higher frequencies. Meidan et al. (1995) reviewed the subject and could find no trend in ultrasound exposure conditions or structure of molecules and degree of enhancement. Convincing results have been demonstrated when skin was exposed to ultrasound before application of the drug, indicating that it may indeed be changes to the stratum corneum that are important (William et al. 2007).

1.9.2 Sonoporation

Sonoporation is the term used for the phenomenon by which ultrasound may transiently alter the structure of the cellular membrane, and therefore allow enhanced uptake of low and high molecular weight molecules into the cell. There have been a large number of studies in which a synergistic effect between ultrasound and different drugs has been sought. These have

been comprehensively reviewed by Mitragotri (2005) (Mitragotri et al. 2005). Many of the studies reported have been carried out *in vitro*. It should be noted that while effects may be identified in these studies, the mechanisms of action in the aqueous *in vitro* environment, where acoustic cavitation and streaming may predominate and significant amount of heating are not to be expected, may not be relevant when exposures are carried out *in vivo*. Kremkau et al. (1976) showed that mice injected with the L1210 leukaemia cells that had been exposed to ultrasound, survived longer than those challenged with cells that had had no ultrasound exposure. Studies with different drugs showed that 50% of the subjects showed similar enhancement, but no mechanistic pattern was found (Kremkau et al. 1979).

There is a growing body of evidence that cavitation either induced in tissue by the ultrasound exposure or facilitated by micro-bubbles introduced into the tissue, is instrumental in enhancing drug delivery (Unger et al. 2004). The rationale for the use of micro-bubbles is multi-fold. Bubbles increase the local absorption of ultrasound and oscillate or resonate to the pressure field. Depending on the driving parameters and the bubble size, they may break up, releasing a shock wave and creating micro-jets locally.

1.9.3 Gene Therapy

There is considerable interest in facilitating the transfer of genes into diseased tissues and organs. The main aim is to increase the delivery efficiency of exogenous nucleic acid to the intended target (ter Haar et al. 2007). The ideal system would enhance gene expression in the target while having no effect in non-target tissues. Ultrasound might be able to provide this localization. Ultrasound has been shown to enhance gene transfer into cells *in vitro* (Bao et al.

1997). This has also been demonstrated *in vivo* (Bao et al. 1998). Significantly more enhanced transfection is achieved in presence of cavitation (Greenleaf et al. 1998). Enhanced gene transfer is found either when the exposed bubbles are in the vicinity of the genetic material, or when the genes are encapsulated within, or bound to the bubbles. Both strategies have been investigated *in vitro* with certain degree of success (Frenkel et al. 2002) and *in vivo* (Taniyama et al. 2002).

1.9.4 Bone Healing

There is evidence in the literature that while high intensities of ultrasound can damage bone or delay healing (Arden et al. 1957), low intensities can enhance repair rates and reduce healing times (Pilla et al. 1990).

It has been shown experimentally in rat fibulae that when ultrasound exposures are carried out during the inflammatory and early proliferative phases of bone repair following fracture, healing can be accelerated, with direct ossification being observed (ter Haar et al. 2007). If treatment is delayed until the late proliferative phase, it is cartilage growth that is stimulated. 1.5 MHz ultrasound has been found to be more effective than 3 MHz (pulsed 2 ms and 8ms for 5 min) (Dyson and Brookes, 1983). This suggests a non-thermal mechanism of action. Pilla et al. (1990) showed that the strength of fractured rabbit fibulae returned to that of the uninjured bone following osteotomy in 17 days following ultrasound exposure (1.5 MHz, 0.03 $W.cm^{-2}$) whereas it took 28 days for the untreated controls.

There is also a considerable number of other reports that suggests low intensities are effective in stimulating bone repair (Mayr et al. 2001; Heybeli et al. 2002). For example, Heybeli

et al., (2002) reports successful stimulation of fracture repair following five exposures at ‘’diagnostic’’ levels of ultrasound (7.5 MHz; 10 min; 5-day intervals).

In summary, there is experimental and some clinical evidence of the beneficial effects of very low ultrasound intensities on bone repair. However, the mechanisms by which this is produced are unclear, and warrant further study. At these low exposure levels, thermal effect are unlikely to be involved.

1.9.5 Lithotripsy

Since the early 1980s, lithotripsy has been the most common treatment for kidney stones and continues to be the favored method for uncomplicated, upper urinary tract calculi, even with the advent of percutaneous surgical techniques (Watkin et al. 1997). Lithotripters produce short focused microsecond pulses as opposed to a burst of many cycles at a characteristic frequency in HIFU. A common lithotripter waveform at focus point is shown in figure 1.13. Typical peak positive pressure is 20-140 MPa and peak negative pressure is -8 to -15 MPa. A few hundreds of pulses are delivered in a treatment at rates of 1-2 Hz. Higher rates would accelerate treatment but cause more tissue injury. Lithotripters sources are usually tens of centimeters in aperture with F-numbers around one. Acoustic coupling with the patient is achieved through water baths or liquid-filled pillows. Finally, orthopedic applications are driving the development of compact designs (Bailey et al. 2003).

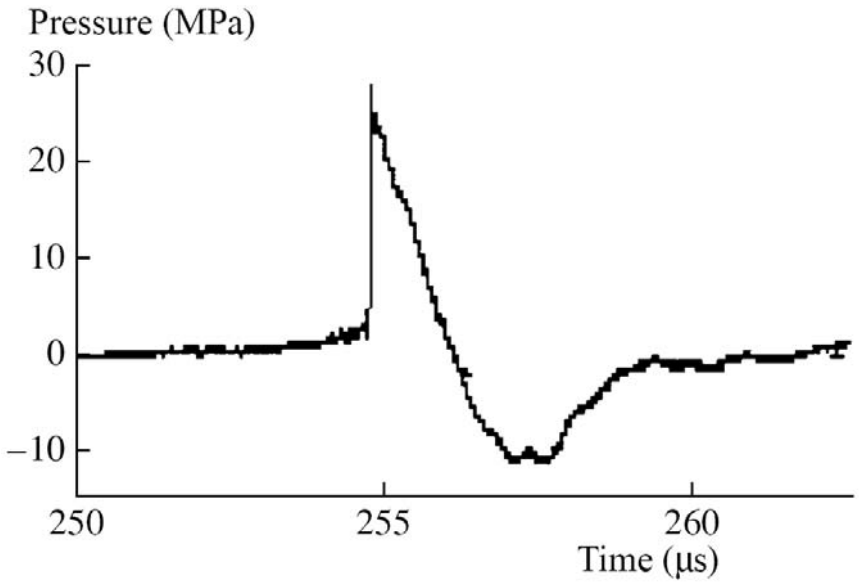

Figure 1.13 – A typical lithotripsy pulse measured at the focus of a lithotripter, peak positive pressures are 20 to 140 MPa with peak negative pressures around -8 to -15 MPa – courtesy of Bailey et al. 2003

1.9.6 Histotripsy

Histotripsy is a noninvasive focused ultrasound technology where energy is delivered extra-corporeally to a target volume within the body (Tavakkoli et al. 1997). Unlike HIFU where thermal coagulative necrosis is induced, histotripsy treatment consists of high amplitude, very short pulses that induce mechanical cavitation with very negligible thermal contribution (Tavakkoli et al. 1997). The cavitational process can be conceptualized as formation, oscillation, and violent collapse of micro-bubbles that results in precise mechanical disruption of tissues at the cellular and sub-cellular level (Cain et al. 2005).

1.9.7 High Intensity Focused Ultrasound (HIFU)

The physical properties of megahertz ultrasound in tissue mean that it can be brought to a tight focus at a distance from its source (ter Haar et al. 2007). This can be used in therapeutic benefit when a focused source is driven at high power. High temperatures can be generated solely within the focal region, with surrounding areas remaining largely unheated. It has been shown that, at 1.7 MHz, when focal peak intensities of 1500 $W.cm^{-2}$ are held for 1-2 s, temperatures in excess of 56 degrees Celsius are achieved in *ex vivo* liver tissue (Tavakkoli et al. 2010). This leads to instantaneous cell death through coagulative necrosis, with a margin of 6-10 cells between live and dead cells at the edge of the focal zone (ter Haar et al. 1995). This is the principle of HIFU.

The first to demonstrate that focused ultrasound beams could produce regions of highly localized biological effect were Lynn and Putnam (1944), Lynn et al. (1942). HIFU was developed for local tissue destruction in the brain by Fry et al. (1955). Burov (1956) was the first to suggest its use for cancer therapy. Early use was made of HIFU in the treatment of Parkinson's disease (Fry et al. 1960) and for a number of ophthalmological problems (Coleman et al., 1985). However the introduction of L-dopa drug for treatment of Parkinsonism, and of lasers for eye surgery inhibited the further development of these applications.

By comparison, HIFU delivers intensities that are 4 to 5 orders of magnitude higher than those used in diagnostic ultrasound imaging systems. HIFU systems can produce acoustic intensities greater than 1000 $W.cm^{-2}$ at the focus, and use frequencies in the range of 0.5-5 MHz. The great advantage of HIFU is that it can focus energy to a small region inside the body without damaging intervening tissue (Foley et al. 2006) (Figure 1.14).

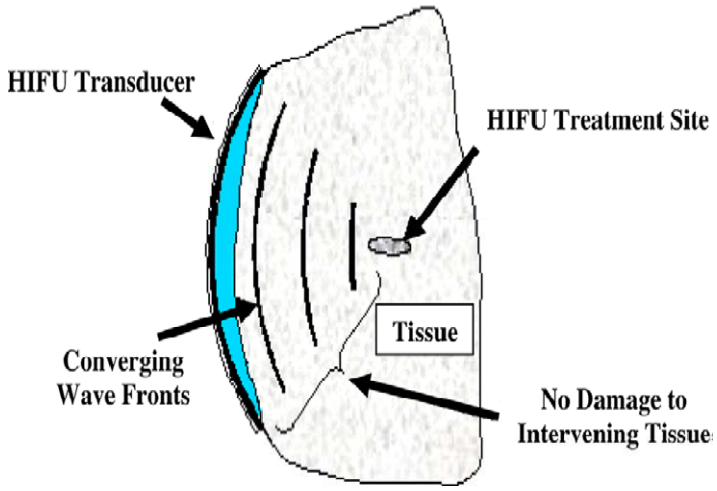

Figure 1.14 – Schematic of HIFU effects on deep tissues – courtesy of Foley et al. 2006

The biological effects of HIFU are dependent upon the specific tissue being treated and the parameter of HIFU operation. Different parameters of HIFU, particularly the intensity of the HIFU beam and the duration of exposure, could result in different effects on a tissue being targeted. HIFU application to a specific structure within the body can be described using the standard treatment parameter of ‘’dose’’. Dose, defined as intensity multiplied by the duration of the exposure [$J.cm^{-2}$], is an important parameter in the production of biological effect during HIFU treatment.

Furthermore, different tissues in the body will absorb different amounts of acoustic energy and therefore, the same HIFU dose may result in different biological effects when applied to a range of tissue types. Absorption coefficients are dependent on the frequency of the acoustic energy and so frequency becomes an important parameter to be considered. Higher frequencies will be absorbed at a greater rate by tissue and will require lower HIFU doses to produce a desired biological effect. The focal dimensions of the HIFU beam are also dependent on the frequency of the acoustic field and higher frequencies produce smaller focal regions. It is thus

important to investigate the role of parameters of dose and frequency in the production of biological effects in the specific tissue of interest, in order to develop the most optimal HIFU systems and treatment protocols. The earliest work with HIFU included investigation of the dose-dependent effect of ultrasound in different tissues including red cells and nerve tissue (ter Haar et al. 2007).

1.10 Applications of HIFU in Neurology and Neurosurgery

Research investigating the applications of focused ultrasound in medicine and biology began over 60 years ago. There was significant development in the early years to use focused ultrasound to produce changes in the central nervous system, particularly the brain (ter Haar et al. 2007), and apply this technology to treat the brains of patients with neurological disorders such as Parkinson's disease; though promising, HIFU was not accepted as a clinical treatment at that time, due in part to the inability to precisely guide and monitor HIFU treatment.

In recent years, with significant advancements in diagnostic ultrasound imaging as well as other imaging modalities, many research groups have begun to investigate the promising therapeutic effects of HIFU. For instance, HIFU integrated with confocal ultrasound image-guidance enables real-time treatment monitoring, including the observation of the hyper-echoic region that develops at the focus during HIFU exposure (Foley et al. 2006). Alternatively, MRI has the capability of monitoring the temperature rise of tissue as HIFU treatment is performed (Gavrilov et al. 1995) which could enable precise control of tissue ablation. Since the inception of HIFU, there have been many exciting areas of technology development and clinical applications within the broad field of acoustic therapy. The most commonly investigated

applications of HIFU have included: necrosis of tumors, coagulation of bleeding, and treatments of various urological and gynecological disorders (Foley et al. 2006). For instance, HIFU targeted to the site of a tumor produces heat that can result in coagulative necrosis of death of the tumor cells. Additional mechanical effects of the acoustic energy can produce further biological changes such as cell disruption or production of pores in biological membranes. Furthermore, the application of HIFU therapy to treat neurological disorders has been of interest for years and has begun to mature into a promising area of ultrasound research.

In the last 50 years, several groups of researchers have shown interest in the development of therapeutic ultrasound devices to treat neurological disorders. Many works investigated the use of focused ultrasound to lesion selective areas of the brain such as those that could be responsible for the development of hyper-kinesias in Parkinsonian patients (ter Haar et al. 2007). Meyers et al. treated 41 patients with either Parkinsonian symptoms or interact-able pain using such selective lesioning; for most patients, the treatment was successful in temporarily alleviating their symptoms (ter Haar et al. 2007). Although this treatment was promising, the invasiveness of the procedure and the difficulties in control of the treatment resulted in postponement of adoption of the technology clinically. In recent years there has been a renewed interest in using focused ultrasound to treat neurological disorders due to improved imaging modalities for guidance and monitoring and new advancements in HIFU transducer technology.

There have been several studies that have used electrophysiological methods to investigate the effects of ultrasound on action potentials in the brain, spinal cord, and peripheral nerves (Wang et al. 2005). Most of these studies have been *ex vivo* investigations. They have demonstrated that focused ultrasound at intensities above 1000 $W.cm^{-2}$ can be used to block axonal conduction in nerves, either reversibly or irreversible, dependent on the dose of HIFU

application (Foley et al. 2006). For example, Young and Henneman exposed *ex vivo* frog sciatic nerves to 2.7 MHz focused ultrasound and observed changes to the size and shape of evoked potentials in the nerves (Foley et al. 2006). At doses above 23,000 $J.cm^{-2}$ (1150 $W.cm^{-2}$, 20 s exposure) the evoked potentials (an electrical response recorded from the nervous system of a human, detected by EEG (Electroencephalography) or EMG (Electromyography)) were completely suppressed, whereas at doses below 4600 $J.cm^{-2}$ (1150 $W.cm^{-2}$, 4 s exposure) no effects on conduction were observed. At intermediate HIFU doses, variable effects on evoked potentials were dependent upon the size of the nerve fibers in addition to the dose; higher doses were required to block bigger fibers as compared to smaller fibers.

A similar study by Takagi et al. investigated the effects of 1 MHz focused ultrasound on the electrical excitability of *ex vivo* myelinated frog nerves. Results indicated that the evoked potentials were enlarged 10 to 30% after application of ultrasound with dose of 1920 $J.cm^{-2}$ (16 $W.cm^{-2}$, 2 min exposure) (Takagi et al. 1960). When the dose was increased to above 4200 $J.cm^{-2}$ (35 $W.cm^{-2}$, 2 min exposure) however, the evoked potentials were inhibited, but not completely suppressed. These results suggest that there are dose-dependent effects of ultrasound on nerves that could possibly be used to produce a range of biological effects.

Mihran et al. exposed *ex vivo* myelinated frog sciatic nerves to single, short-duration and low-energy pulses of 2 MHz focused ultrasound (100-800 $W.cm^{-2}$) (Mihran et al. 1990). This level of ultrasound exposure altered the amplitude of evoked potentials in the nerve that remained until 50 ms after cessation of the ultrasound pulse. Both enhancement and suppression of the nerve excitability were observed, however, the low doses of ultrasound produced only transient changes.

Young and Henneman (1961) studied isolated frog nerves and demonstrated reversible and irreversible block in nerves that were placed in a groove made of a sound absorbing rubber. A 2.7 MHz frequency at exposure times of 2-3 s was used. In surgically-exposed cat spinal cord, reversible effects of reflexes were also induced by 3 to 300 bursts with a frequency of 2.7 MHz sonication (Hynynen et al. 2009).

The specific electrophysiological studies mentioned here have shown that ultrasound can have variable effects on neural structures (Foley et al. 2006). Suppression of action potentials suggests that ultrasound could potentially be used to block conduction in nerves, including peripheral nerves involved in spasticity and pain. The *ex vivo* conditions of previous studies however have not enabled investigation of the effects of such suppression of nerve action potentials on the ability of the nerves to stimulate muscle contraction. Furthermore, the variance of the quantified effects on evoked potentials (An evoked potential (or "evoked response") is an electrical potential recorded from the brainstem or cerebral cortex of a human or other animal following presentation of a stimulus) (Foley et al. 2006). seems to indicate a possibility that ultrasound could play a role in producing variable biological effects ranging from partial conduction block to complete block, and from reversible conduction block to irreversible axon degeneration.

Extending such electrophysiological investigations to *in vivo* models and also studying the effects of focused ultrasound on the function of neurological tissues must be addressed in order to ultimately use this technology for clinical procedures. Foley et al. have used ultrasound-guided HIFU to selectively target and block sciatic nerves of rabbits (Foley et al. 2007). The device included a 3.2 MHz spherically curved transducer with an intra-operative imaging probe such that the HIFU focus was within the image plane. The sciatic nerve of rabbits was imaged in

cross-section and identified between two muscle planes, and the HIFU treatment was directed to the nerve, using a scanning method the entire nerve was monitored in real time. *In situ* acoustic intensity of 1480-1850 $W.cm^{-2}$ were applied to nerves for 36 s (53280-66600 $J.cm^{-2}$), which resulted in complete conduction block of the nerves in 22 rabbit legs. Lesions on the nerve at the HIFU treatment site appeared blanched, suggesting coagulative necrosis of the nerve.

These studies indicate the use of HIFU for producing selective suppression of nerve function, which could potentially be used to minimize conditions of spasticity that are often associated with disorders of the central nervous system including multiple sclerosis, stroke and traumatic injury to the brain or spinal cord (Foley et al. 2007).

Another recent investigation showed a permanent nerve block created by thermally coagulating a rabbit sciatic nerve in an *in vivo* study by Foley et al. (2004). A 3.2 MHz transducer was used with 30 s of sonication (57000 $J.cm^{-2}$). Persistence of the block occurred with repeated 5 s sonications at the intensity of 1.9 $kW.cm^{-2}$ (Foley et al., 2004). Therefore, this can be used a proof that HIFU exposure can permanently block mammalian nerves.

Yu et al. (2008) used an electrophysiological method to investigate the time-dependent effect of focused ultrasound on the conduction properties of toad's sciatic nerve. It was noticed that focused ultrasound could make the CAPs descend significantly and rapidly after a short time (26s) of radiation (a 1.2 MHz single element transducer with an electric power of 180 W) (Figure 1.15). However, before the nerve was totally damaged, the CAPs had some recoverability once focused ultrasound was stopped (Yu et al. 2008).

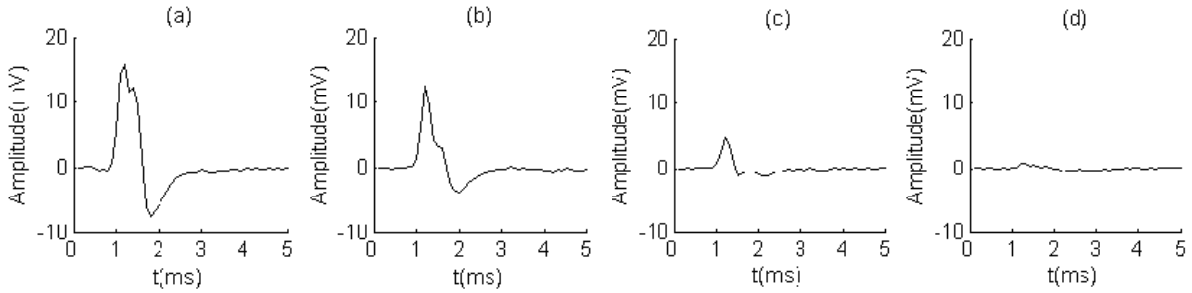

Figure 1.15 – 4 segments of one CAP during conduction suppression under focused ultrasound – Showing a decrease in the CAP amplitude from (a) to (d) – courtesy of Yu et al. 2008

In a more recent study, Hynynen et al. (2009) performed an *in vitro* study (Figure 1.16) to further extend the knowledge of potential use of HIFU on nerves. The sciatic nerves from the bullfrog were subjected to focused ultrasound with frequencies of 0.661 and 1.986 MHz (acoustic power of 16 W). The nerve compound action potential was shown to decrease in the experiments and correlated with temperature elevation measured in the nerve.

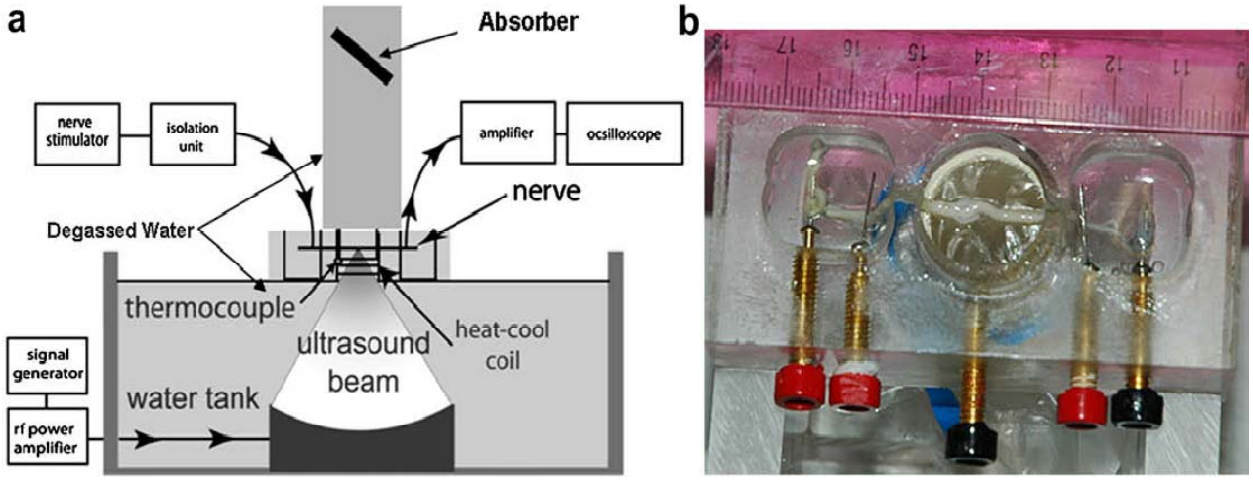

Figure 1.16 –Experimental set-up used by Hynynen et al. (2009); a; Schematic vertical cross section of the sonication set-up, b; Photograph of the nerve chamber – courtesy of Hynynen et al. 2009

The compound action potential recovered either completely, partially or not at all, depending on the parameters of the ultrasound exposure. A detectable reduction in the action potential was induced with both frequencies at an intensity of 200 $W.cm^{-2}$ with reducing signal as a function of increasing intensity. For both frequencies, the action potential amplitude was halved at 350 $W.cm^{-2}$. There was also a residual action potential up to 575 and 875 $W.cm^{-2}$ at the low and high frequency, respectively.

As shown in figure 1.17 the CAP amplitudes decreased significantly over time after the sonication. CAP baseline measurement is showing the biggest amplitude, while waiting 1, 2 and 3 minutes after the exposure is decreasing this value.

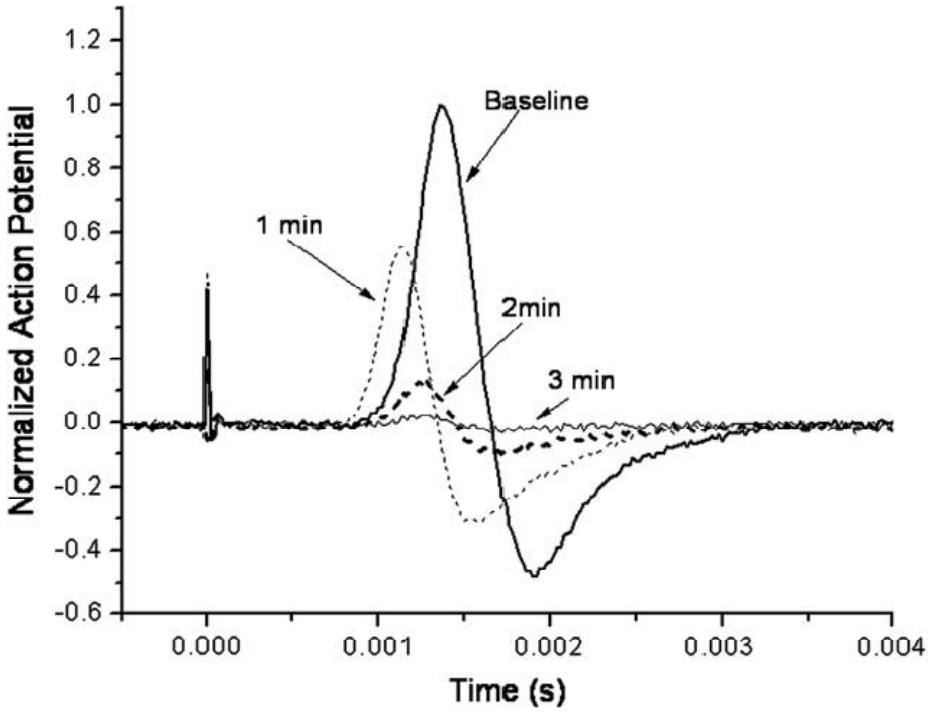

Figure 1.17 – An example of the reduction of the action potential after a 30 s sonication at the frequency of 0.661 MHz – A CAP baseline is measured, the CAP is also measured after 1, 2 and 3 minutes after the sonication – courtesy of Hynynen et al. 2009

In this study, the reduction of the baseline nerve temperature by circulating cooling fluid through the sonication chamber did not prevent the collapse of the nerve action potential; however, higher power was required to induce the same endpoint as without cooling (Hynynen et al. 2009). These results indicated that a thermal mechanism of focused ultrasound can be used to block nerve conduction, either temporarily or permanently.

1.11 Hypothesis of the Research Work

The hypothesis of the research work is that controlled changes in neural tissues and structures are achievable by using different parameters (intensity, frequency, exposure duration, and duty cycle) in HIFU systems.

To test the above hypothesis a series of experiments based on an animal *in vitro* nerve model (lobster abdominal nerve) was designed. Changes in the neural compound action potential (CAP) values caused by the HIFU exposure were used as an indicator to changes in nerve functionality.

Chapter 2 Materials and Methods

2.1 HIFU Transducer

A handheld HIFU transducer was used in this project. The transducer had a spherical concave geometry with radius of curvature of 120 mm and aperture diameter of 50 mm (F number of 2.4 – F number is defined as the focal length divided by transducer diameter) (Figure 2.1). The resonance frequency of the transducer was 1.94 MHz. The transducer was connected to a Plexiglass (methyl methacrylate) nose that accommodates degassed water and had a height of 117 mm (Figure 2.2); making it easier to target the nerve right at the focal point. Once the nose piece was connected to the transducer and was filled with water, an ultrasound-transparent Mylar sheet (polyester film) of thickness 0.025 mm covered at the top; making an interface to couple the transducer to the tissue.

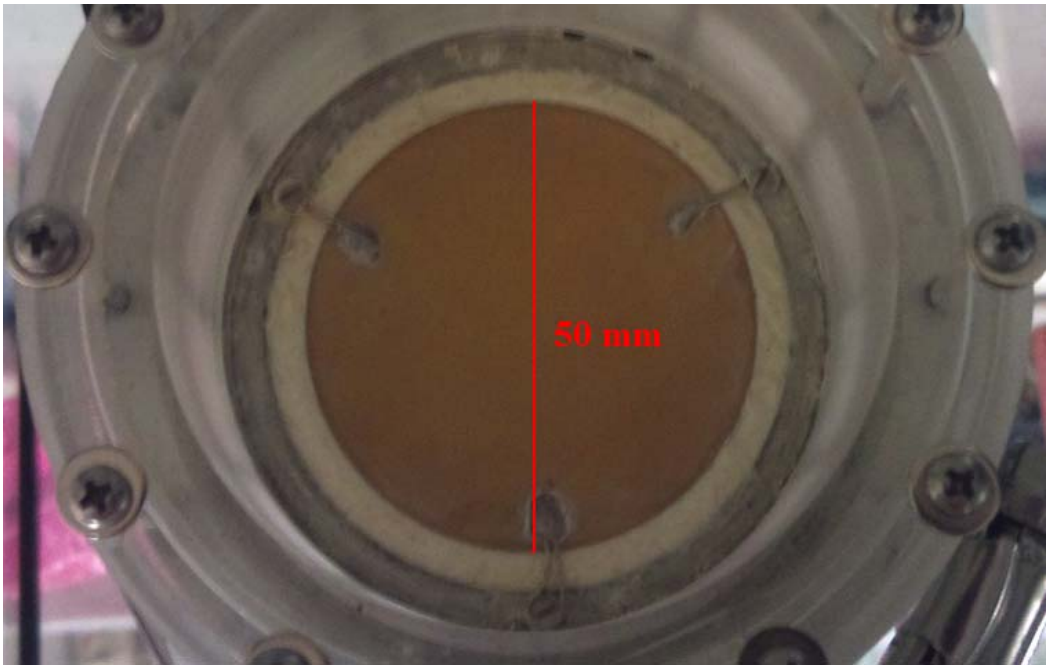

Figure 2.1 – Geometry for the surface of HIFU transducer

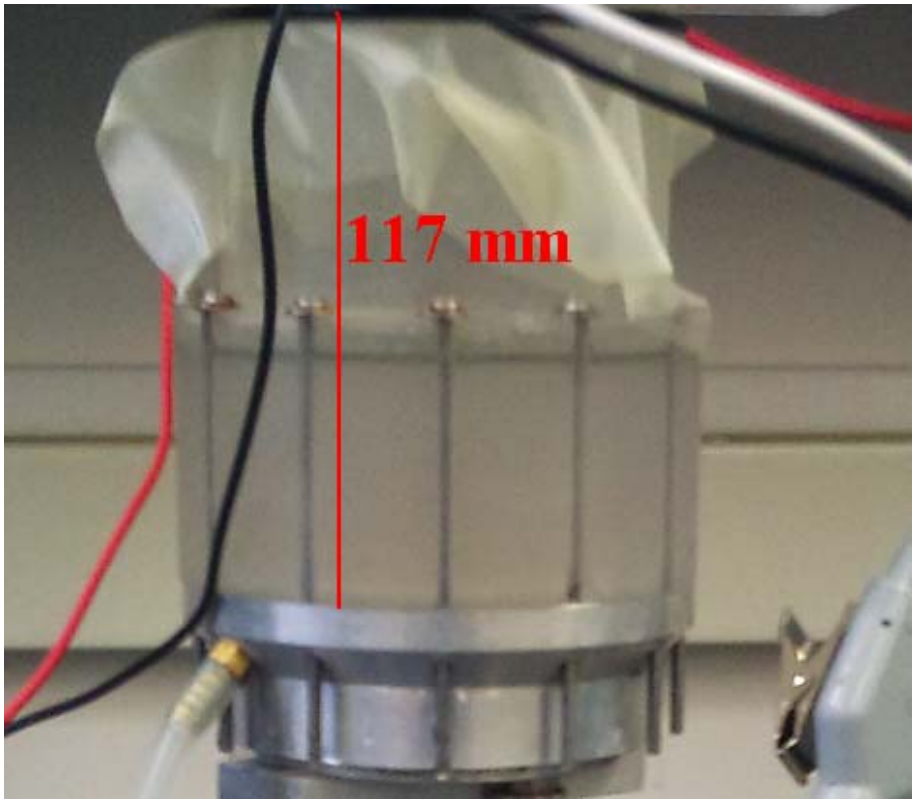

Figure 2.2 – Geometry for the HIFU Plexiglass nose

2.1.1 Characterization of the HIFU Transducer

2.1.2 Ultrasound Field Simulations

The ultrasound field is simulated using an approximate expression for the sound pressure amplitude; p_0, at a point, when the transmitting element is a small rectangle of size Δw by Δh surrounded by a plane rigid baffle. The array elements are divided into small rectangular sub-elements for which the approximation holds, and the computed complex pressures are summed up in order to get the pressure at all the elements (Zemp et al. 2000). The pressure equation used here is:

$$Po = \frac{j\rho c \Delta w \Delta h \exp(-(\alpha + jk)R)}{\lambda R} sinc\left(\frac{kx' \Delta w}{2R}\right) sinc\left(\frac{ky' \Delta h}{2R}\right) \quad (2.1)$$

where ρ is density of the medium, c is speed of sound, Δw is width of the element, Δh is height of the element, α is the attenuation coefficient, k is wave number, and R is the radial distance from the centre of the element to the point at which the pressure is being computed (Figure 2.3).

The coordinate values *x'*, *y'* and *z'* are in a coordinate system based on the element orientation, where the x direction is determined by the edge of the element having dimension Δw, and the y direction is determined by the edge of the element having dimension Δh, and the origin of the coordinate system is based on the centre of the small element.

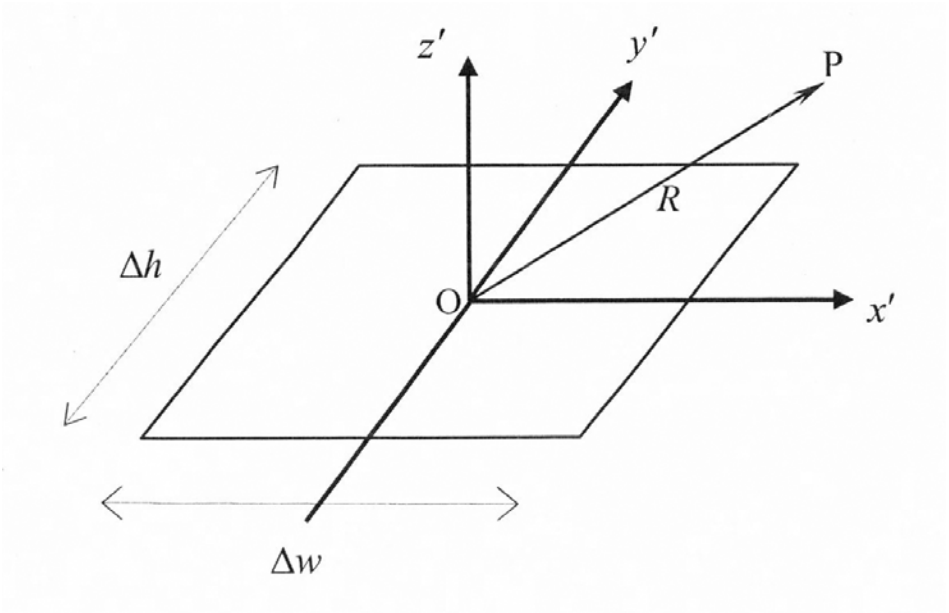

Figure 2.3 – Definition of parameters used in formula (2.1)

The field simulation program also converts the computed pressure values to intensity values, using the equation (1.6) given in chapter 1.

The field simulation program used in this study is a full 3D model in which all the parameters pertinent to the source and the propagation medium are input to the model and the resulting 3D intensity field is the output from the model. Ultrasound field simulation of the HIFU transducer will be presented in the next chapter.

2.2 Total Acoustic Power (TAP) Measurements

During the past decades, high power ultrasound transducers have found many applications in medicine and industry (Wells et al. 1992). Apart from some traditional industrial applications, such as ultrasonic cleaning, ultrasonic plastics soldering and metal welding, some new and promising medical applications of high power ultrasonics, such as sonochemistry and ultrasonic therapy have also received more and more attention (Campos-Pozuelo et al. 1996).

In the case of high power ultrasonic energy applications, the vibrational characteristics of a transducer used are essential for the optimized design and safe work of the system. The measurement of these characteristics of the transducer is vital for the evaluation of the transducer performance and the practical process the transducer is involved in. Some of these characteristic include the output acoustic power, the electro-acoustic efficiency, intensity and the temperature rise.

Measurement of power output levels of these high power ultrasonic transducers is very important to determine exact exposure levels in order to have accurate results. Two different acoustic power measurement systems will be used to measure the output TAP of the HIFU transducer used in this study: an Ohmic power meter and an Onda radiation force balance.

2.2.1 Ohmic Radiation Force Balance Power Meter

Ohmic power meter model UPM-DT-100AV (Ohmic Instruments Co., Maryland, USA), is designed to measure the ultrasound power output of diagnostic and therapeutic transducers up to 30 watts acoustic. The Ohmic power meter is shown in figure 2.4. These series of power meters have been in use worldwide since 1986 and conform to the testing guidelines recommended by FDA (Food and Drug Administration), JCAHO (Joint Commission for the Accreditation of Hospitals and Healthcare Organizations), AAMI (Association for the Advancement of Medical Instrumentation) and AIUM (The American Institute of Ultrasound in Medicine).

Figure 2.4 – Ohmic Ultrasound Power Meter – UPM-DT-100AV – courtesy of Ohmic Instruments Co.

The most reliable and repeatable means of measuring ultrasound power is the radiation force balance method. The transducer was centered above a 45 degrees air-backed aluminum cone target in water media, which is linked to a precision balance capable of resolving 1.0 mg. When acoustic energy is applied to the cone, the resultant force exerted on the load cell of the balance is directly proportional to the total radiated power. The test tank wall was covered with sonic absorbent rubber to prevent power reflection. The balance was calibrated to convert milli-Newton magnitude forces directly to readouts in watts with resolution of 0.002 watt. Verification of the system was easily accomplished by placing a calibrated weight on the arm of the target cone.

Small variations of water surface motion, air currents in the test room, or mechanical vibrations may cause uncertainties in power measurements. Therefore, any mechanical and air movements should be avoided while making power measurements.

As mentioned earlier, the measurements are to be performed in de-gassed water, since ultrasound propagation in water closely approximates the propagation of an ultrasound beam in tissues with the exception of the effect of attenuation. The use of water also prevents measurement in a more highly attenuating material such as tissue-mimicking gels from representing the highest possible intensities which might be encountered in the body. Water temperature can also affect accuracy of the power measurements. Therefore it is recommended to perform the measurement in a temperature of 21 to 27 degrees Celsius ambient (Lin et al. 1999). Measurement should be limited to a few minutes since prolonged testing, particularly at higher power levels, will drive out dissolved air and air bubbles will be visible on surfaces in the tank – gently brushing off these bubbles is also recommended.

The transducer should be positioned above the cone target. Various positions above the cone target should be tried in order to obtain a stable power reading from the system.

2.2.2 Onda Radiation Force Balance Power Meter

The Onda radiation force balance power meter (RFB-2000) (Onda Instruments Co., California, USA) is designed especially for easy ultrasound power measurements on medical ultrasound devices, especially for high power therapeutic devices. The RFB-2000 carries the feature of automatic temperature correction as well as accommodating variety of targets. The device operates with a personal computer (PC) that makes the calibration of the system easy and accurate. This system comes with two targets; cone and brush target, each allowing acoustic power ranges up to 30W and 100W, respectively. The Onda RFB-2000 system is illustrated in the figure 2.5.

Figure 2.5 – Onda RFB-2000 system – Showing Radiation force balance, Vacuum lid for in-tank degassing and Brush target for HIFU measurements – courtesy of Onda Instruments Co.

The RFB-2000 system also carries the degassing feature to prepare degassed water to be used with the cone/brush target. Once the transducer is adjusted and placed in the right position; calibrating the system can start. The tank of the RFB-2000 was connected to a generator system via a sensor cable as shown in figure 2.6. The RFB-2000 controlling program ran on a PC which communicated with the generator system by means of a USB cable. Once all the initial connections were made the acoustic power measurements for the desired transducer were detected.

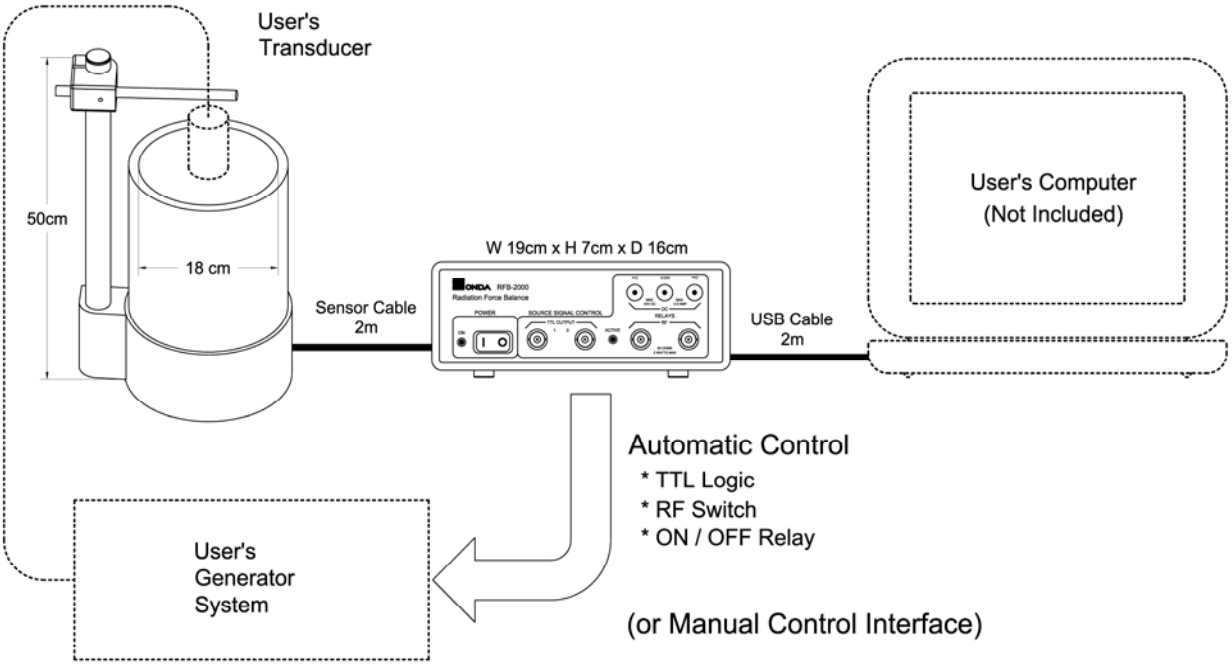

Figure 2.6 – Onda RFB-2000 – Showing a diagram of the system and its connections – courtesy of Onda Instruments Co.

As mentioned in chapter one, sound is a form of energy that sets the particles in the isonated medium into vibrational motion. The particles then possess a kinetic energy. If dP_m is

the rate of the flow of this energy about an area of *dA*, then the mean acoustic intensity will be calculated as:

$$I = \frac{dPm}{dA} \tag{2.2}$$

When a plane sound wave propagates through a uniform non-absorbent medium (such as water); the intensity must be the same for all points in the wave. When the sound energy passes through a unit cross-sectional area with a speed *c*, the intensity is:

$$I = cE \tag{2.3}$$

where *E* represents the energy density per volume in $Js.cm^{-3}$.

The radiation pressure effect can be explained by analogy to the application of an alternating electric voltage to a non-linear load (Ohmic Instruments Co. 2005). With the non-linear load it appears that both AC and DC components are present. In an ultrasonic field the non-linear element is the density of the fluid and hence acoustic impedance (load) varies in the same periodical manner as the density. Therefore, in ultrasound the two components of pressure, one alternating and the other direct present. The average AC pressure per cycle is zero, but the DC pressure of radiation is:

$$P\tau = I/c \tag{2.4}$$

where *I* is intensity and *c* represents speed of sound.

Therefore, from the above two equations, the pressure of radiation ($P\tau$) is equal to the energy density (*E*).

$$P\tau = E \tag{2.5}$$

It is this DC pressure of radiation that can be measured. At low frequencies, below 100 kHz, a standard high frequency acoustic microphone can be used. For higher frequencies however, generally used in medical applications, 1-15 MHz, hydrophones are used. At these frequencies the ultrasound radiation force can be measured using a precision balance and a radiation force target that is perfectly absorptive. The conversion from force to power can be accomplished using the equation:

$$p = Fgc \tag{2.6}$$

where F is the measured force, g is acceleration in dynes, c is the velocity of sound and p is power in J/s. At last, by combining all constants together and converting from J/s to Watts, a simplified equation that is used to calculate the ultrasonic power once the force is measured can be written as:

$$P = 14.65F \tag{2.7}$$

where P stands for the ultrasonic power in Watts, while F represents the ultrasonic force in grams.

2.3 Biopac Electro-physiology System

In this section we will describe a specialized electro-physiology system used to stimulate and record Compound Action Potential (CAP) from a dissected nerve (Biopac system, MP36, Biopac Systems, Inc., CA, USA). The Biopac system comes with different parts that are each

tailored for specific physiological signal measurements. Each application needs certain software and a number of different connecting cables (such as Stroke Volume, Force, Pulse and Autonomic Nervous System). The system used in this study was equipped with a specialized software and cables/connectors that allowed one to measure CAP waveforms, conduction velocity and record the effect on the ability of the nerve to conduct impulses before and after the application of HIFU energy. In order to stimulate the nerve and record CAP waveforms, specific knowledge about the software and the hardware of the Biopac system is needed.

2.3.1 Biopac System Hardware

The Biopac system hardware comprises of data acquisition unit (MP36), SS58L low-voltage stimulator, nerve conduction chamber, stimulator to nerve chamber, BNC adapter cable, BSLCBL1 banana plug or BSLCBL2A 2mm banana plug and nerve response recording cable, and 2mm banana plug (BSLCBL3A or BSLCBL4B), all shown in figure 2.7.

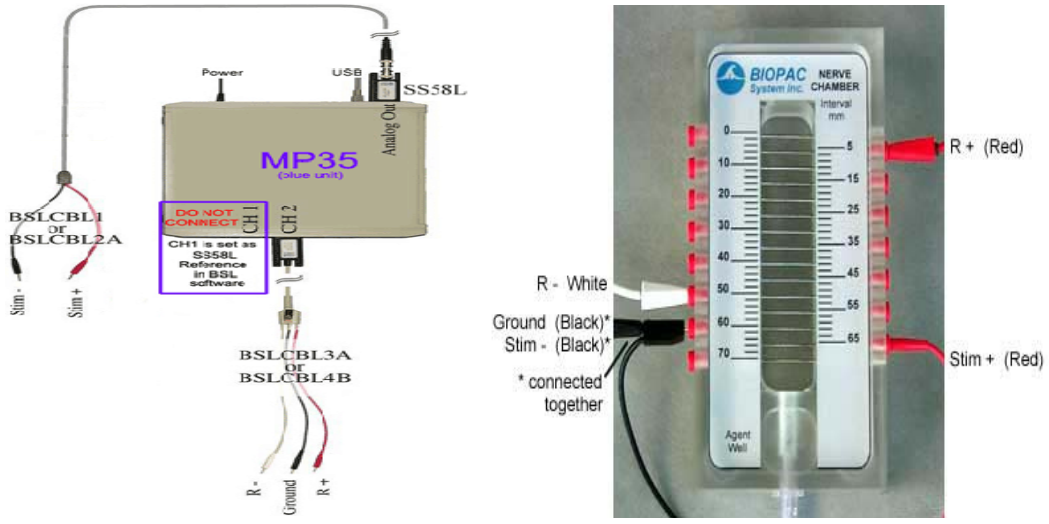

Figure 2.7 – Biopac System Hardware and a Biopac Nerve Chamber – courtesy of Biopac Systems, Inc.

There are many different types of nerve chambers that the Biopac system can work with. There are certain rules of cable connection that are common for all of them, therefore it is necessary to have the ability to connect them accordingly resulting in accurate and desired measurements. In figure 2.7, R denotes the recording cable (BSLCBL3A or BSLCBL4B). The Ground cable is the black lead of the recording cable. The Ground leads of the recording cable and stimulator cable (Black, Stim-) should be connected to the same point on the nerve chamber. As mentioned earlier, any nerve chamber can be used for CAP measurements as long as these sets of connection rules have been followed. Furthermore, the positive response lead (Red, R+) must be positioned further from the stimulator leads than the negative response lead (White, R-) (Figure 2.8), however, both may be positioned on the same side of the nerve chamber being used to accommodate the dissected nerve.

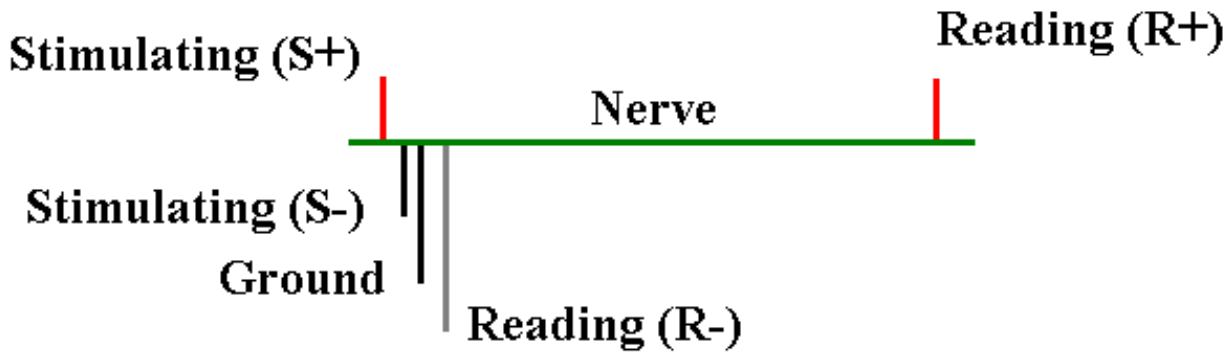

Figure 2.8 – A diagram showing the nerve and all cable connections

It is very important to have a good electrical connection between the BSL leads and the nerve chamber. If there is corrosion on any lead or socket, it must be cleaned off prior to the beginning of the measurement process. It is also crucial to have a tight fit between the lead and

the socket to ensure good electrical connection. It is also essential to have a good electrical connection between the nerve and the wires of the chamber, therefore, it is recommended to lightly abrade the top of the nerve chamber wires with an abrasive pad, and then clean them with alcohol before each experiment session. Placing the dissected nerve on the wires follows sets of rules itself, which will be discussed in the upcoming sections.

2.3.2 Biopac System Software

The Biopac system comes with user-friendly software (BSL PRO 3.6.6). This software is upgradable which enables the user to have a broad use involving various applications. As mentioned earlier, the Biopac MP36 is an integrated unit which comes with a low voltage stimulator, allowing it to have voltages in the range of -10 to +10 Volts. The Biopac stimulator window is shown in the figure 2.9.

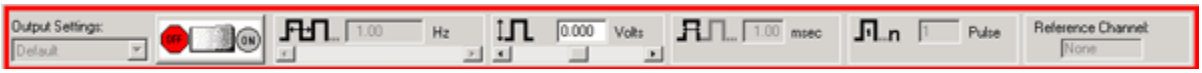

Figure 2.9 – Biopac Stimulator Window – Enabling the user to change the frequency, voltage and on and off time of the pulses sent to the nerve – courtesy of Biopac Systems, Inc.

The Biopac is a complete system for acquiring almost any form of physiological signals. As mentioned before, this system can perform a range of recording tasks, from high speed acquisition (up to 100,000 samples/sec) to long duration acquisitions. Some of the features of this system which become very handy and useful in analyzing the data obtained from any measurements are; output control panels, segment overlap, marker controls, digital channels recording, rewind, horizontal scale, standard curve, data selection and display enhancements.

This Biopac software performs two basic functions; acquisition and analysis as well as controlling the frequency, voltage and on and off time of the signals sent to the nerve. The acquisition settings determine the basic nature of the data to be collected, such as the amount of time and rate of collection, while other commands pertain to analysis functions such as viewing, editing and transforming data. The latest version of the Biopac software gives the user the ability to change the scaling, zooming in and out in order to get the best reading and measuring possible. A simple change of scaling and settings of the Biopac software can be seen in figure 2.10.

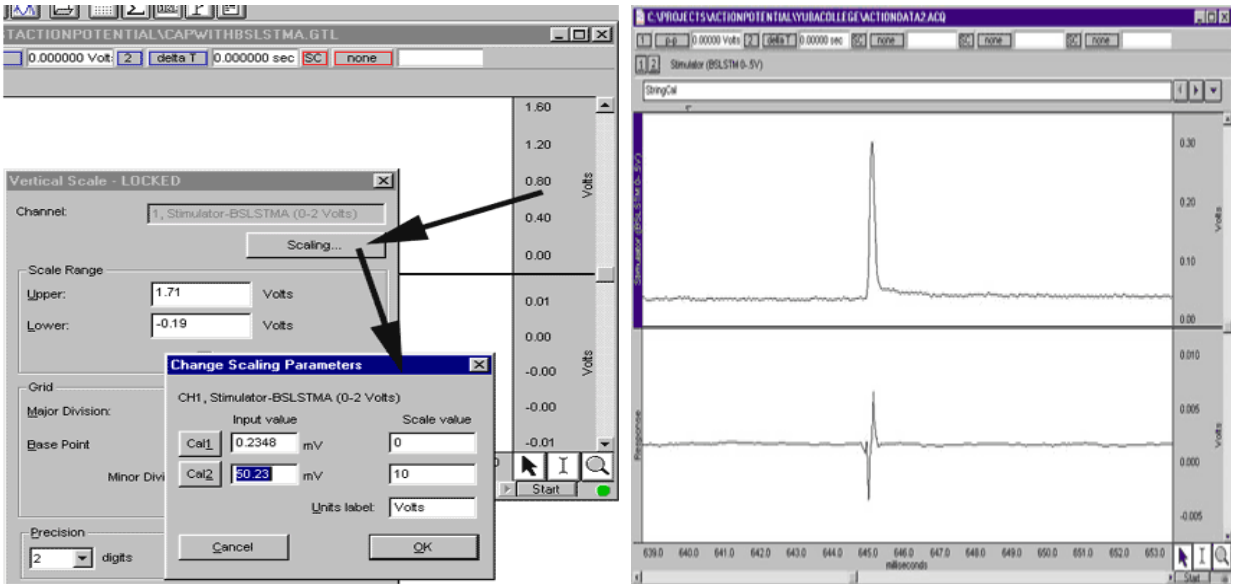

Figure 2.10 – Biopac Software – Change of scaling parameters and a stimulating pulse + CAP – courtesy of Biopac Systems, Inc.

Using the Biopac PRO software for CAP measurements will require having two different channels, one belonging to the stimulating pulse, and one showing the actual CAP waveform. Along with the CAP signal, the system always picks up an electrical artifact one needs to be careful in order to recognize the electrical artifact that is being created before the actual CAP

signal. The difference between the two is shown in figure 2.11. The artifact is a result of electrical coupling between the stimulating and recording electrodes. The size of the artifact is also affected by the geometrical arrangement of the stimulating and recording electrodes. The lengths of unshielded wires should be kept as small as possible in order to get the smallest stimulus artifact possible. Electrical current can flow across the nerve, so a response voltage can be measured. This is identical to what happens when stimulus voltage is applied to the outside of the nerve. This also initiates an electrochemical response once it has made the connection with a dissected nerve. This software also allows the user to increase the sampling rate, change the range of voltages being sent out and also alter the duration and frequency of the stimulating pulses.

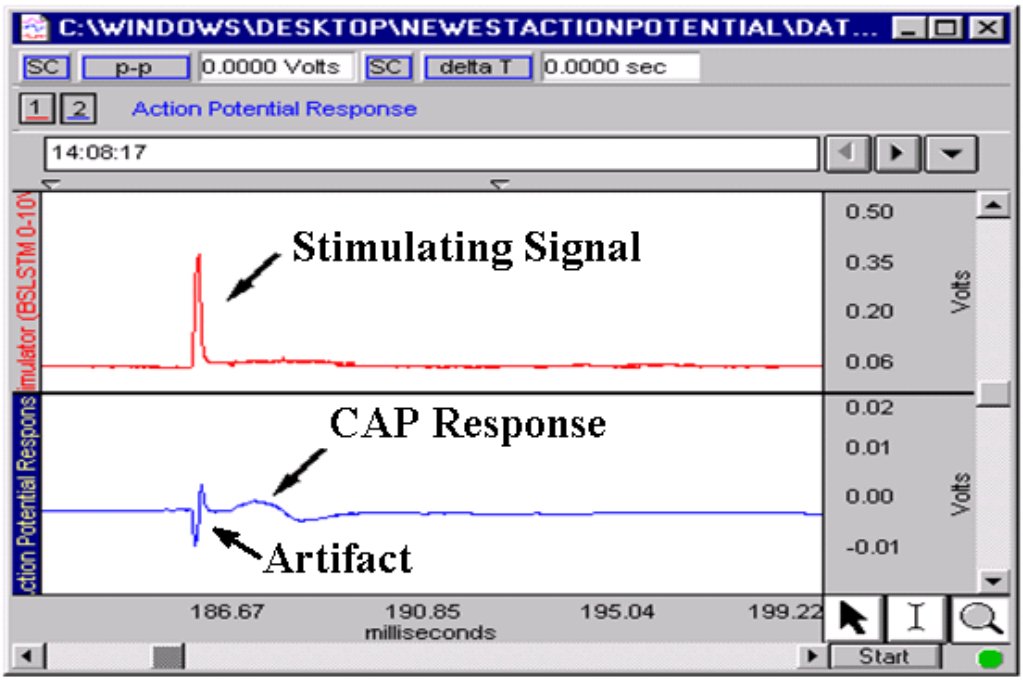

Figure 2.11 – Biopac Software showing CAP – A close look at the stimulating signal, an artifact and a real CAP – courtesy of Biopac Systems, Inc.

2.4 Nerve and Nerve Chamber

The Biopac nerve chamber and its cables are illustrated in figure 2.12. A nerve placed on the nerve chamber is also shown in the figure.

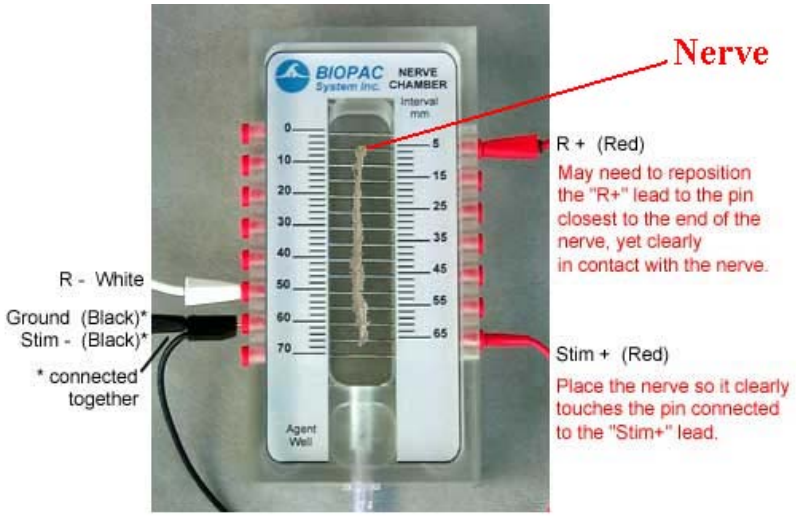

Figure 2.12 – The Biopac nerve chamber with a nerve placed in it– courtesy of Biopac Systems, Inc.

It is vital for the dissected nerve to have a good electrical connection with the wires of the nerve chamber being used. Therefore, the stimulus should be off when the nerve is being placed on these wires. The nerve should be kept moist at all times, while it is being laid over the silver wires in the nerve chamber with the large end of the nerve over the closely spaced stimulating electrodes. If a thread is being used to carry the nerve, it needs to be extended so that the nerve comes to its original length while sitting on the wires. A small drop of Ringer's solution should be laid at each electrode-nerve crossing to ensure electrical connection. Extra care should be taken not to short-circuit the electrodes by putting excessive amount of Ringer's solution. Once the nerve is securely sitting on the wires of the nerve chamber, the measurements of CAP can be

started. The three closely-spaced electrodes (two stimulating electrodes and one ground) are used for electrically stimulating the nerve, while the remaining two electrodes are used for recording.

2.5 Lobster Nerve Ringer's Solution

Lobster nerve Ringer's solution approximates the ionic composition of the extra-cellular fluids of the lobster, and a nerve bathed in Ringer's solution can remain electrically responsive for hours. The predominate ions in Ringer's solution are Na^+ and Cl^-, which are typical for normal extra-cellular fluids. Lobster Ringer's solution contains both NaCl and KCl, so that the solution has the same osmolarity as the other solutions being used for different types of nerves. As mentioned before, it is vital to use lobster nerve Ringer's solution in order to make the nerve conductive and also to provide nutrients and ions required for optimum CAP response (Hynynen et al. 2009). Throughout the dissection and the course of the experiment, the lobster nerve should be kept moist in Ringer's solution. There are different compositions of bathing solutions for each type of nerve; therefore, the right solution needs to be chosen for the desired nerve. Table 2.1 is listing all the ingredients and their concentration for making the lobster Ringer's solution (Biological Bulletin Publications).

Ingredients	NaCl	KCl	CaCl2	MgCl2	Hydroxymethyl	Maleic Acid	Glucose
Concentration	462 mM	16 mM	26 mM	8 mM	10 mM	10 mM	11 mM

Table 2.1 – Lobster Ringer's Solution – Ingredients and their concentration – courtesy of Biological Bulletin Publications

The solution used in this study was made in the lab. Distilled water was used in mixing the ingredients since no extra ions are needed. The ingredients are added one by one to the distilled water while continuously stirring the solution, as each dissolves the next ingredient should be added. CaCl2 seems to not dissolve if added too early to the solution, this might be pH related, and therefore it is recommended for this ingredient to be added last into the mix.

2.6 Lobster Nerve

Dissection of the nerve from the animal should be performed with extra care since they have strong reactions, therefore, placing the lobster in the freezer for 5 to 10 minutes prior to dissection is highly recommended. This action will calm the animal's nervous system down, giving it much slower reaction and movements. Once the lobster is taken out of the freezer the head should be cut off immediately. Next step would be removing the tail (abdomen) from the thorax by cutting around the joint (seam) connecting these two parts. The anatomy of lobster is shown in the figure 2.13. The tail needs to be pinned down with the ventral surface up in the preparation dish giving the possibility to work on the abdominal part of the animal. All the swimmerets need to be removed, while one pin is pushed down through the shell in the first abdominal segment and another pin through the telson (tail-fan) (Brusca, 2003). The tails needs to be held in order to make a longitudinal cut along each side of the abdomen to loosen the ventral shell from the dorsal shell. The tail swimmerets may be left attached to the dorsal exoskeleton.

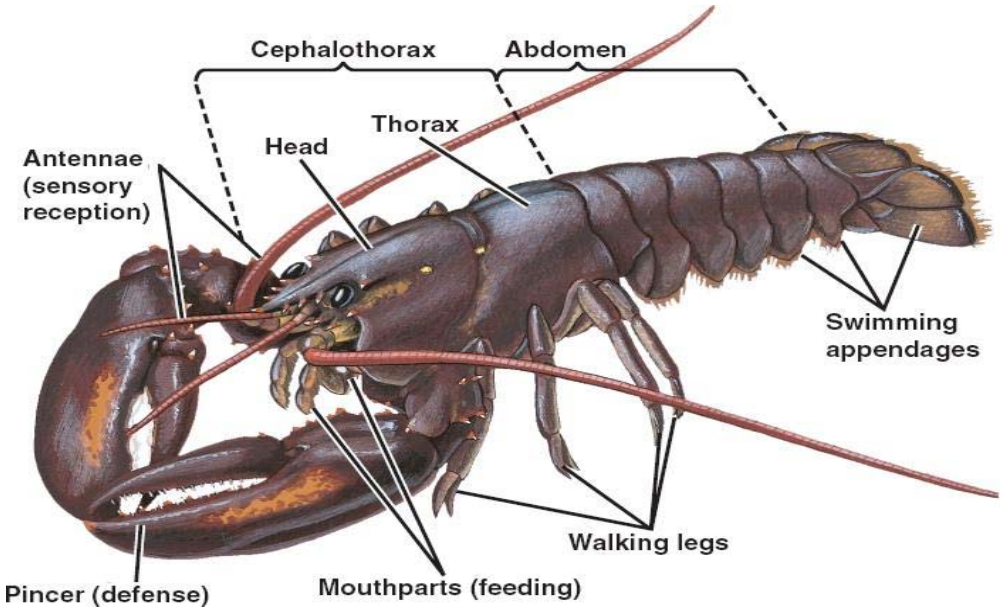

Figure 2.13 – Lobster's anatomy – Showing the joint connecting the tail to thorax

The ventral and dorsal halves of the shell need to be separated by beginning at the end of the abdomen of the lobster. The anterior border of the ventral shell needs to be lifted while making a scratch with pair of scissors as close as possible to the ventral shell. In addition, any muscle tissue attached to the ventral shell needs to be scratched and cut. The ventral portion of the shell can be discarded once the telson is reached.

Once the above procedure is performed, the ventral nerve cord of the lobster will be noticeable, running along the middle of the tail. The anterior portion of the nerve should be carefully lifted in order to separate the nerve from the tail. The nerve can be separated from surrounding connective and muscle tissue by aid of scalper. Once the nerve is completely free, a piece of thread may be attached under the anterior end of the nerve in order to align the nerve in the nerve chamber. As mentioned before, the nerve should be kept moist with Ringer's solution at all times. Once the above process has come to an end, the nerve can be placed in the nerve

chamber and CAP measurements may begin. An instruction to obtain a lobster nerve is shown in figure 2.14.

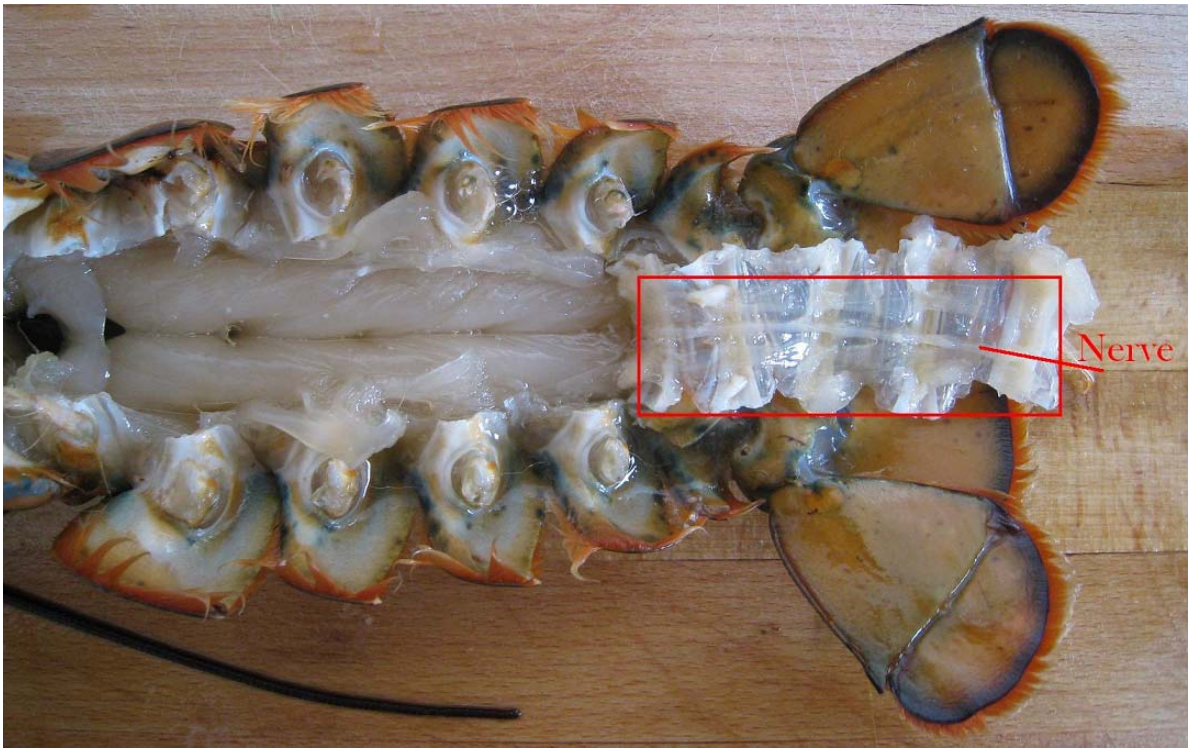

Figure 2.14 – Lobster nerve dissection – Showing a dissected nerve without any damages

Chapter 3 **Results**

3.1 Characterization of the HIFU Transducer

3.1.1 Ultrasound Field Simulations

A MATLAB code (Appendix A) and a C function were used to numerically calculate intensity profiles of our HIFU transducer. As mentioned in chapter two; these programs compute 3D linear intensity field of an ultrasound source in a homogenous medium defined in front of the source. The program was used in this study to complete the calibration chart for the HIFU transducer. For more information about the code refer to (LATS User Manual, 2010). Once the code runs, it provides us with different profiles of the given transducer. Lateral and axial profiles are also obtained which will help in calculating the exact focal spot dimensions of the transducer. Figure 3.1 shows the surface of the HIFU transducer geometry that was used in the simulation code (50 mm in diameter, and 120 mm in radius of curvature).

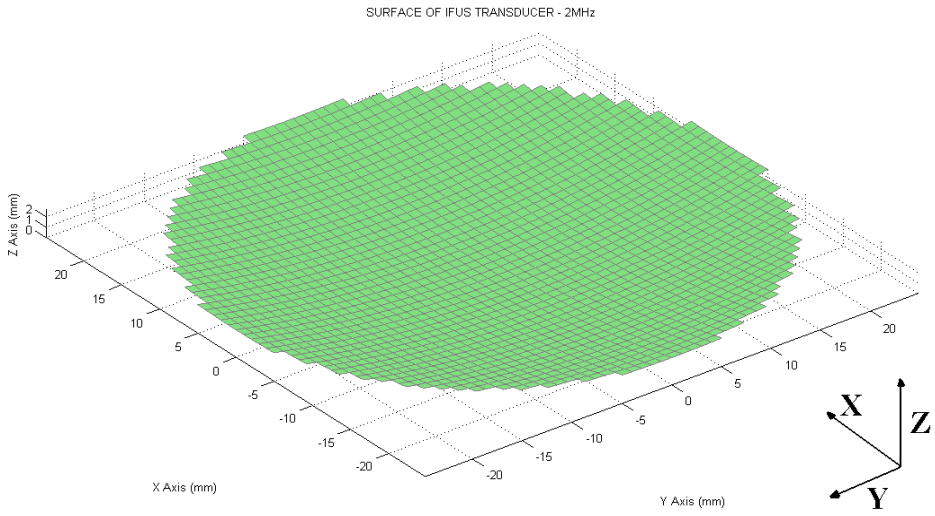

Figure 3.1 – Geometry of HIFU transducer

Lateral and axial intensity profiles of the HIFU transducer are shown in figures 3.3 and 3.4, respectively. Based on these simulations, the full width at half maximum (FWHM) lateral and axial lengths of the focal spot were found to be 1.8 mm, and 28.8 mm, respectively.

3.1.2 Hydrophone Measurements

In order to fully characterize the system, profile comparison between the simulations and hydrophone measurements were carried out. Figure 3.2 shows the HIFU transducer and a calibrated needle hydrophone (HP Hydrophone – 1139, Precision Acoustics LTD, Dorchester, England) submerged in degassed water. The hydrophone with an active sensor diameter of 0.2 mm is attached to a 3D micro-positioning scanning system with an increment size of 1 mm in X and Z axis in order to get the lateral and axial profiles of the transducer, respectively. Values of 1.8 mm and 26.5 mm were found to be the lateral and axial lengths of the focal spot of our HIFU transducer. The measured value for axial length has a 7.9 % of difference when compared to the simulated value, which might be due to some errors in our hydrophone measurement and approximations in the simulations. Figures 3.3 and 3.4 show the measured lateral and axial intensity profiles of the HIFU transducer, respectively.

Figure 3.3 shows a small asymmetry at the intensity peak of the hydrophone scan, which might be due to some errors in the 3D positioning system that was used to carry out the hydrophone measurements. As mentioned above, lateral profile of the transducer was obtained by a scan in the X axis coordinate, therefore any small non-alignment on this axis could also cause the asymmetry that is shown.

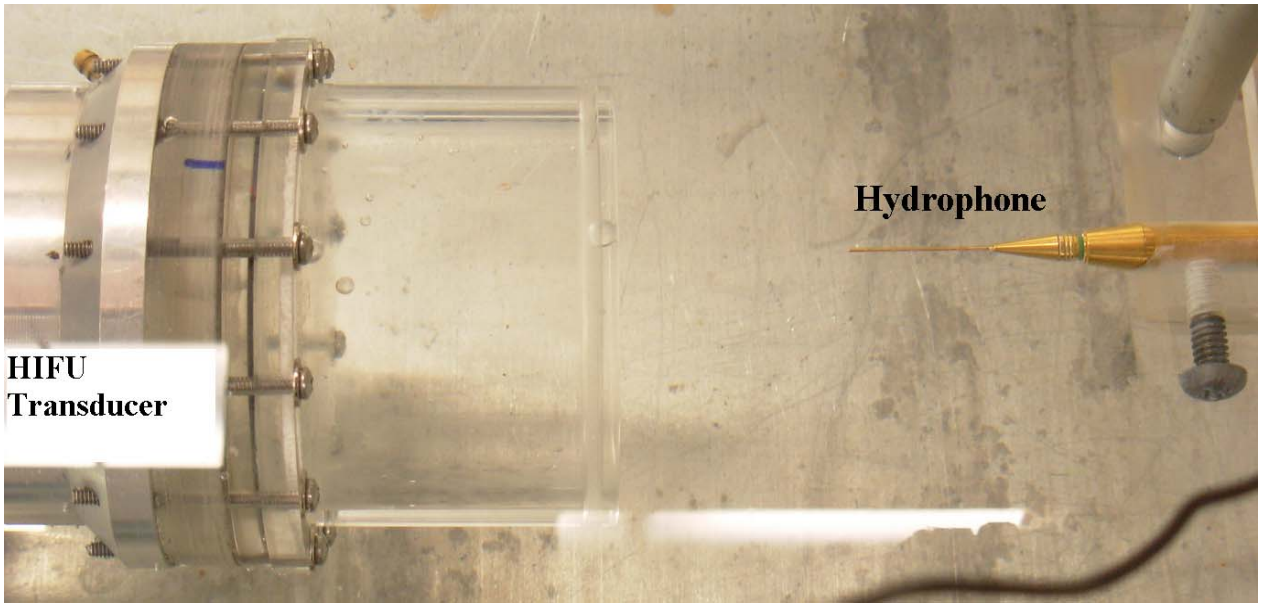

Figure 3.2 – Hydrophone measurement of the HIFU transducer field

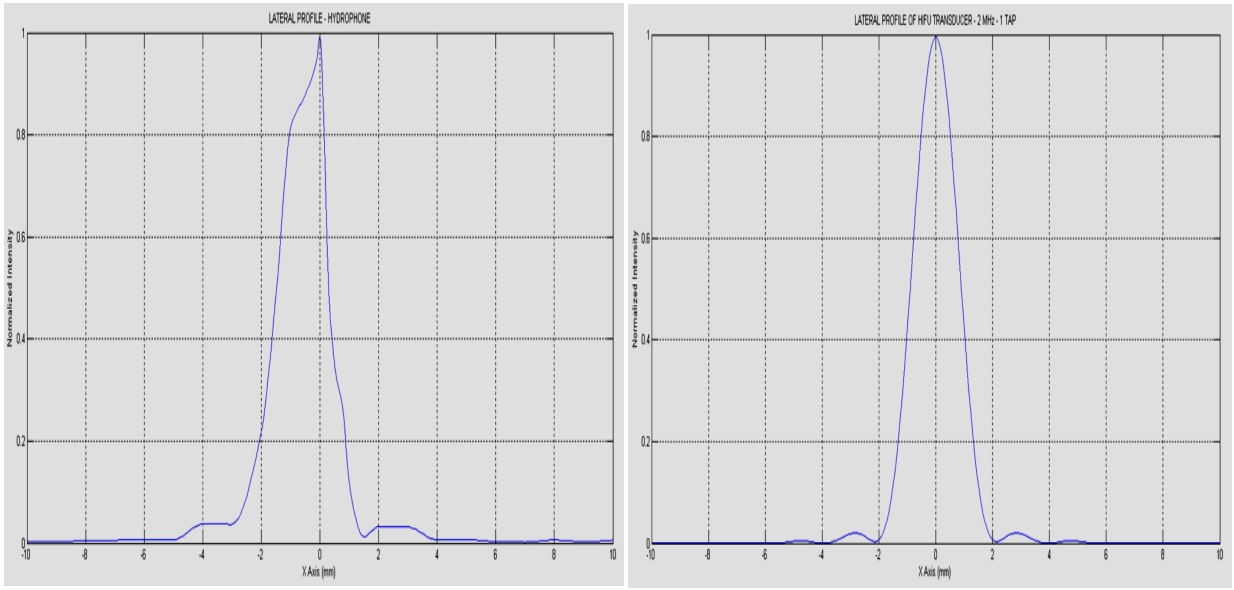

Figure 3.3 – Lateral intensity profiles – Left: measured lateral intensity profile of the HIFU transducer – The width of the focal spot was found to be 1.8 mm – Right: simulated lateral intensity profile of the HIFU transducer – The width of the focal spot was calculated as 1.8 mm

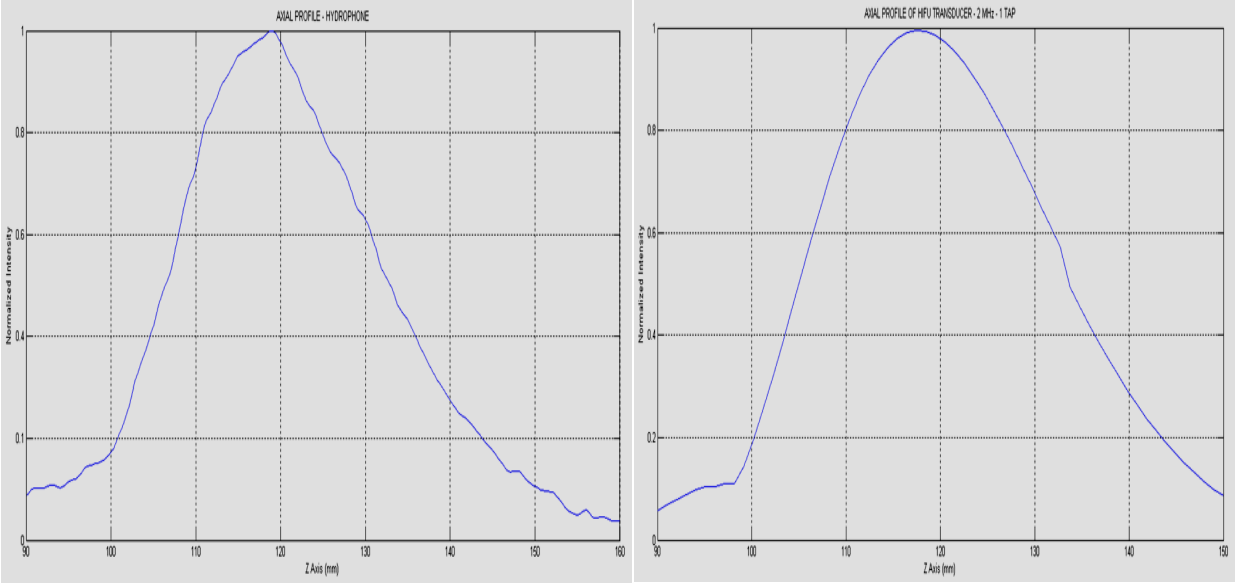

Figure 3.4 –Axial intensity profiles – Left: measured axial intensity profile of the HIFU transducer – The width of the focal spot was found to be 26.5 mm – Right: simulated axial intensity profile of the HIFU transducer – The width of the focal spot was calculated as 28.8 mm

3.1.3 Total Acoustic Power (TAP) Measurements

Measurement of the acoustic power output levels of our HIFU transducer is very important to determine exact exposure levels in order to have accurate results. As mentioned in chapter two, two different acoustic power measurement systems were used to measure the output TAP of the HIFU transducer used in this study: Ohmic and Onda radiation force balance power meters. Figure 3.5 shows our HIFU transducer during a power measurement process using the Ohmic radiation force balance system. Figure 3.6 shows a graph of our power measurement with the Ohmic system that shows output acoustic power vs. input voltage.

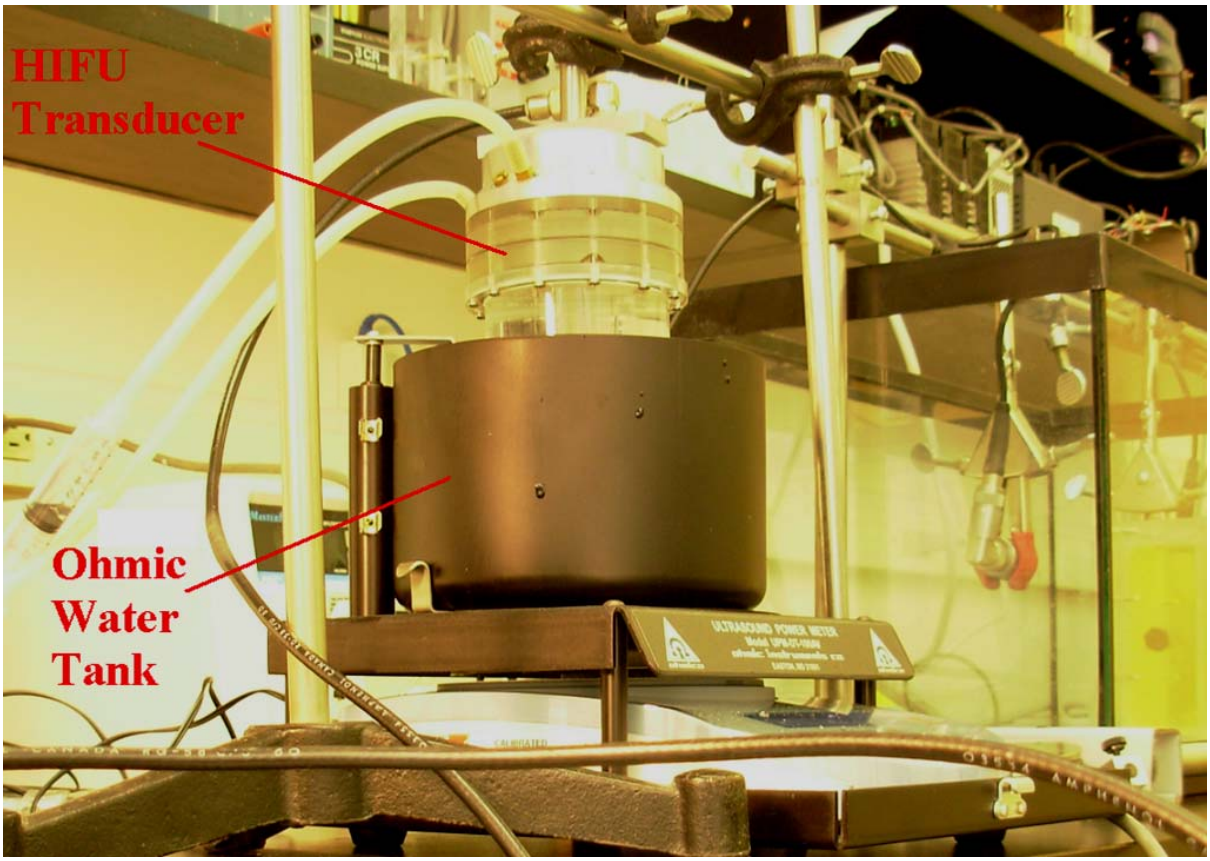

Figure 3.5 – Power measurement setup – Showing the HIFU transducer inside of the water tank of the Ohmic radiation force balance power meter

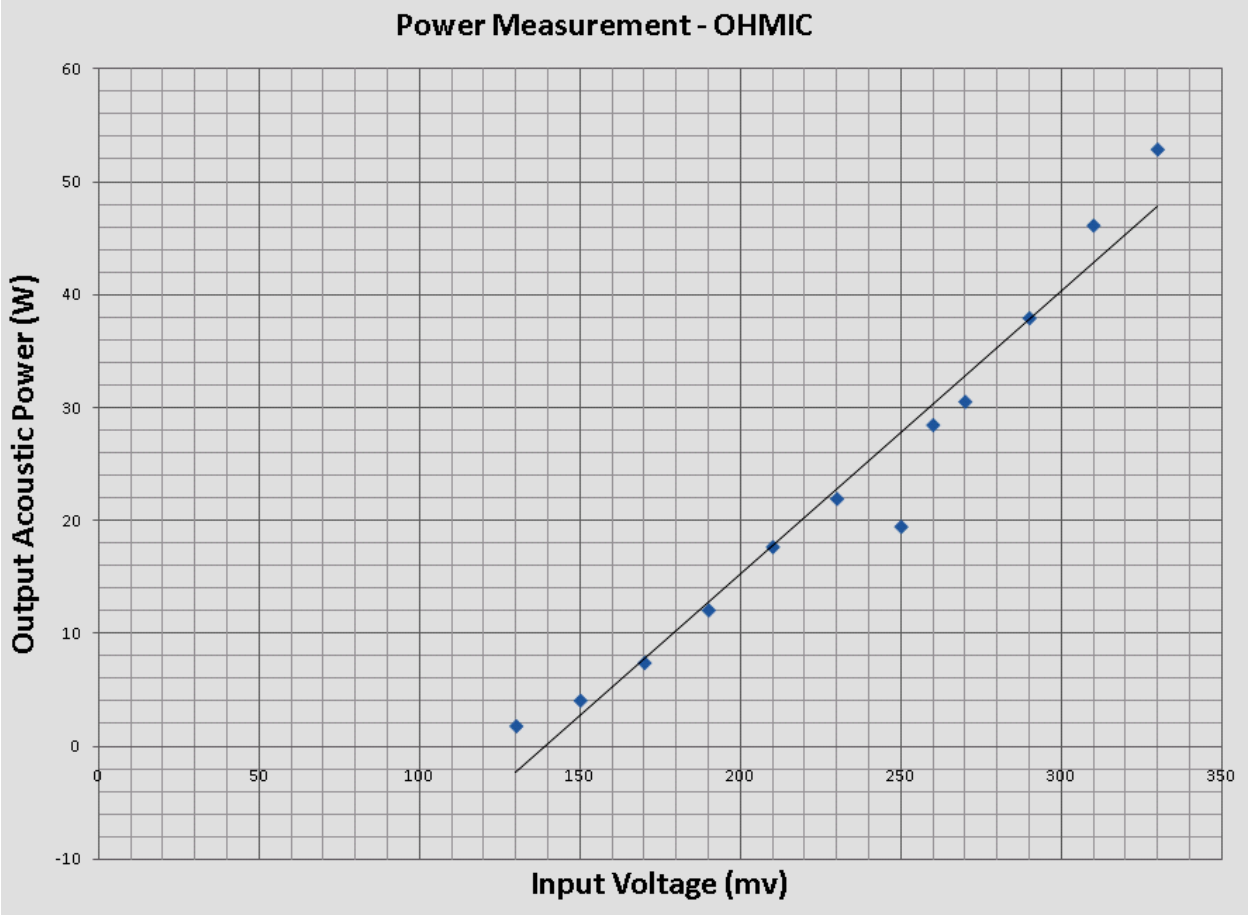

Figure 3.6 – Power measurement – Ohmic system – Output acoustic power vs. Input voltage – The solid line in the graph represents the best fitted line through the measured points in the power measurement experiment

The same measurements were carried out with the Onda system, the results of this measurement is shown in figure 3.7.

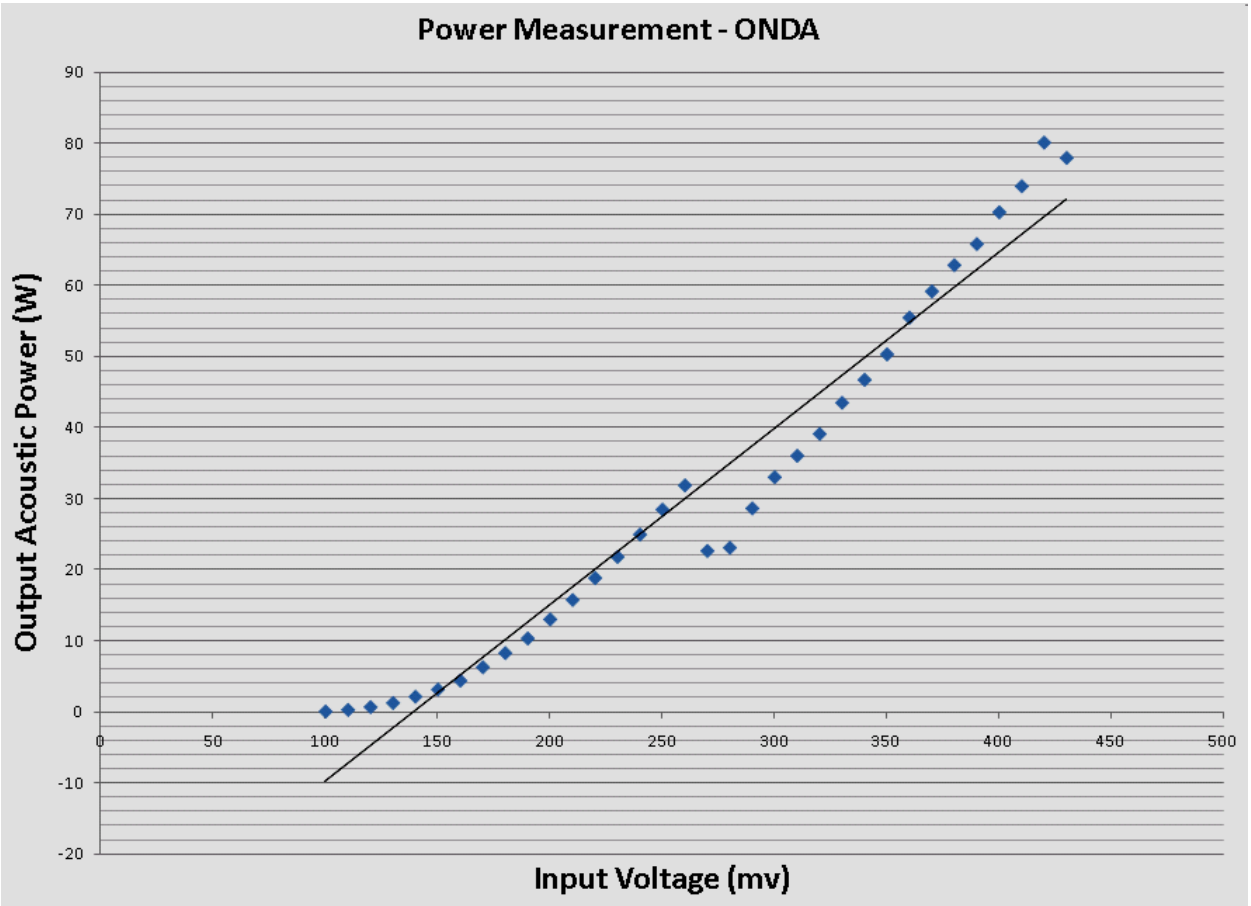

Figure 3.7 – Power measurement – Onda system – Output acoustic power VS. Input voltage – The solid line in the graph represents the best fitted line through the measured points in the power measurement experiment

A comparison between the two systems was carried out in order to use the best and most accurate values in our calibration chart. Both systems were found to be accurate. Figure 3.8 is showing this comparison.

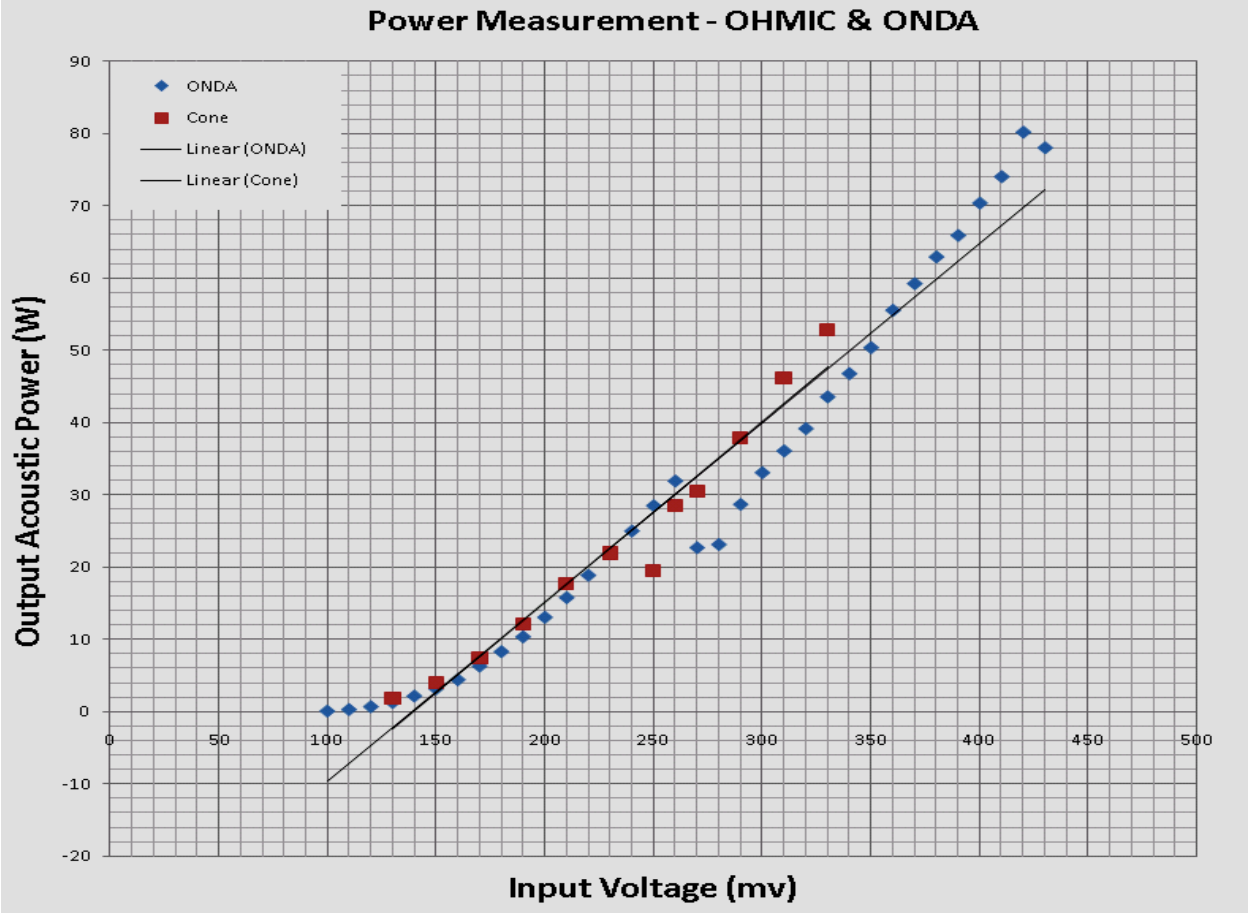

Figure 3.8 – Power measurement – Ohmic & Onda systems – The solid line in the graph represents the best fitted line through the measured points in the power measurement experiments

3.1.4 HIFU System Calibration Chart

The calibration chart that specifies the output total acoustic power and the focal intensity of the HIFU system for a given input electrical signal excitation was obtained. The experimental setup used in this study will be presented in the next section. Combining the values measured in our power measurements with the values calculated in our simulations gives us the HIFU system calibration chart. This chart includes values such as the input voltage, output acoustic power and

focal intensity which will enable the user to choose the exact power/intensity desired to be used. Table 3.1 is showing the calibration chart that includes free-field focal intensities ranging from about 2 to more than 1500 $W.cm^{-2}$.

Input Voltage (mV)	Total Acoustic Power (W)	Focal Intensity in Water Medium ($W.cm^{-2}$)
100	0.09	2.24
110	0.31	7.72
120	0.71	17.6
130	1.29	32.1
140	2.17	53.9
150	3.19	79.3
160	4.43	110
170	6.32	157
180	8.31	206
190	10.37	258
200	13.06	324
210	15.79	392
220	18.88	469
230	21.85	543
240	25	622

250	28.51	709
260	31.91	793
270	32.7	813
280	33	821
290	33.9	843
300	33.07	872
310	36.08	897
320	39.16	974
330	43.55	1083
340	46.77	1163
350	50.36	1252
360	59.22	1381
370	62.91	1473
380	65.88	1565

Table 3.1 – HIFU system calibration chart

3.2 Nerve Study

3.2.1 Nerve and Nerve Chamber Preparations

A minor adjustment to the Biopac nerve chamber was applied. The bottom of the nerve chamber was removed, enabling the ultrasound beam to go through and reach the nerve once it is placed on the chamber wires. The transducer was heading upwards, making it possible for the chamber to be placed on top of the transducer nose section. The nose section was filled with degassed water and a Mylar sheet of thickness 0.025 mm was fixed on top of the nose piece in order to provide a support and an ultrasound interface to the nerve chamber. The chamber was placed on top of the transducer, sitting above the Mylar sheet while the 1 cm gap between the nerve and the Mylar sheet was filled with ultrasound gel allowing no air bubbles between this sheet and the nerve. Once the chamber was placed on its right position, more ultrasound gel was placed on top of the nerve (centre part of the nerve only) in order to decrease reflection once the ultrasound beams are coming through. Figure 3.9 is showing the Biopac nerve chamber on top of the HIFU transducer during the nerve study.

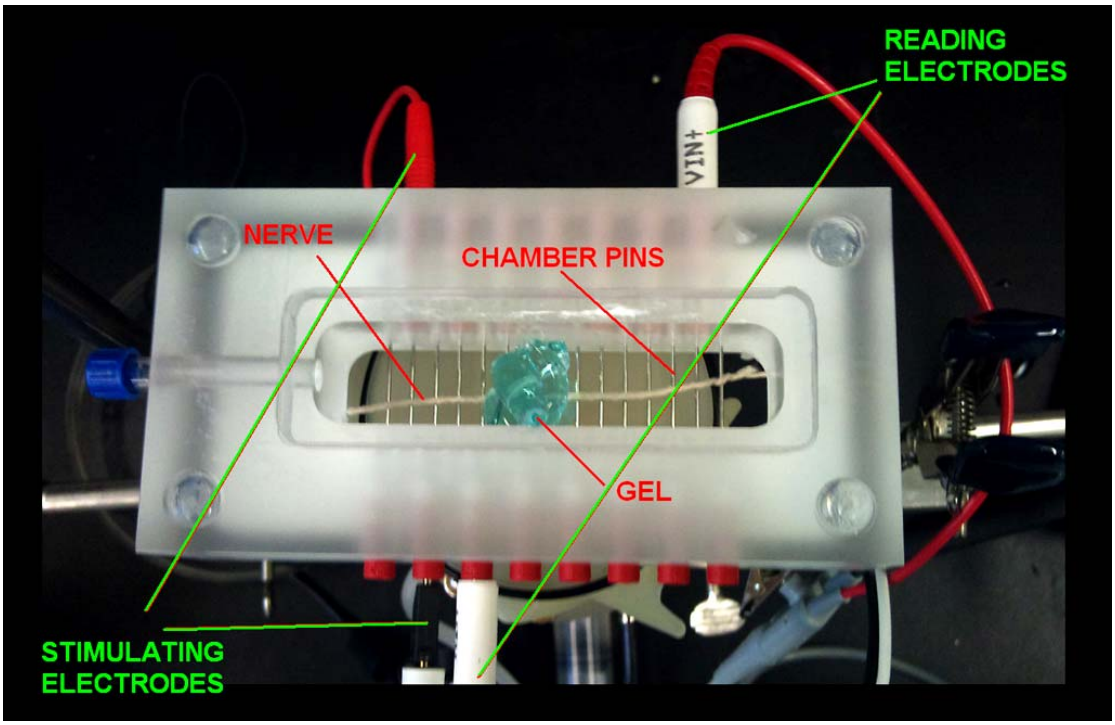

Figure 3.9 – Nerve chamber – Showing the Biopac nerve chamber during an experiment. The nerve sits on the wires of the chamber, while the centre of the nerve is covered with ultrasound gel

3.2.2 Experimental Setup

The transducer was connected to an RF power amplifier (2100L, Electronics & Innovation Ltd., New York, USA) with a maximum output electric power of 100 W, and a frequency range of 10 kHz to 12 MHz. The amplifier is fed by a signal generator (AFG 3022B, Tektronix Corp., Oregon, USA) with a bandwidth of 25 MHz. Figure 3.10 shows all components of the experimental set up. Figure 3.11 also shows a block diagram of the experimental set up and all the connections. The excitation signal was initiated by the Tektronix signal generator which gets amplified through the E&I RF amplifier and then is sent to the transducer. The exact power/intensity needed was read from the calibration chart calculated earlier, which tells the user

what input voltage should be used for a desired focal intensity. The focal intensities chosen for these studies were as following: 100, 175, 275, 400, 525 and 700 $W.cm^{-2}$.

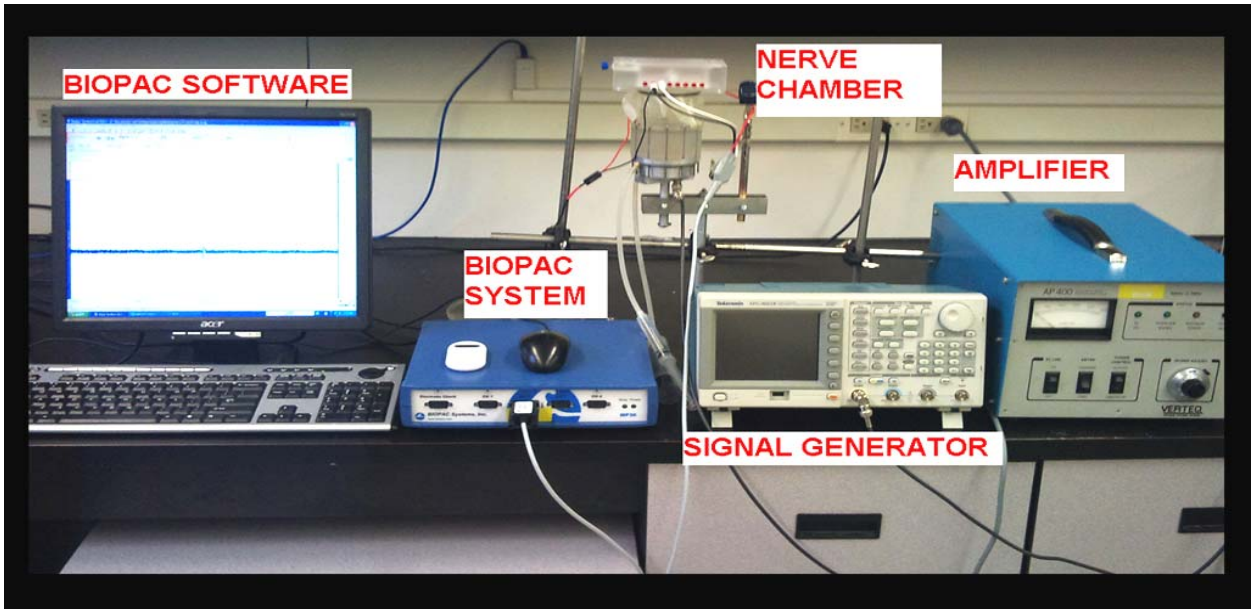

Figure 3.10 – Experimental setup – Showing the Biopac device and system, the nerve chamber, E & I power amplifier and Tektronix signal generator

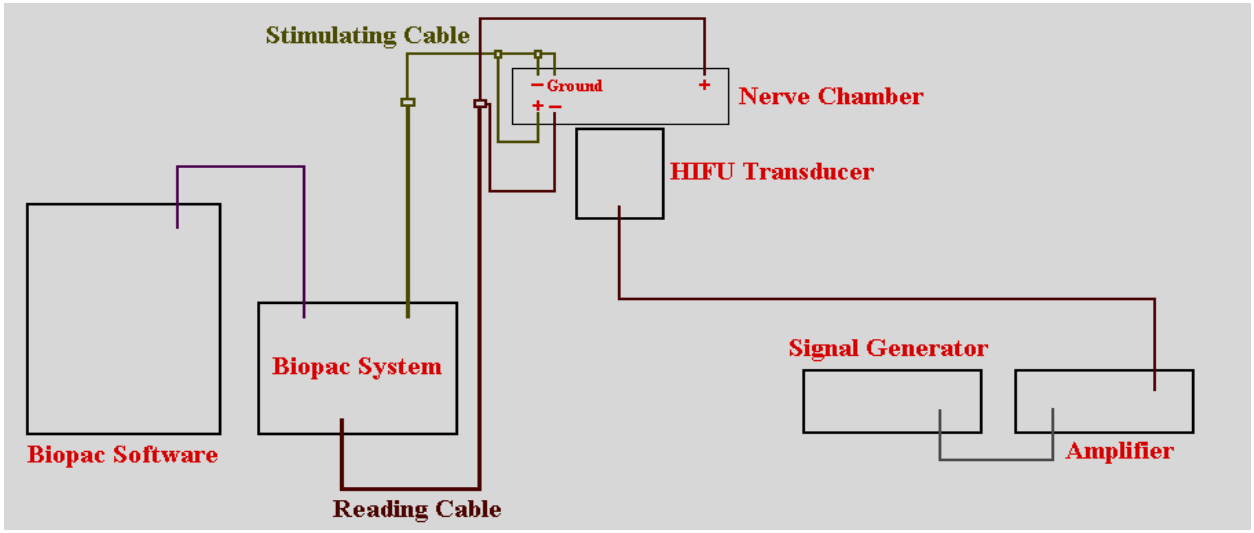

Figure 3.11 – Block diagram of the experimental setup – Showing the Biopac system and software, the nerve chamber, power amplifier and a signal generator – All the connections are also shown in this diagram

3.2.3 Nerve Experiment Results

Once the experimental setup was ready, control nerves were studied first. All the control nerves were fully functional even after 30 minutes of their dissection (the amount of Ringer's solution used on these nerves had to be minimal since it would interfere with the CAP measurements). The CAP values for these nerves were found to be 14±2 µv. A total number of 40 nerves were studied under the same conditions and were stimulated with 5 volts and were exposed to 10 seconds of the HIFU exposure. The stimulation pulse was off during the 10 second HIFU exposure; therefore no CAP signals were recorded during the on-time of the HIFU system (figure 3.12).

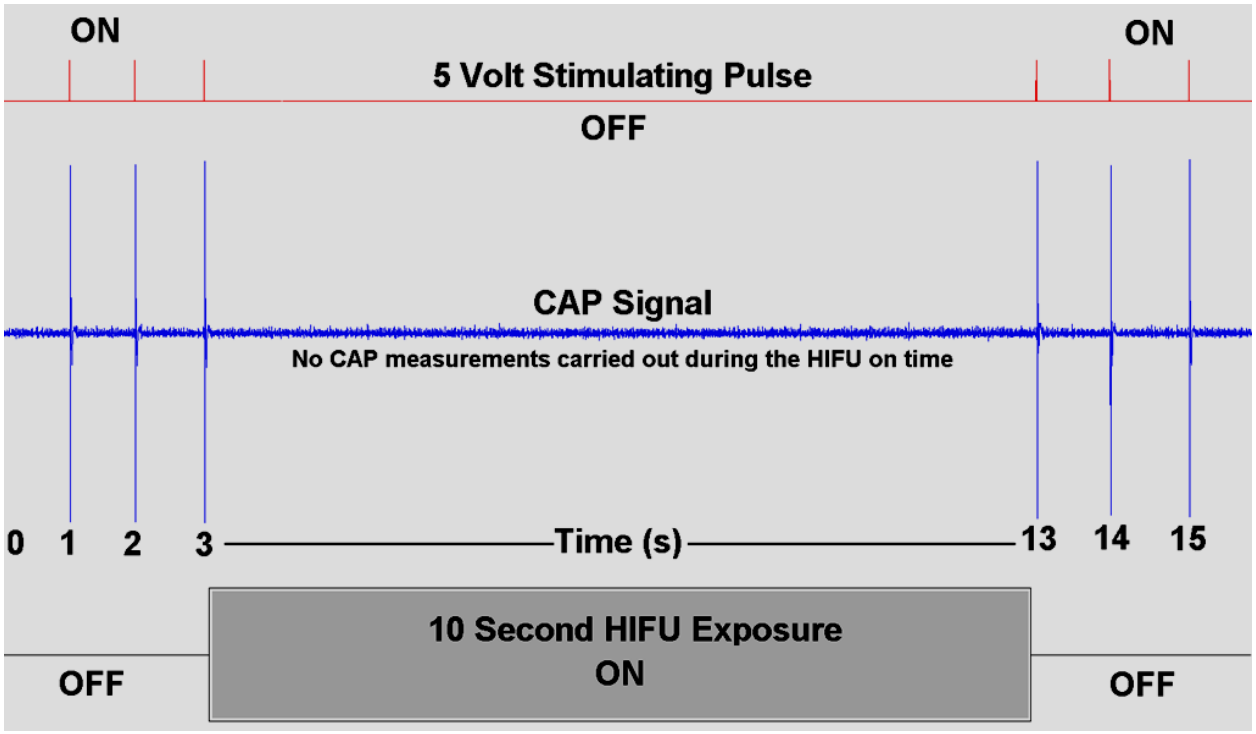

Figure 3.12 – Time sequence diagram for HIFU exposure and CAP recording – Showing the method which was used to record CAP signals before and post exposure

At the intermediate intensities of 100 to 525 W.cm^{-2} it was observed that the CAP amplitude increases, while with higher intensities a significant decrease could be observed. At a focal intensity of 700 W.cm^{-2} a total degeneration of the nerve and a total suppression of the CAP were achieved. Figures 3.13 – 3.24 show the typical CAP measurements before and after each HIFU exposure.

Delay time (time between the stimulation and the occurring of the CAP) was also measured for each nerve before and post exposure. These values were found to be 12.3±0.1 ms in length which showed no change in the conduction velocity of CAPs.

At the lowest focal intensity of 100 W.cm^{-2} the baseline CAP amplitude of the nerve was measured to be 12.9 µv, this amplitude is illustrated in figure 3.13. Once the nerve was exposed the 10 s HIFU exposure, the CAP amplitude increased to 16.2 µv shown in figure 3.14. The error bars in the following figures represent the range for different CAP amplitudes in different nerves studied.

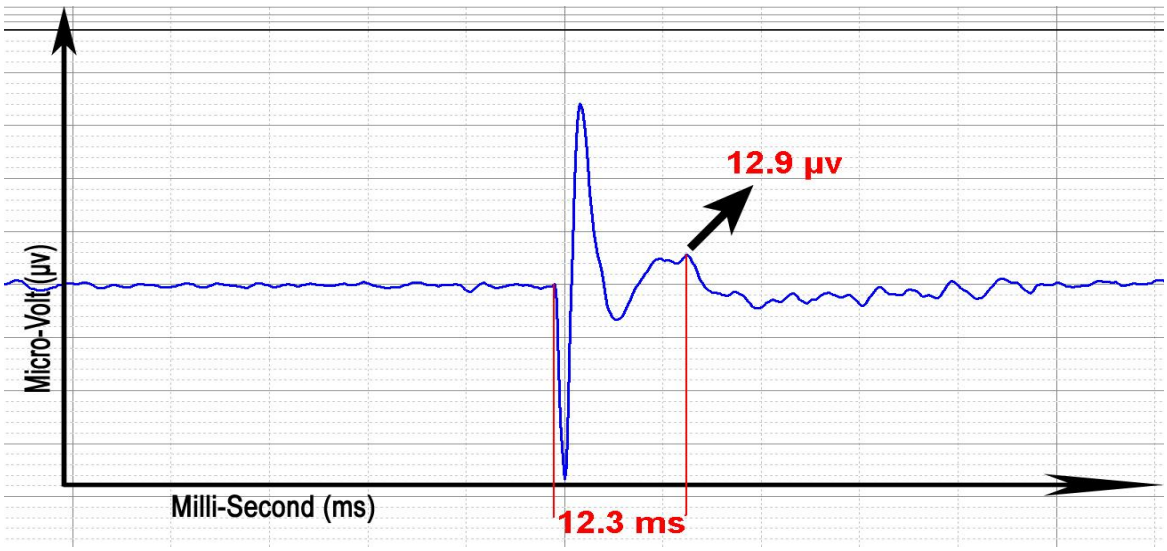

Figure 3.13 – Baseline CAP measurement –Showing the CAP amplitude before the HIFU exposure of 100 W.cm^{-2}

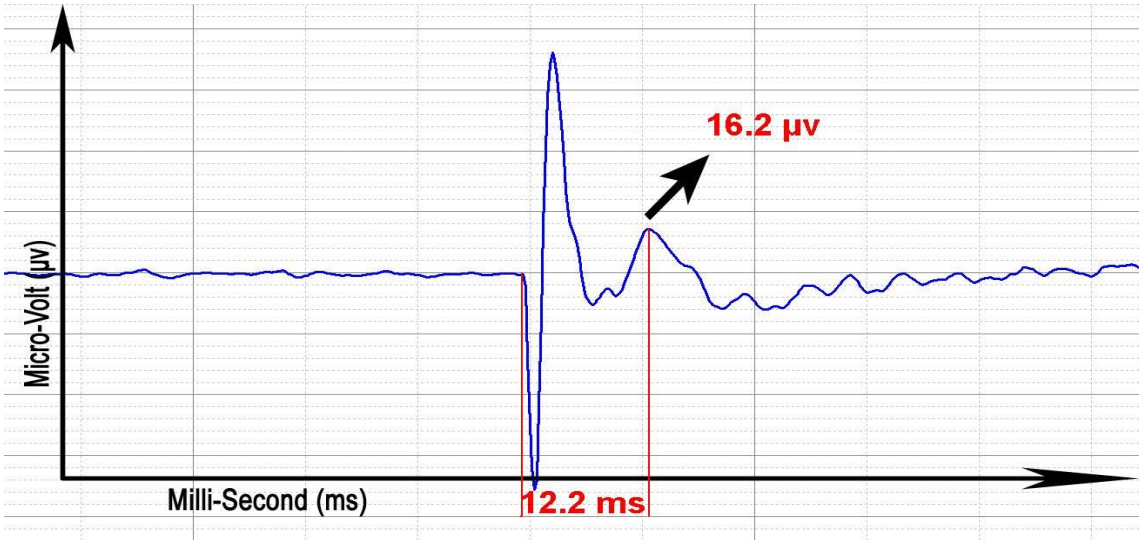

Figure 3.14 – CAP measurement after exposure to 100 W.cm^{-2} for 10 s.

The baseline CAP amplitude before and post exposure to an intensity of 175 W.cm^{-2} were measured as 14.4 and 18 µv, respectively (figures 3.15 and 3.16).

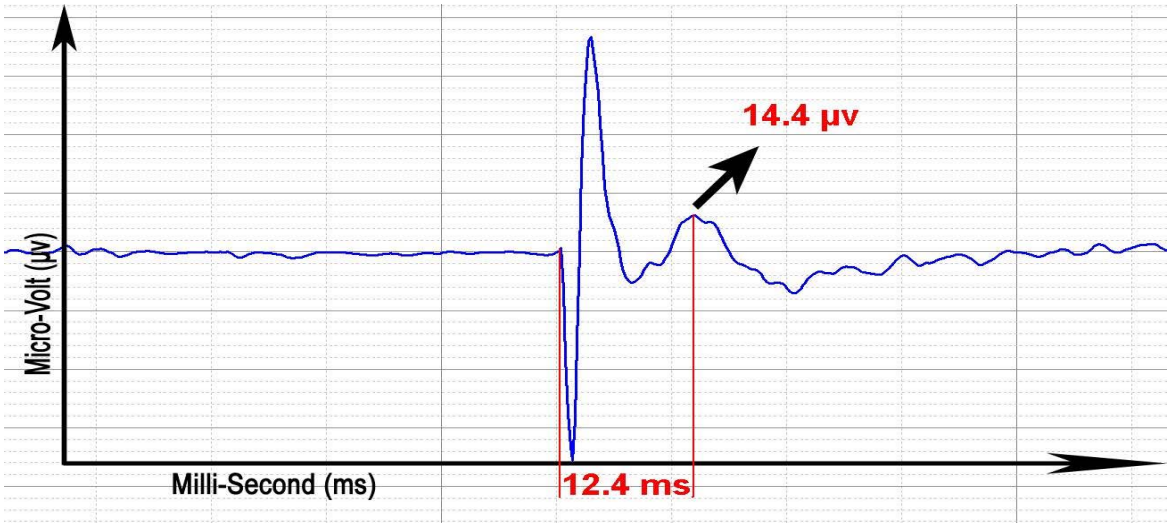

Figure 3.15 – Baseline CAP measurement - Showing the CAP amplitude before the HIFU exposure of 175 W.cm^{-2}

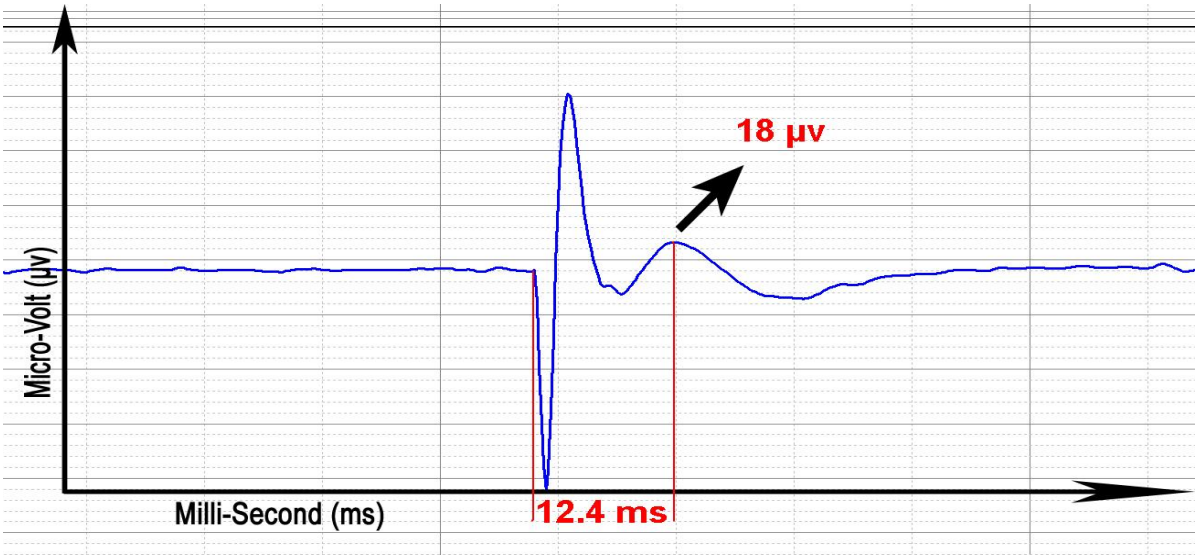

Figure 3.16 – CAP measurement after exposure to 175 W.cm^{-2} for 10 s

The next intensity was chosen as 275 W.cm^{-2}. The baseline and post exposure CAP amplitudes were found to be 9.5 and 11.7 µv, respectively. The increase in the CAP amplitude after the nerve being exposed to the HIFU exposure was still evident. The baseline and post exposure CAP values are illustrated in figures 3.17 and 3.18, respectively.

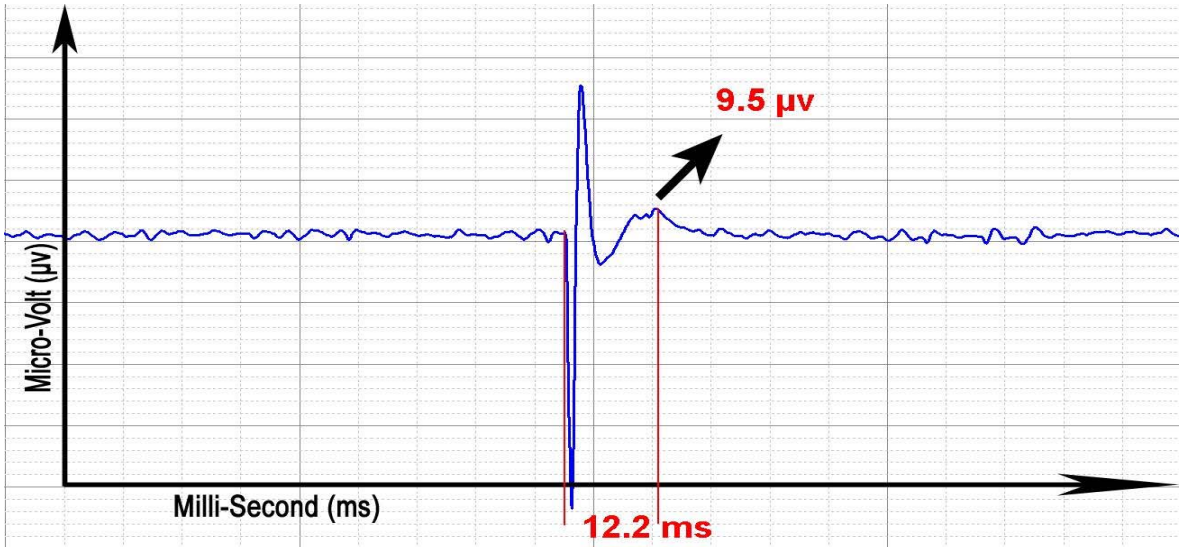

Figure 3.17 – Baseline CAP measurement - Showing the CAP amplitude before the HIFU exposure of 275 W.cm^{-2}

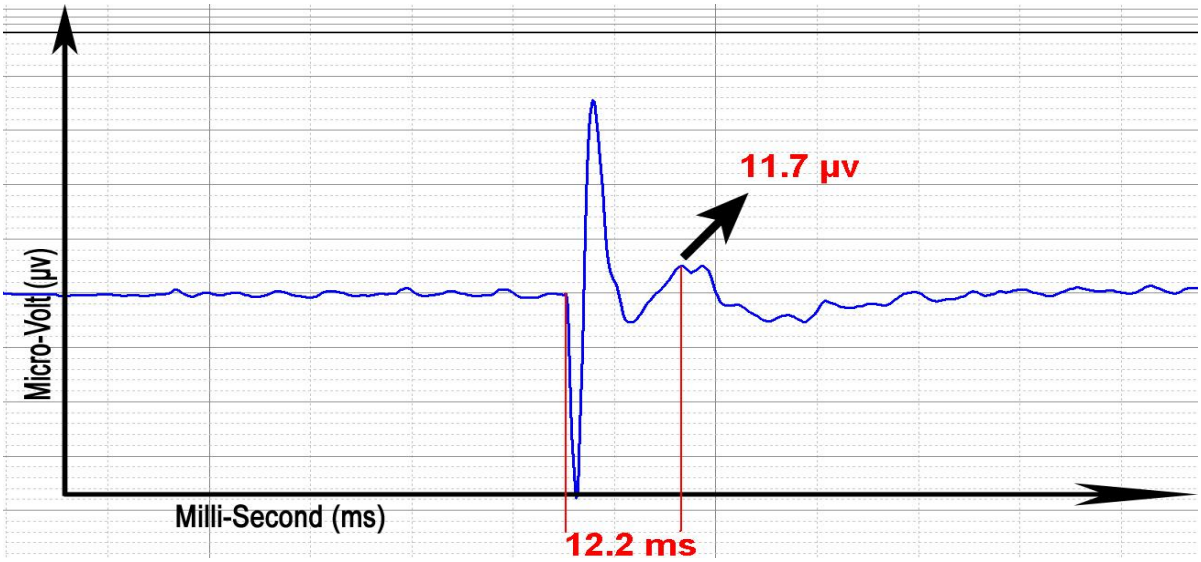

Figure 3.18 – CAP measurement after exposure to 275 W.cm^{-2} for 10 s.

The nerve was also exposed to 400 W.cm^{-2}. The baseline CAP was measured as 8.5 µv (figure 3.19) while it increased once again to the value of 10 µv shown in figure 3.20.

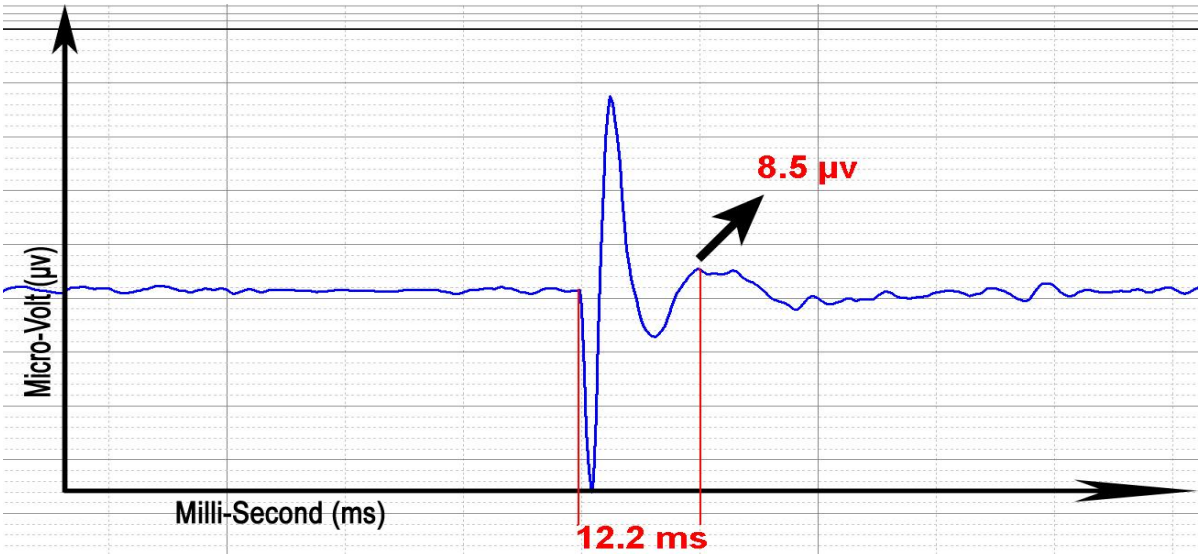

Figure 3.19 – Baseline CAP measurement - Showing the CAP amplitude before the HIFU exposure of 400 W.cm^{-2}

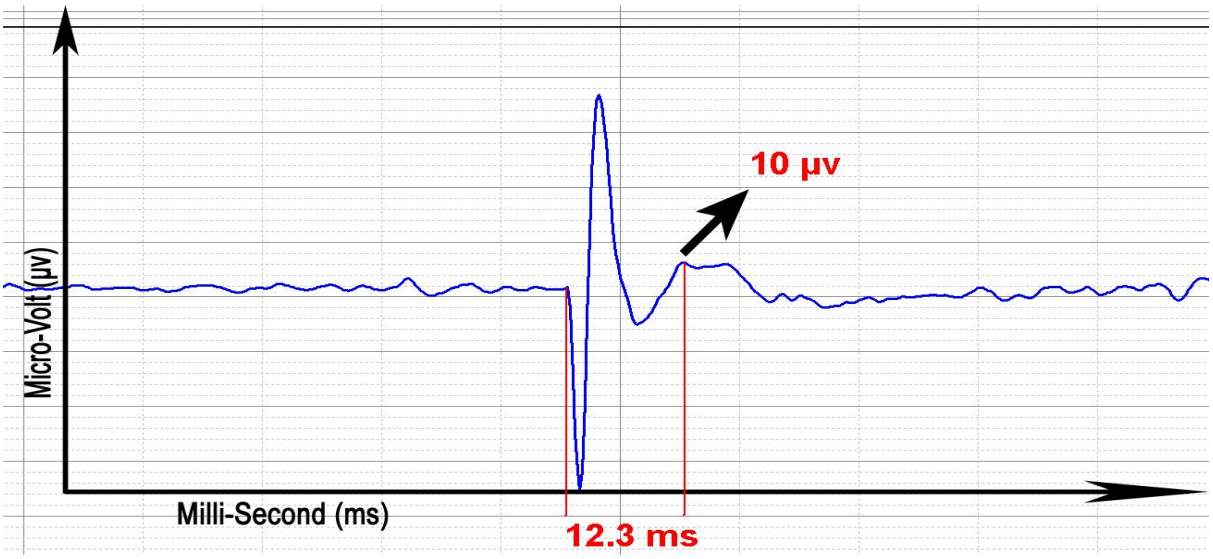

Figure 3.20 – CAP measurement after exposure to 400 W.cm^{-2} for 10 s

Another intensity was chosen as 525 W.cm^{-2}. The baseline and post exposure CAP values were found as 11.5 (figure 3.21) and 13.8 µv (figure 3.22), respectively.

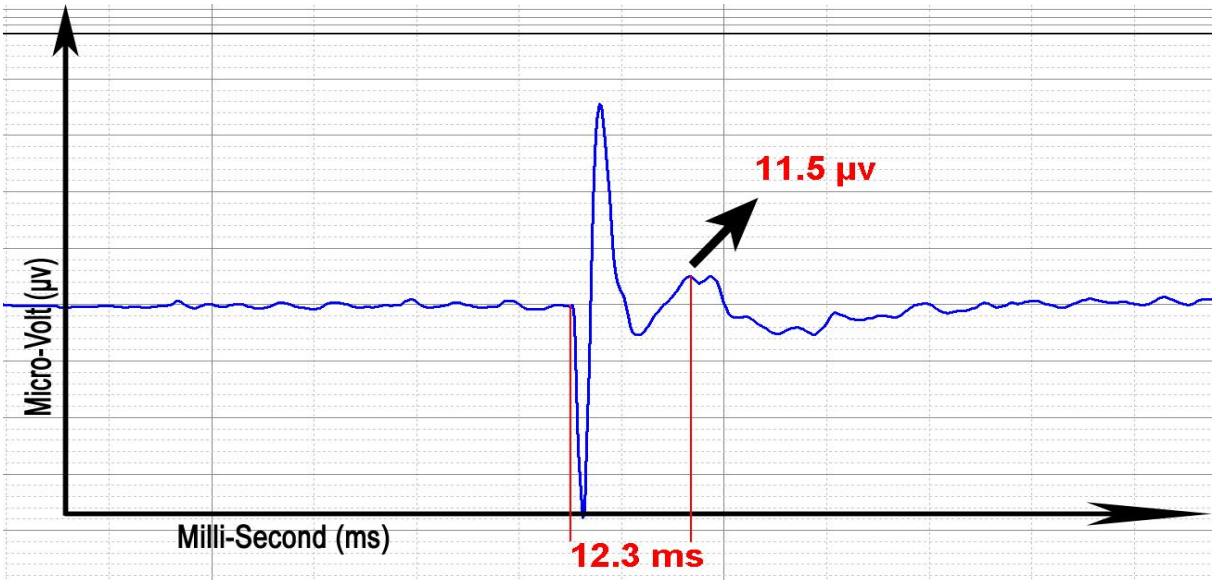

Figure 3.21 – Baseline CAP measurement - Showing the CAP amplitude before the HIFU exposure of 525 W.cm^{-2}

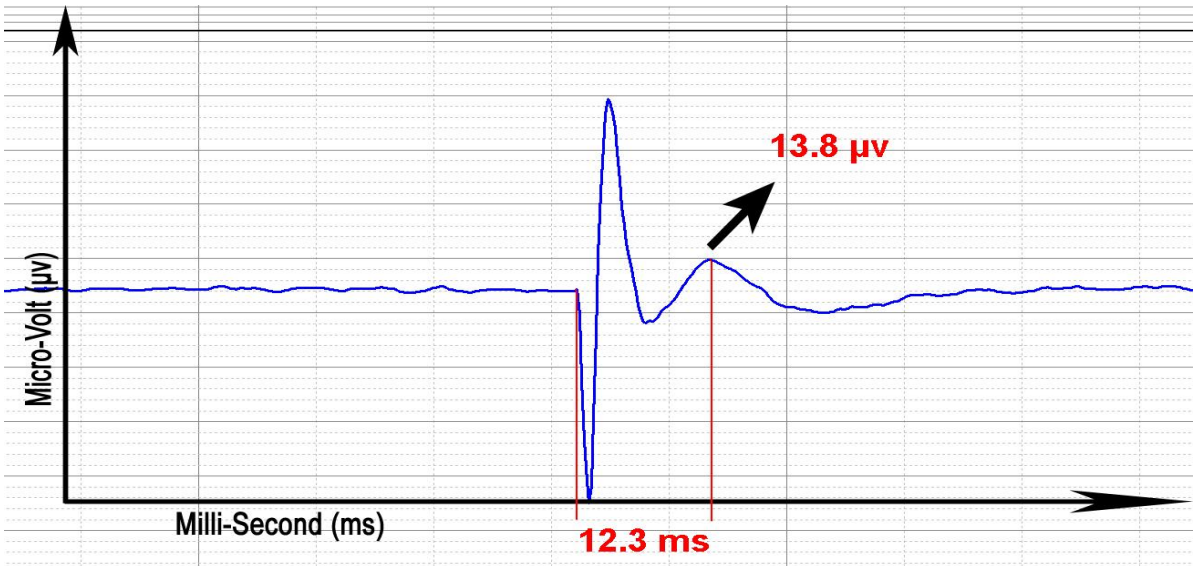

Figure 3.22 – CAP measurement after exposure to 525 W.cm^{-2} for 10 s

The highest focal intensity was chosen as 700 W.cm^{-2}. Unlike all other intensities complete or partial nerve degeneration/coagulation could be observed (comparing the physical properties of these nerves with normal and functional nerves and undergoing CAP measurement process) at this high power. The baseline CAP was measured at 16.1 µv illustrated in figure 3.23, while once the nerve was exposed to the 10 s HIFU exposure this value decreased to 7.1 µv shown in figure 3.24. The nerve was also tested after this high power exposure, however, it found to be completely or partially degenerated and dysfunctional, meaning no further CAP value could be detected. Figure 3.25 is showing one of the nerves after exposure to this high intensity. The green box in the image represents the coagulated section of the nerve. Looking closely, one can observe some changes in the color of this section in comparing to other parts of the nerve.

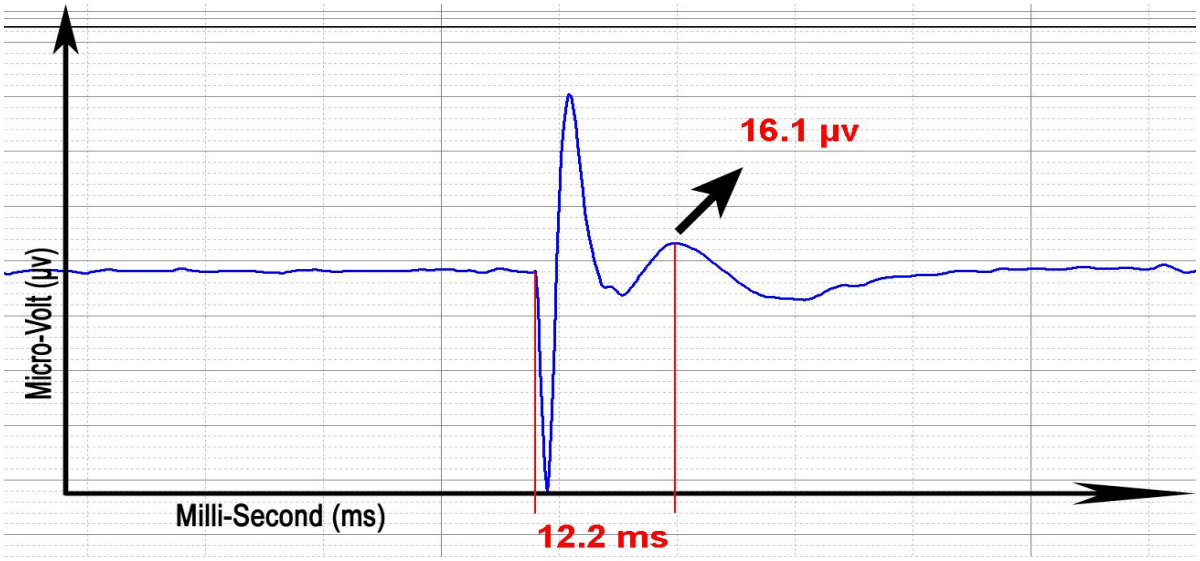

Figure 3.23 – Baseline CAP measurement - Showing the CAP amplitude before the HIFU exposure of 700 W.cm^{-2}

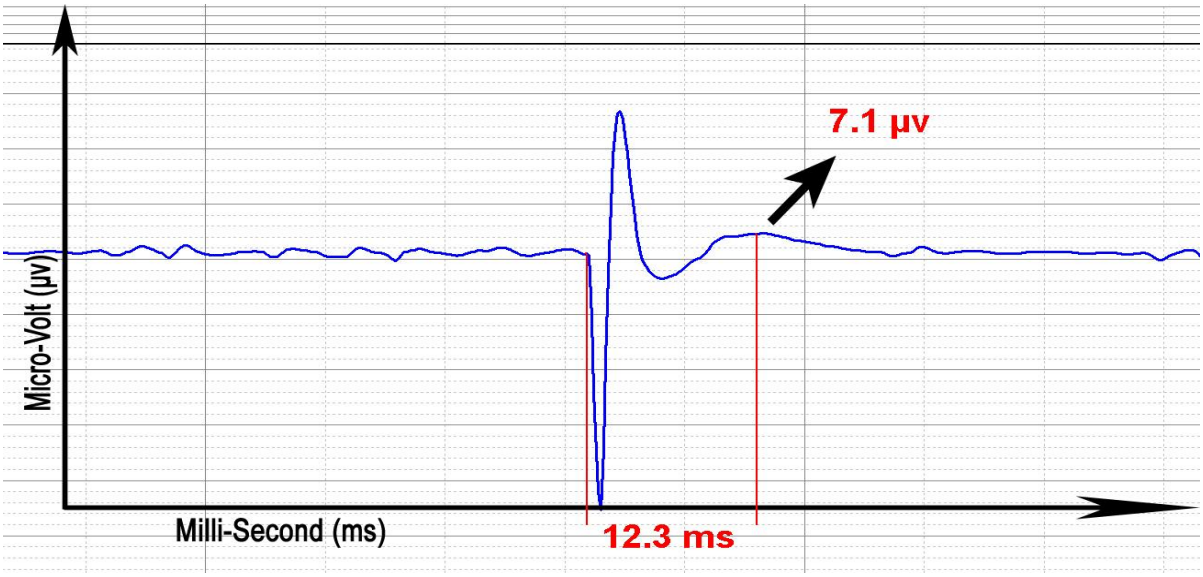

Figure 3.24 – CAP measurement after exposure to 700 W.cm^{-2} for 10 s

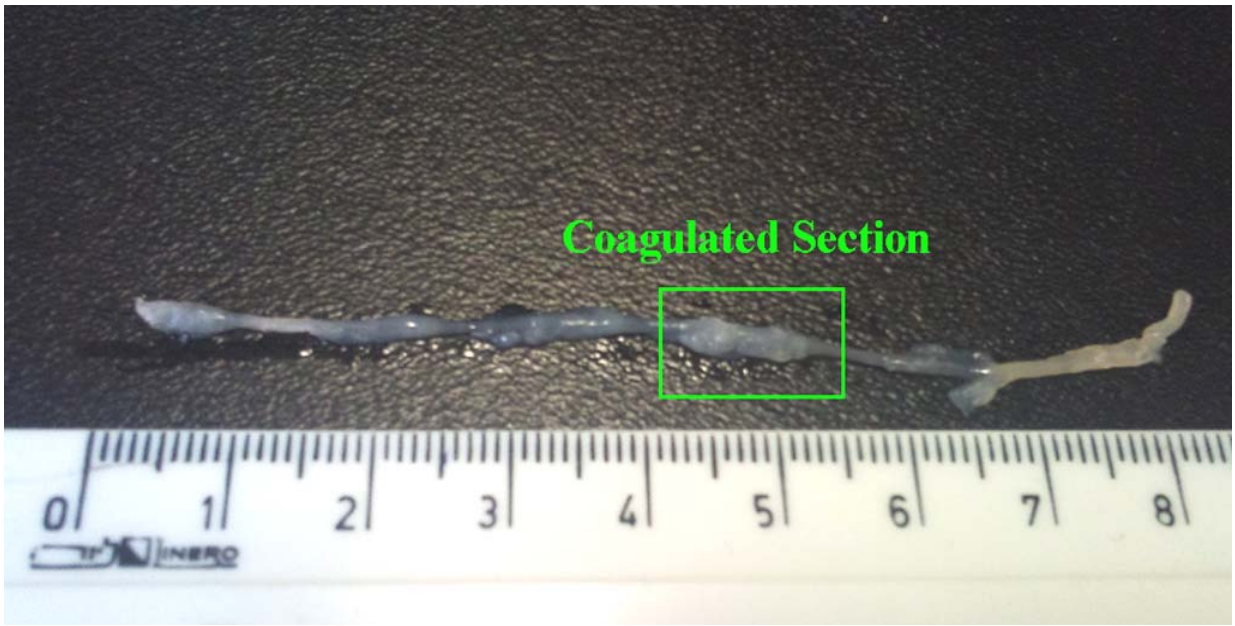

Figure 3.25 – Coagulated nerve after HIFU exposure of 700 W.cm^{2} for 10 s –The green box is showing the degenerated section of the nerve

A total number of 40 nerves were studied in this project, each showing slightly different values and effects, however, summing up the entire studies proved an increase in the CAP amplitude at low and intermediate intensities while complete degeneration and permanent nerve block was achieved at a higher intensity level of 700 $W.cm^{-2}$ or above. The graph in figure 3.26 is showing the baseline and post exposure average CAP values against the focal intensity levels used.

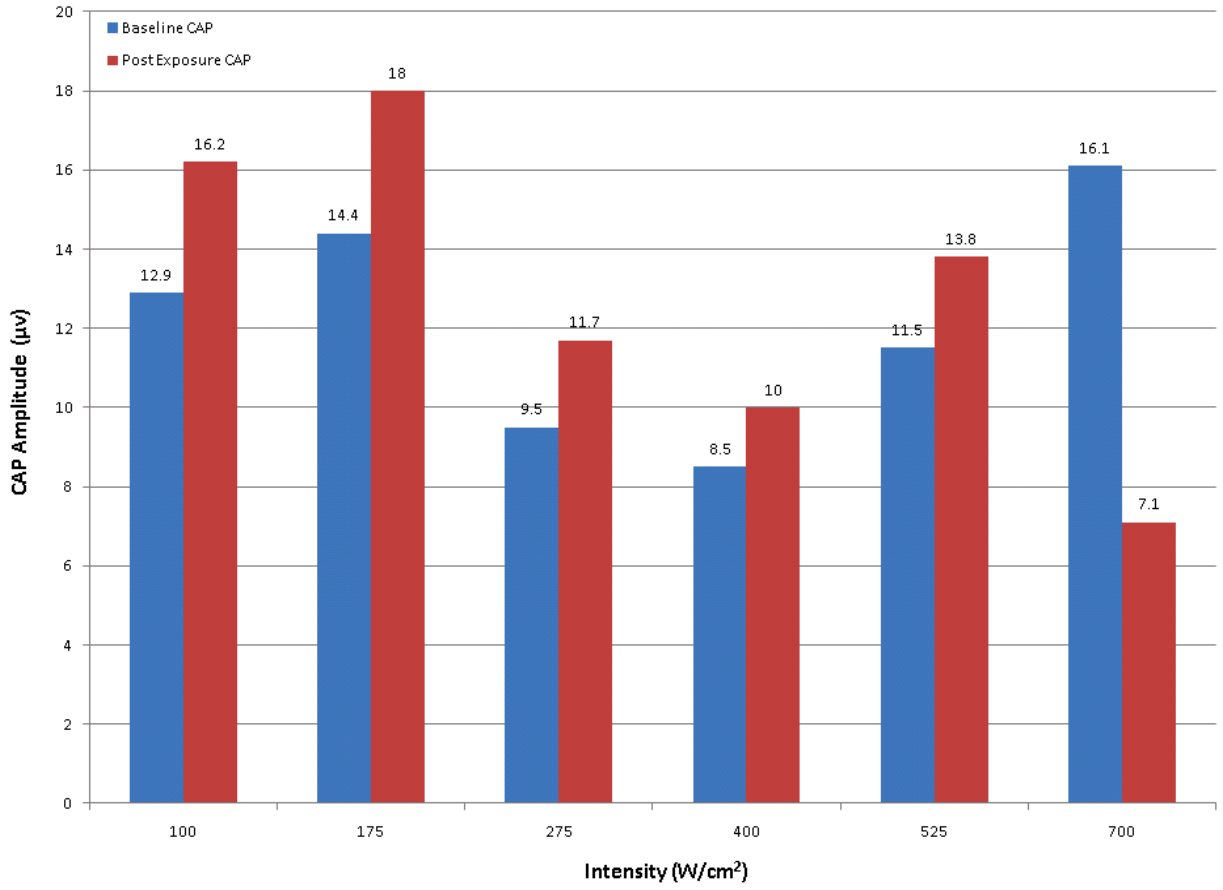

Figure 3.26 – Baseline and post exposure CAP amplitudes vs. focal intensity of a 10-s HIFU

In order to better visualize the data the CAP values were normalized. First the rate of the change of the CAP after the exposure was found (figure 3.27). All the obtained data were divided by the maximum rate of change. As the result, the value corresponding to the maximum rate of change will equal to one. Afterwards all the new data were subtracted by one. After this process the value corresponding to maximum rate of change will equal to zero indicating an irreversible damage to the nerve. Equations 3.1 and 3.2 illustrate the used normalization method.

$$Rate\ of\ change = \frac{|A-B|}{B} \qquad (3.1)$$

where *B* is the baseline CAP amplitude and *A* represents the post CAP amplitude.

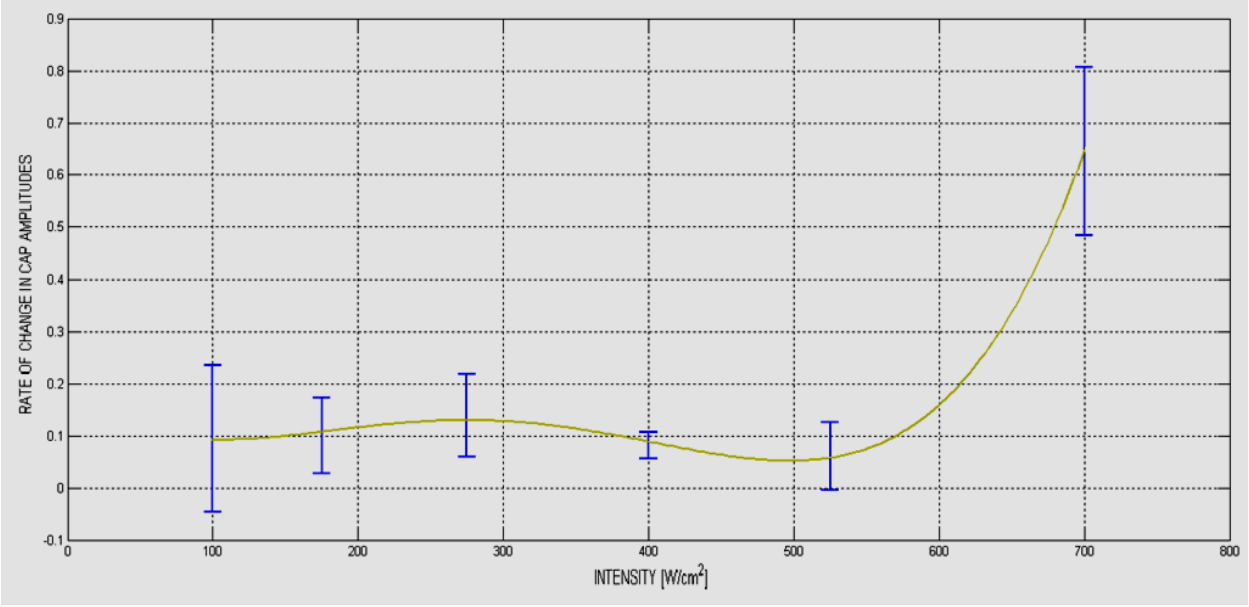

Figure 3.27 – Rate of change in CAP amplitudes vs. focal intensity of a 10-s HIFU exposure

Once the rates of change of all CAPs in different intensity levels were found, a maximum value of the calculated values will be marked as the Maximum Rate of change. Applying

equation 3.2 will normalize the calculated rates of change to 1. This will result in having a zero normalized action potential on the 700 W.cm^{-2} where the rate of change has its maximum value while having the same amplitude as the Maximum rate of change which will make a division of two identical numbers, resulting in a value of 1. Following the equation 3.2 will have a result of subtracting 1 from 1 which will result in having a zero on the normalized action potential axis.

$$Nomalized\ Action\ Potential = 1 - \frac{Rate\ of\ change}{Maximum\ Rate\ of\ change} \qquad (3.2)$$

Once all normalized action potential values are calculated for each intensity level, a graph of these values against the intensity levels will be plotted (figure 3.28).

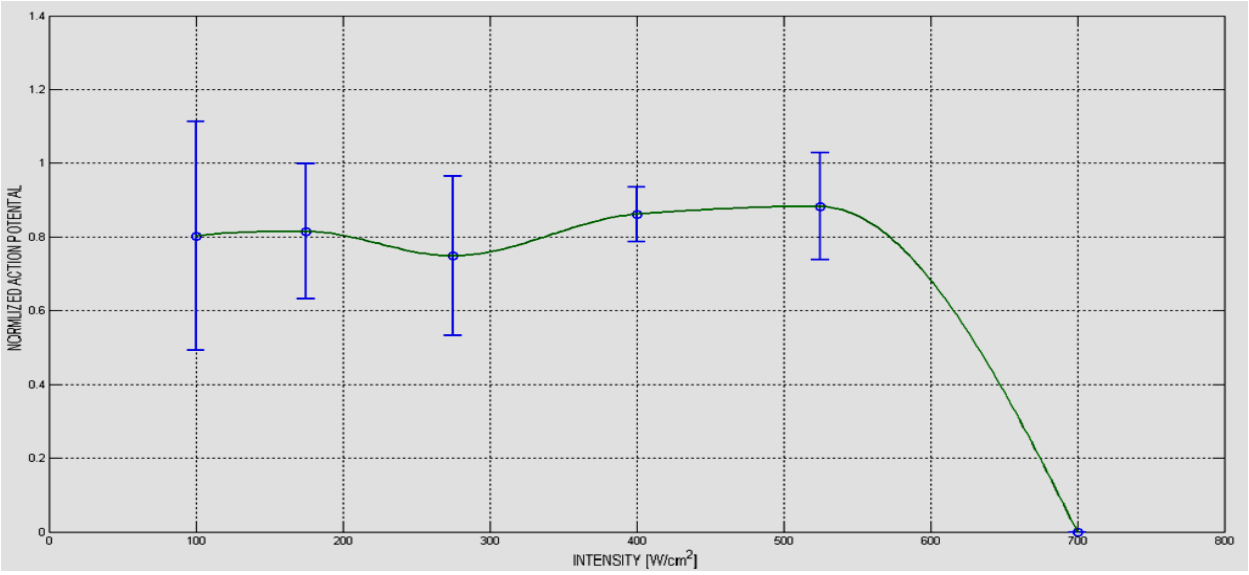

Figure 3.28 – Normalized compound action potential (CAP) vs. focal intensity of a 10-s HIFU exposure. It shows a complete block at 700 W.cm^{-2} while a trend of small changes in CAP amplitude can be seen at lower intensity levels

Chapter 4 Discussions and Conclusions

In this chapter we will provide discussions and conclusions from the results obtained in our study. We will also lay out a road map for future works.

4.1 Discussions

In this study, a total number of 40 lobster nerves were exposed to 10-second HIFU exposures. Setting up all the equipment in a fashion that could reliably accommodate a nerve piece was the biggest challenge in this study. Precise targeting of the nerve while located in the nerve chamber also had vital effects on the results obtained. As mentioned in chapter three, the lateral size of the HIFU focal spot was found to be 1.8 mm, hence finding the right location and placing the nerve at the focal spot took a lot of practice. However, choosing the right size of the plexiglass nose piece that was attached to the transducer made it much easier to target the nerve right at the focal spot in the axial direction.

Using the Biopac system, all the nerves were electrically stimulated with 5 volts of stimulation prior and during the experiment. As seen in the results section, a wide range of CAP values was measured in the lobster nerves used in this study. This might be due to the fact that the nerves were dissected from several lobsters with different living conditions, making the baseline CAP values different for each nerve. Furthermore, error bars in figure 3.28 suggest a range in post exposure measurements which could be due to the challenge of adequate positioning of the nerve and hitting it with the exact intensity level.

4.2 Conclusions

It was shown in this research work that the application of HIFU energy causes some changes to the amplitude of compound action potentials of *in vitro* lobster nerves when the nerves were exposed to a 10-s HIFU sonication.

The nerve conduction velocity parameter did not play a role in this study due to the fact that the lobster abdominal nerve is not protected by myelin sheath. As mentioned in chapter 1, the myelin sheath protects the nerve while it speeds up the signal conduction. Furthermore, not any specific trend in the delay time (time between the electrical stimulation and the occurring of the CAP) was observed in the nerves undergone the exposure. In other words, in these experiments, the velocity of the CAP signal did not change after the exposure to the HIFU sonication.

The CAP measurement results obtained in this study suggested that the nerves exposed to focal intensity levels ranging from 100 $W.cm^{-2}$ to 525 $W.cm^{-2}$ showed slight increases in their CAP values. This may be attributed to excitation of the nerve by the HIFU energy (acoustic excitation) due to HIFU-induced thermal and/or mechanical stresses applied to the nerve.

A significant decrease of CAP amplitude occurred in the last group of nerves studied. The nerves in the intensity group of 700 $W.cm^{-2}$ showed an average baseline CAP at 16.1 μv while once the nerves were exposed to the 10-s HIFU exposure this value decreased to 7.1 μv. These nerves were found not to be functional after the exposure, suggesting a total dysfunctioning of the exposed nerve and a complete nerve block.

In conclusion, it was shown that the HIFU energy used in this study resulted in a slight increasing in the CAP amplitude at low and intermediate intensity levels, while a drastic change

in the CAP amplitude and complete nerve block and degeneration of the nerve was achieved with the application of higher intensities.

When comparing the intensity groups, the highest intensity level appeared to have much stronger effect on nerves being exposed to the HIFU energy, while all the intermediate groups showed a minor changing regime which could only slightly change the CAP value of the nerves studied.

This study contributes to the advancement of our knowledge towards the electro-physiological effects and changes that can occur in nerves once exposed to high intensive focused ultrasound exposures. It also contributed to setting up a CAP measurement system which could be used in the ultrasound field.

4.3 Future Work

The results from this study suggest a wide range of future work and research projects with different set of assumptions. Among others, new nerve models can be studied while being exposed to HIFU systems. Below are a few suggestions for future works based on the current study:

- A new nerve model can be used to investigate the effects of HIFU on nerves. Frog's sciatic nerves can be chosen as the next model because of their close comparison to human's nervous system. These nerves are also protected by the myelin sheath which will add a nerve conduction velocity change parameter to the research.

- A longer and more focused study on each intensity level may also add some significant results on the changes that can be achieved by exposing nerves to different levels of ultrasound. Changing the exposure time and the conditions that nerves are being exposed to HIFU system can also play a big role in achieving some scientific contribution.
- Further investigation on CAP changes in an *in vivo* nerve model may also lead to the development of a non-invasive method to block and unblock nerve conduction. This research would hopefully result in enhanced treatment of chronic pain as well as new methods to achieve non-invasive localized anesthesia.
- A great deal of effort in this thesis has been put into the understanding of the electro-physiological aspects of the study. However, the HIFU system and the experimental set-up used for this study limited the parameters that could be changed in order to get the best results possible. Having a smaller hand-held transducer and a more accurate set-up could lead to more control in experiments and more effective results.
- A more fundamental study is needed to investigate the effects of mechanical and/or thermal stresses on nerves through well-controlled experimental protocols toward understanding of biophysical mechanisms of actions of HIFU with nerves. This study has just started in our research group.

Appendix A

The MATLAB code and C function – Field simulations

```
close all;
clear all;
TAP=1;          % Total Acoustic Power (Normalize to 1 W)
sos=1500;       % speed of sound, [m/s]
density=1000;   % density [kg/m^3]
f0=2;           % Center (resonance) frequency in [MHz]
freq=f0*1000;   % Center frequency in [kHz]

alpha_actual=0  %1.01*10^-4 % Attenuation coefficient in water at f0, [Np/mm]

factor=20;      % integration factor
esize=1;        % element size in x, [mm]
espac=1;        % element spacing in x, [mm]
dimx=50;        % size of transducer in x, [mm]
dimy=50;        % size of transducer in y, [mm]
radcurv=120;    % radius of curvature, [mm]
dh=0;           % diameter of central hole, [mm]

elements=truncsphshell(espac,esize,dimx,dimy,radcurv);

focus=[0,0,radcurv]';
x=[-10,10];      % [mm] compute pressure field over these dimensions
y=[-10,10];      % [mm]
z=[90,150];      % [mm]
step=[0.5,0.5,0.3];
xx=x(1):step(1):x(2);
yy=y(1):step(2):y(2);
zz=z(1):step(3):z(2);

elements=set_power(elements,sos,density,TAP);

[row,col]=size(elements);
Po = sqrt(2*density*sos*TAP/(esize*esize*1e-6*col));
for i=1:col
    if sqrt(elements(1,i)^2+elements(2,i)^2) <= dh/2,
        elements(15,i)=0;     % Set the amplitude of the elements inside the
hole to zero
        elements(16,i)=0;     % Set the phase of the elements inside the hole
to zero
    end
end

save crystal1 elements x y z step freq factor density alpha sos xx yy zz
focus
save alpha_actual alpha_actual
drawarray(elements,'mag'), axis equal, grid on;  % Draw the array geometry
```

(1) To compile the field_2008.c file:

```
>> mex field_2008.c
```

(2) Creating transducer geometry

```
>> crystal1
>> load crystal1.mat
>> drawarray(elements,'non')
```

(3) 3D intensity field calculation (Linear)

```
>> field_2008('crystal1.mat','crystal1_field.mat');
>> load crystal1_field.mat
>> dims                          % Dimensions of the 3D intensity matrix
>> xx, yy, zz                    % Get index to the desired plane
>> Ix=islice(intensity,dims,i_index
>> Ix=Ix ';
>> imagesc(yy,zz,Ix), colorbar;

>>plot(zz,Ix(:,index of yy –it's an integer number))
Kslice – lateral profile
Islice – axial profile
```

References

Aury, J. M., O. Jaillon. (2006). Global trends of whole-genome duplications revealed by the ciliate Paramecium tetraurelia, Nature 444, 8-171

Arden, N.I., Janes, J.M., Herrick, J.F. (1957). Ultrasonic energy and defects in bone, J. Bonne Joint Surg. Am. 39, 394-402

Barnett M.W., Larkman P.M. (2007). The action potential, Pract. Neurol. 3, 192-197

Bailey, M.R., Khokhlova, V.A., Sapozhnikov, O.A., Kargl, S.G. and Crum. (2003). Physical mechanisms of the therapeutic effect of ultrasound, Acoustical Physics 49, 437-464

Bao, S., Thrall, B.D., Gies, R.A., Miller, D.L. (1998). In vivo transfection of melanoma cells by lithotripter shock waves, Cancer Res. 23, 953-959

Bao, S., Thrall, B.D., Miller, D.L. (1997). Transfection of reporter plasmid into cultured cells by sonoporation in vitro, Ultrasound Med. Biol. 58, 219-221

Becker, B.M., Hefrich, S., Baker, E. (2005). Ultrasound with topical anesthetic rapidly decreases pain of intravenous cannulation, Acad. Emerg. Med. 12, 289-295

Bhatheja K, Field J. (2006). Schwann cells: origins and role in axonal maintenance and regeneration, National Center for Biotechnology Information, Pub. Med. 38, 9-1995

Burov, A.K. (1956). High intensity ultrasonic vibrations for action on animal and human malignant tumors. Dokl. Akad. Nauk. SSR 106, 239-241

Biological Bulletin Publications, Recipes (Amphibia, Mammals), Marine Biology (www.mbl.edu)

Biopac nerve conduction manual (2003). Biopac Systems, Inc.,

Charles A. Cain, T. L. Hall, J. B. (2005). Fowlkes. Imaging feedback of tissue liquefacation (histotripsy) in ultrasound surgery, IEEE Ultrasonics Symposium, 5, 7803-9383

Colin W. (2004). The lobster coast, Viking/Penguin (New York)

Coleman, D.J., Lizzi, F.L., Driller, J., Rosado, A.L., Chang, S., Iwamoto, T., Rosenthal, D. (1985). Therapeutic ultrasound in the treatment of glaucoma experimental model, Ophthalmology 92, 339-346

Carson P.L., Physics of ultrasound propagation. In Goldman L.W., Fowlkes J.B. (1995). Medical CT and ultrasound, American Association of Physicists in Med.

C. Campos-Pozuelo. (1996). Limiting strain of metals subjected to high-intensity ultrasound, Acustica 82 (6), 823-828

Cobbold Richard S. C. (2007). Foundations of biomedical Ultrasound, Oxford University Press

Davick, J.P., Martin, R.K., Albright, J.R. (1988). Distribution and deposition of tritiated cortisol using phonophoresis, Phys. Ther. 68, 1672-1675

Dukhin, A.S. and Goetz, P.J. (2002). Ultrasound for characterizing colloids, Elsevier,

Dyson, M., Brookes, M. (1983). Stimulation of bone repair by ultrasound, Ultrasound 82, Pergamon Press (Oxford), 61-66

Duncan D. (1934). A relation between axon diameter and myelination determined by measurement of myelinated spinal root fibers, J. Comp. Neurol. 60, 33-45

Doyle D.A., Morais Cabral J., Pfuetzner R.A., Kuo A., Gulbis J.M., Cohen S.L. (1998). The structure of the potassium channel, molecular basis of K^+ conduction and selectivity, Science 280, 7-56

E.A. Neppiras. (1972). Macrosonics in industry, Ultrasonics 10, 9-13

Foley, J.L., Little, J.W., Starr, F.L., Frantz, C., Vaezy, S. (2004). Image-guided HIFU neurlysis of peripheral nerves to treat spasticity and pain, Ultrasound Med. Biol. 30, 1199-1207

Foley, J.L., Vaezy, S. and Crum. (2006). Applications of high-intensity focused ultrasound in medicine: Spotlight on neurological applications, Appl. Acoust. 68, 245-259

Foley, J.L., James, W.L., Vaezy, S. (2007). Effects of high-intensity focused ultrasound on nerve conduction, Muscle and Nerve 37, 241-250

Fry, W.J., Fry, F.J. (1960). Fundamental neurological research and human neurosurgery using intense ultrasound, IRE Trans. Med. Electron. ME-7, 166-181

Fry, W.J., Barnard, J.W., Fry, F.J., Krumins, R.f., Brennan, J.F. (1955). Ultrasonic lesions in the mammalian central nervous system, Science 122, 517-518

Frenkel, P.A., Chen, S., Thai, T., Shohet, R.V., Grayburn, P.A. (2002). DNA-loaded albumin microbubbles enhance ultrasound mediated transfection in vitro, Ultrasound Med. Biol. 28, 817-822

Gavrilov, L. R., I. Davies. (1995). Application of focused ultrasound for the stimulation of neural structures, Ultrasound in Med. & Biol. 22, 179-192

Greenleaf, W.J., Bolander, M.E., Sarkar, G., Goldring, M.B., Greenleaf, J.F. (1998). Artificial cavitation nuclei significantly enhance acoustically induced cell transfection, Ultrasund Med. Biol. 24, 587-595

Gibson, Frank, Lord, and Phillip. (2008). Minimum information about a neuroscience investigation electrophysiology, Nature Preceding

Hartline D.K., Colman D.R. (2007). Rapid conduction and the evolution of giant axons and myelinated fibers, Curr. Biology 17, 29-35

Hanajiri, K. (2006). Microbubble-induced increase in ablation of liver tumors by high-intensity focused ultrasound, Hepatology Research 36, 14-308

Hang J. Lee, Joel A. Delisa. (2004). Manual of nerve conduction study and surface anatomy for needle electromyography (4^{th} ed.)

Heybeli, N., Oyar, O., Gulsoy, U.K., Tekinsoy, M.A., Mumcu, E.F. (2002). Diagnostic ultrasound treatment increases the bone fracture healing rate in an internally fixed rat femoral osteotomy model, J. Ultrasound Med. 21, 357-1363

Hedrick W., D.L. Hykes and Dale E. Starchman. (2005). Ultrasound physics and instrumentation, Elsevier Mosby (4^{th} ed.)

Hynynen K., Vincent C., Gary S., Ferenc J., Natalia V. (2009). Focused ultrasound effects on nerve action potential in vitro, Ultrasound in Medicine and Biology 35, 1737-1747

Holt, R.G. and Roy, R.A. (2001). Measurements of bubble-enhanced heating from focused, MHz-frequency ultrasound in a tissue mimicking material, Ultrasound in Medicine and Biology 27, 412-1399

Hueter, T.F., Ballantine J., H.T., Cotter, W.C. (1956). Production of lesions in the central nervous system with focused ultrasound: as study of dosage factors, J. Acoust. Soc. Am. 28, 192-201

Hunt, F.V. (1982). Electroacoustics: The analysis of transduction, and its historical background, Acoustical Society of America (New York)

Jiang Y., Lee A., Chen J., Ruta V., Cadene M., Chait B.T., MacKinnon R. (2003). X-ray structure of a voltage-dependent K^+ channel, Nature 423, 33-41

Kalat, James W. (2007). Biological psychology, Thompson Learning, (USA) (9^{th} ed.)

Kremkau, F., Gramiak, R., Carstensen, E., Shah, P., Kramer, D. (1970). Ultrasonic detection of cavitation at catheter tips, Am. J. Roentgenol. Radium Ther.-Nucl. Med. 110, 177-183

Kremkau, F.W. (1979). Cancer therapy with ultrasound: a historical review, J. Clin. Ultrasound 7, 287-300

Kremkau F.W. (2002). Diagnostics ultrasound: principles of instruments, Philadelphia (6th ed.)

LATS (Linear Acoustic and Temperature Simulation) User Manual (2010), Fouad Butt and Jahan Tavakkoli

Lin S. (2000). Measurement of ultrasonic power and electro-acoustic efficiency of high power transducers, Ultrasonics 37, 549-554

Lynn, J.G., Zwemer, R.L., Chick, A.J., Miller, A.F. (1942). A new method for the generation and use of focused ultrasound in experimental biology, J. Gen. Physiol. 26, 179-193

Mayr, E., Laule, A., Suger, G., Ruter, A., Claes, L. (2001). Radiographic results of callus distribution aided by pulsed low intensity ultrasound, J. Orthop. Trauma 15, 407-414

Marieb E.N., Hoehn K. (2007). Human anatomy & physiology, (7th ed.)

Mihran R.T., Barnes F.S., Wachtel H. (1990). Temporally specific modification of myelinated axon excitability in vitro following a single ultrasound pulse, Ultrasound Med. Biol. 3, 297-309

Mitragotri, S., Edwards, D.A., Blankschtein, A., Langer, R. (1995). A mechanistic study of ultrasonically enhanced transdermal drug delivery, J. Pharm. Sci. 84, 697-706

Mitragotri, S. (2005). Healing sound: the use of ultrasound in drug delivery and other therapeutic applications, NAT. Rev. Drug Discovery 4, 255-260

O'Brien, J., W.D. (1998). Assessing the risks for modern diagnostic ultrasound imaging, Jpn. J. Appl. Phys. 37, 2781-2788

Ohmic Instruments Corporation Operator's Manual (2005)

Purves D., Augustine G.J., Fitzppooatrick D. (2008). Neuroscience, Sinauer Associates, (4th ed.)

Pilla, A.A., Mont, M.A., Nasser, P.R., Khan, S.A. (1990). Non-invasive low intensity pulsed ultrasound accelerates bone healing in rabbit, J. Orthopaed. Trauma 4, 246-253

Pinto A., Morecroft J.H. and Curry W.A. (1921). Principles of radio communication, John Wiley & Sons Inc. (New York)

P.N.T. Wells. (1992). Ultrasonics: a window into biomedical science, Ultrasonics 30, 3-7

Richard C. Brusca & Gary J. Brusca. (2003). Invertebrates (2nd ed.), Sinauer Associates

Schmitt Francis O. and Betty B. Geren. (1956). On the significance of the Schwann cell in the structure and function of peripheral nerve, (USA), 46, 659-662

Sjoberg, A., Stable, J., Johnson, S., Sahl, R. (1963). Treatment of meniere's disease by ultrasonic irradiation. Acta Otolaryngol. Suppl. 178, 171-175

Skauen, D.M., Zenter, G.M. (1984). Phonophoresis, Intern. J. Pharmaceut. 20, 235-245

Shona Mcsheehy & Zoltán Mester. (2004). Arsenic speciation in marine certified reference materials, Journal of Analytical Atomic Spectrometry

Tavakkoli J., Birer A., Arefiev A., Prat F., Chapelon J.Y., Cathignol D. (1997). A piezocomposite shock-wave generator with electronic focusing capability: application for producing cavitation-induced lesions in rabbit liver, Ultrasound Med. Biol.

Tavakkoli J., Sanghvi N.T. (2010). Ultrasound-guided HIFU and thermal ablation. In: Frenkel V., ed. "Therapeutic Ultrasound: Mechanisms to Applications", Chapter 6, Nova Science Publishers, Hauppauge (New York)

Taniyama, Y., Tachibana, K., Hiaola, K. (2002). Development of safe and efficient novel nonviral gate transfer using ultrasound: enhancement of transfection efficiency if naked plasmid DNA in skeletal muscle, Gene Therapy 9, 372-380

Takagi, S.F., Higashino, S., Shibuya, T., Osawa, N. (1960). The actions of ultrasound on the myelinated nerve, the spinal cord and brain, Jpn. J. Physiol. 10, 93-183

Ter Haar, G. (2007). Therapeutic applications of ultrasound, Progress in Biophysics and Molecular Biology 93, 111-129

Traill R.R. (1988). The case that mammalian intelligence is based on sub-molecular memory coding and fiber-optic capabilities of myelinated nerve axons, Speculations Sci. Technology 3, 173-181

Unger, E.C., Porter, T., Culp, W. (2004). Therapeutic applications of lipid-coated microbubbles, Adv. Drug Delivery Rev. 56, 1291-1314

Wang, S., Tsui, P., Huang, C. (2005). In vitro effects of ultrasound with different energies on the conduction properties of neural tissues, Ultrasonics 43, 560-565

Watkin, N.A., Morris, S.B., Rivens, Haar, G.T. (1997). High intensity focused ultrasound ablation of the kidneys in a large animal model, J. Endourol. 11, 191-196

Wells, P.N.T., Bullen, M.A., Follett, D.H., Freundlich, H.F., James, J.A. (1963). The dosimetry of small ultrasonic beams, Ultrasonics 1, 106-110

Wells P.N.T. (1977). Biomedical ultrasonics, Academic Press, (New York)

Whitton John, B.A. and Brook, A.J. (2002). The freshwater algal flora of the British Isles, Cambridge University Press

Whittingham T.A. (1999). Broadband transducers, Eur. Radiol

Wood, R.W., and Loomis, A.L. (1927). The physical and biological effects of high frequency sound waves of great intensity, Phil. Mag. (VII) 4, 417-436

William, W. Roberts, Timothy L., Hall, Kimberly Ives, J. Stuart Wolf. (2006). Pulsed cavitational ultrasound: A noninvasive technology for controlled tissue ablation (Histotripsy), The Journal of Urology 175, 734-738

Wu, Y., Liang, H., Chen, W., Lai, J., Luh and Chong F. (2008). Electrophysiological and functional effects of shock waves on the sciatic nerve of rats, Ultrasound in Med. & Biol. 34, 1688-1696

William, D. O'Brien, J. (2007). Ultrasound-biophysics mechanisms, Progress in Biophysics and Molecular Biology 93, 212-255

Yu., W., Wang, S., Zhao, N., Wan, M. (2008). Focused-ultrasound modifications on the conduction properties of toad's sciatic nerve, IEEE International Ultrasonics Symposium Proceedings

Zagzebski, J.A. (1996). Essentials of ultrasound physics, St. Lousis, Mosby-Year Book

Zemp, R. J. (2000). Modeling non-linear ultrasound in tissue MS.c. Institute of Biomaterials and Biomedical Engineering